WAVES AND STRONGLY-SHEARED CURRENTS: EXTENSIONS TO COASTAL OCEAN MODELS

BY

SAEIDEH BANIHASHEMI AND JAMES T. KIRBY

RESEARCH REPORT NO. CACR-19-06

FALL 2019

CENTER FOR APPLIED COASTAL RESEARCH

University of Delaware
Newark, Delaware 19716

ACKNOWLEDGEMENTS

This study was supported by the National Science Foundation, Physical Oceanography Program under Grants Number OCE-1334325, OCE-1435147, and OCE-1756355.

TABLE OF CONTENTS

LIST OF TABLES

LIST OF FIGURES

ABSTRACT

Interaction between surface gravity waves and mean flows has implications for wave propagation, breaking and changes in the mean circulation pattern. These physical processes subsequently modify material transport and mixing in the coastal ocean. Most of the existing wave-current interaction modeling approaches are based on the assumptions of weak current or strong current with weak vertical shear. Few of the former studies consider the interaction of waves with strongly sheared current, in which the current vertical shear can affect linear wave dynamics at the leading order. In real world, however, in coastal zones where fresh riverine water meets salty seawater, such as in a river mouth, flow structures can be highly complex and the current becomes strongly sheared due to stratification and tidal effects.

In this study we investigate the shortcomings in numerical modeling of waves and vertically sheared currents. The influence of an arbitrary current profile on wave dispersion and evolution equation is studied. We demonstrate that the widely used depth-weighted average current value of Kirby & Chen (1989)(KC89), is not the correct current speed to use directly in the action equation in SWAN or similar wave models, as this approach neglects the contribution from the derivative of the wavenumber-dependent weighted current during calculation of the group velocity. We correct this error and also suggest a strategy for determining the current contribution to group velocity as a function of frequency, employing a Taylor series expansion about the peak frequency, significantly extending the range of accuracy of current information with minimal additional programming or data passage. The expressions for energy density and intrinsic frequency used to construct the wave action density are similarly investigated, using perturbation approximations in the general action balance equation of Voronovich (1976). The results suggest that the action density $N = E_0/\sigma$ may be

consistently constructed using the usual expression for energy density, $E_0 = 1/2\rho g a^2$, together with a $\sigma = \omega - k\tilde{U}$ based on the KC89 current speed. The wave action flux approximation also suggests the use of the current $\hat{U}$ as the correct current speed to be used in the advection velocity, which is the vector form of the advection velocity suggested by KC89 and discussed by Banihashemi *et al.* (2017). We have further extended the suggested Taylor expansion around the peak wave number in a modeled spectrum, with extensions covering the specification of action, flux and intrinsic frequency as well as an extension to a general 2D horizontal setting. These results provide an avenue for calculating wave action and action flux in spectral wave models, using a compact set of information about the current field evaluated at the spectral peak wave number. Lastly the coupled wave-current model $NH\overline{WAVE}$, which couples the wave model SWAN with a wave-averaged version of the non-hydrostatic model NHWAVE Ma *et al.* (2012), is validated using laboratory experiments on wave-current interaction. We have chosen the experiments done by Kemp & Simons (1982) on the interaction of non-breaking waves with currents in a laboratory flume. The results from our 3D non-hydrostatic model agree reasonably well with data from the experiment for wave following currents.

Chapter 1

INTRODUCTION

Wave-current interaction plays a key role in understanding coastal ocean dynamics and near shore sediment transport. To analyze and model wave-current interaction, it is useful to have a clear understanding of the relative magnitude of time and length scales for both the waves and currents. In most frame works, waves are considered to vary more frequently than the currents. Therefore, in many situations and over most coastal and open-ocean areas, there is a clear separation between waves and currents in horizontal space and time scales. This provides a basis for deriving the conservative wave-current interaction equations. The theories have been incorporated in numerical models to include wind wave effects in ocean circulation without resolving surface gravity wave motions for computational efficiency. Within the modeling system, ocean circulation models are coupled with wave generation and propagation models to resolve the effect of waves on circulation and vice versa. The spectral wave models include evolution of wave action density affected by the mean flow, and the ocean circulation models account for the wave-averaged forces driving or modifying the mean flow.

1.1 Current Effects on Waves

To describe the wave group evolution, wave action, which is defined as the total wave energy divided by intrinsic frequency, is often adopted because of its conservative characteristics without growth and dissipation effects (Bretherton & Garrett, 1968). Existing, widely used wave models such as SWAN (Simulating Waves Nearshore, Booij *et al.*, 1999) are typically based on the underlying dynamics for monochromatic waves being governed by the wave action balance of Bretherton & Garrett (1968).

Studies have recently been carried out using SWAN model for example in the Wadden Sea (Caires *et al.*, 2006; Haskoning, 2007; Groeneweg *et al.*, 2007), in which model results were compared with buoy observations in tidal inlets. The objective of these studies were to determine the predictive skill of SWAN for a number of severe storm conditions, including a range of wind and wave directions, high water levels and strong tidal currents through the tidal inlet. These hind casts indicated that, at the buoy locations positioned around the tidal inlet, the largest discrepancies between model results and observations are found at short fetches at the lee of the barrier islands, and in the main tidal channel. Wave-current interaction was shown to have a significant influence on wave conditions in the tidal channel. In particular, under conditions of opposing current, wave heights and mean absolute wave periods were found to be overestimated by the model Groeneweg *et al.* (2007). It is therefore important to verify the performance of wave-current interaction in wave models such as SWAN, and to investigate refinements to its implementation.

A specific aspect considered in the wave evolution models is the influence of the current profile on the dispersion of the waves. Presently, the SWAN model assumes a depth uniform current when computing wave-current interaction to evaluate the propagation velocities. The effect of weak vertical current shear has recently been accounted for in models using a depth-weighted average current value (Skop, 1987; Kirby & Chen, 1989). Various studies including van der Westhuysen & Lesser (2007); Ardhuin *et al.* (2008) have utilized this depth-weighted current $\tilde{U}(k)$ as the basis for the wave-current interaction in propagation models. In application, this approach is often further truncated to account for the limitations in the standard form for input into the spectral wave model, which only allows the specification of a single current value at each grid location. This limitation is often dealt with by using $\tilde{U}(k_p)$ as the representative value of $\tilde{U}$, where k_p denotes the wavenumber at the spectral peak frequency; see, for example, Elias *et al.* (2012). The effect of choosing a single value for current velocity based on the peak wave frequency is examined in Chapter 3 and an alternate strategy in suggested, involving a Taylor series expansion about the peak frequency, which should

significantly extend the range of accuracy of current information available to the wave model with minimal additional programming.

Presumably, the expression for action density needs to be investigated as well. For the general case, Voronovich (1976) has described the conservation law, in the geometric optics approximation, for an adiabatic invariant corresponding to the wave action density. Recently Quinn *et al.* (2017) have presented an explicit formulation of the wave action equation using known asymptotic solutions of the boundary value problem which exploit the smallness of the current magnitude compared to the wave phase velocity and/or its vertical shear and curvature; the adopted approximations are shown to be sufficient for most conceivable applications. In the limit of vanishing current shear, the new formulation reduces to that of Bretherton & Garrett (1968) without shear, and the invariant is calculated with the current magnitude taken at the free surface. It is shown that in realistic oceanic conditions, the neglect of the vertical structure of the currents in wave modeling might lead to significant errors in wave amplitude. In Chapter 4, using a modification of Kirby & Chen (1989)'s perturbation solution for weakly-sheared currents, where the basic flow is allowed to be a strong current with waves propagating at an arbitrary angle to the surface current direction, we develop approximate expressions for the wave action density and action flux in terms of a weighted integral over depth of the arbitrary current profile.

1.2 Wave Effects on Currents

The study of wave effects on currents was also developed to explain nearshore current generation and modifications. The analytical expressions for surface wave force and wave-current interaction can be classified into two types depending on the treatment of the advection terms in the momentum equation. The formulations for wave forcing are based on either the radiation stress concept (Longuet-Higgins & Stewart, 1960, 1961, 1962, 1964), in which forcing is expressed as the divergence of a stress tensor expressing excess wave momentum flux, or on the vortex-force or CL formalism Craik & Leibovich (1976), where wave forcing appears through a combination of terms

expressing vortex force, divergence of wave volume flux, and the dissipation of wave energy. The difference between the concepts of radiation stress and vortex force lies in the treatment of the advection terms $\mathbf{q}\cdot\nabla\mathbf{q}$ in momentum equation. The advection term, combined with continuity equation, yields wave-averaged forces in radiation stress formalism according to $\mathbf{q}\cdot\nabla\mathbf{q}+\mathbf{q}(\nabla\cdot\mathbf{q}) = \nabla\cdot(\mathbf{q}\otimes\mathbf{q})$, while another operation on the advection term yields the vortex force formalism according to $\mathbf{q}\cdot\nabla\mathbf{q} = \frac{1}{2}\nabla(\mathbf{q}\cdot\mathbf{q}) - \mathbf{q}\times(\nabla\times\mathbf{q})$. The first term on RHS is the gradient of Bernoulli head, which contributes to the pressure gradient force within the water column. The second term on RHS is called the vortex force. The flow vorticity is defined as $\mathbf{\Omega} = \nabla\times\mathbf{q}$.

The classical wave 'radiation stress' concept were originally presented in terms of depth-integrated and short wave-averaged equations. However, when it comes to 3D ocean circulation modeling, it is required that radiation stress be depth-dependent as a forcing term in the momentum equation. Mellor (2003) provided depth dependent formulation for radiation stress terms which has been implemented in publicly available version of ROMS by Warner *et al.* (2008). Nevertheless, it is pointed out that the formula by Mellor are inconsistent in a simple test case of shoaling waves without energy dissipation due to inappropriate treatment of pressure terms in radiation stress (Ardhuin & Belibassakis, 2008). In response, Mellor (2008) modified his original formulation and provided a new approach for depth-dependent radiation stresses to include a Dirac delta function at the sea surface. Bennis & Ardhuin (2011) showed that the new formulation was inconsistent with the known depth-integrated momentum balances in the presence of a sloping bottom. Although they did not discuss the origin of the inconsistency, they stated that Mellor used a different averaging for the pressure gradient term and for the advection terms of the same equation and believe that this was the original reason for the problems discussed in their study. Finally, based on the correct transformation of the horizontal pressure gradient in the equations of Mellor (2003) and with the radiation stress tensor of Mellor (2008), Mellor (2011a) presented a closed set of equations in σ-coordinates which are consistent with Longuet-Higgins & Stewart (1964) and Phillips (1977). Recently Kumar *et al.* (2011) implemented the

Mellor (2008) method including the updates presented in Mellor (2011a) in ROMS, and evaluate an idealized situation of non-breaking and shoaling waves on a steep sloping topography.

Another version of the formulation for wave forcing is the surface wave force initially derived by Garrett (1976) in the study of Langmuir circulation generation. The wave driving forces include the wave dissipation term and the wave-averaged vortex forcing term, identified later by Leibovich (1980) and Smith (1980) as the vertically integrated form of the 'CL vortex-force' derived by Craik & Leibovich (1976). Dingemans *et al.* (1987) also presented a similar formulation of this type of wave driving force. Smith (2006) extended the formulation of Garrett (1976) to include finite-depth effects and provided some insight into physical interpretation of each forcing term in depth-integrated equations. Newberger & Allen (2007) derive wave-averaged forces consisting of a surface stress and a body force. The surface stress is proportional to the wave energy dissipation. The body force includes one term that is related to gradients of part of the radiation stress tensor and a second term that is related to the vortex force and is proportional to a product of the mean wave momentum and the vertical component of the mean vorticity vector. In addition, there is a nonzero normal velocity at the mean surface that arises from the divergence of the mean Eulerian wave mass flux. The formulation is applied to the extended Princeton Ocean Model (POM) and validated with data from DUCK94 experiment. Shi *et al.* (2006) formulate a Craik-Leibovich wave vortex force for a quasi-3D circulation model. The study showed equivalent results when both models were run with continuous coupling between currents and waves. Interestingly, this equivalence breaks down when coupling is updated only intermittently, with a clear indication that the vortex force model retains better accuracy with progressively weakened coupling. This result was thought to be related to the form of the vortex force term, which can utilize the updated current field and thus partially maintains continuous coupling during time-stepping of the circulation model, even if corresponding updates to the Stokes drift are not available.

McWilliams *et al.* (2004) showed a series of equations in different time scales for surface waves, infragravity waves and low-frequency currents in a coupled system, and has provided a careful derivation of the 3-D forcing due to waves acting on currents in a vortex force formulation. Uchiyama *et al.* (2010) presented a wave-current interaction model with the McWilliams *et al.* (2004) vortex force formulation using UCLA/ROMS and SWAN. The model is validated using DUCK94 experimental data. Kumar *et al.* (2012) applies the vortex force formulation by McWilliams *et al.* (2004) in the the coupled ocean-atmosphere-wave-sediment transport (COAWST) modeling system Warner *et al.* (2010), which couples USGS/ROMS with SWAN. Several subsequent studies have used COAWST model with the inclusion of McWilliams *et al.* (2004) wave vortex forces in estuaries and coasts under well-mixed conditions (e.g. Olabarrieta *et al.* 2011, 2014; Benetazzo *et al.* 2013). Recently, wave current interaction effects on mixing and transport in river plumes has received considerable attention (Akan *et al.* 2017; Rong *et al.* 2014) and is found to play important roles in modifying salinity stratification, freshwater transport, and dispersal of river plumes. Gong (2018) have also studied the effects of wave current interaction on salt transport and salt intrusion in estuaries during storm events.

The limitation to weak vertical shear is still present in McWilliams *et al.* (2004) formulation. Recently, Dong (2016) has presented a new framework to describe wave-current interaction for arbitrarily sheared current. Following McWilliams *et al.* (2004), the study has developed a theory to describe the interactions of waves with strongly sheared mean flow. Starting with the multiple scale expansion, they derive governing equations for both waves and mean flow dynamics by applying wave average. With the presence of strongly sheared mean flow, the wave governing equations are manipulated to get into the form of Rayleigh stability equations. The multiple scale expansion and wave averaging are used to separate wave equations and mean flow equations. The resulting formulation for mean flow leads to vortex force formalism incorporating current shear effects.

As mentioned above, most of the existing wave-current interaction modeling

approaches are based on the assumptions of weak current or strong current with weak vertical shear. Few of the former studies consider the interaction of waves with strongly sheared current, in which the current vertical shear can affect linear wave dynamics at the leading order. In real world, however, in coastal zones where fresh reverine water meets salty seawater, such as in a river mouth, flow structures can be highly complex and the current becomes strongly sheared due to stratification and tidal effects (Figure 1.1).

Waves propagating against an opposing current can be stopped if the magnitude of the current, in the direction of wave propagation, exceeds the group velocity of the oncoming waves. This phenomenon is known as wave blocking, and the location where the waves are blocked is called the blocking point. This characteristic feature of wave blocking has drawn the interests of oceanographers and coastal engineers alike for their ability to be used as signature patterns of underlying large scale motion (e.g. internal waves) and for the navigational hazards these regions pose. Around the blocking point, the wave climate transitions rapidly from steepening waves prior to the blocking point to decaying waves beyond the blocking point. One such example of wave blocking can be seen in Figure 1.2 at Indian River inlet. The photograph has been taken 3 hours after high tide, and thus there is a strong current propagating out of the inlet. This strong current blocks waves that are trying to propagate into the inlet.

Field measurements at river inlets are becoming more common with improvements in field observation techniques and instruments. The Columbia River is the largest river on the Pacific coast of North America, accounting for 77% of the total drainage along the coast between San Francisco and the Strait of Juan de Fuca (Hickey *et al.*, 1998). The Columbia plume provides an excellent natural laboratory in which existing numerical and analytical models can be tested and in which the importance of various physical processes can be assessed. Strong river flow, wind forcing, and tidal forcing cause the Columbia River plume to be an extremely dynamic feature, therefore a wide variety of plume processes has been studied by many previous authors. Kilcher & Nash (2010) describe the structure and explore the dynamics of the Columbia River

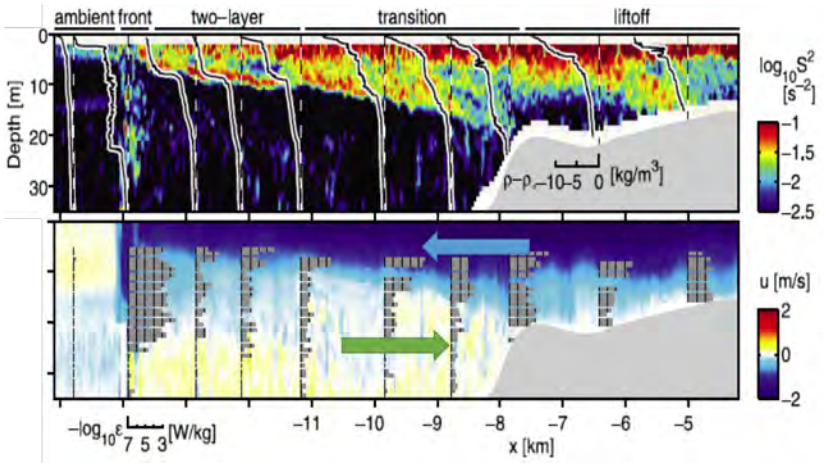

Figure 1.1: Internal plume structure for a moderate ebb near low tide, Columbia River. Upper panel: Log of shear squared (color) and vertical profiles of density deficit $\rho - \rho^{\circ}$(black lines; $\rho^{\circ} = 1026.3 kg/m^3$). Lower panel: Eastward velocity (color) and $log_1 0\epsilon$ (gray bars; tick marks indicate decades above $10^{-7} W/kg$).Kilcher & Nash (2010)

tidal plume and front. Elias *et al.* (2012) have recently reported the first comprehensive field observation (USACEMega-Transect Experiment, Moritz *et al.*, 2007) and numerical modeling (DELFT3D-SWAN; Lesser *et al.*, 2004) efforts for the Mouth of Columbia River (MCR), with surface waves and wave-current interaction being one of their main emphases. In their study, they demonstrated that it is not straight forward to model wave-current interaction over a strongly vertically-sheared surface plume. The distribution of wave height is sensitive to the choice of current intensity experienced by the waves. They suggested that the wave-orbital weighted formulation developed by Kirby & Chen (1989) is shown to have better model skill when comparing with measured data.

Janssen & Herbers (2014) have conducted two pilot experiments in Raccoon Strait located in San Francisco Bay (May and July 2011) and have collected a dataset of wave-current interaction in this area. These pilot experiments were conducted to better understand the current and wave regimes in the area (Figure 1.3). Surface wave energy is enhanced in the blocking zone where the waves are relatively steep

Figure 1.2: Wave blocking at Indian River Inlet, Delaware, USA, (Chawla & Kirby, 2002)

and breaking occurs. Thomson *et al.* (2014) have also presented observations of wave breaking effects at the offshore front of the Columbia River plume. Their observations show that wave breaking is an important source of turbulence at the offshore front, which may contribute to plume mixing. The lateral gradient of current associated with the plume front is sufficient to block (and break) shorter waves.

These initial observations show a complicated interaction between tidal currents, stratification, topography and surface waves, the details of which are not yet fully understood.The interactions between waves and arbitrary strong current can cause significant effects to mass transport, large amplitude wave crests can cause damage to coastal structures, and the turbulence induced by the kinematics can be dangerous for maritime vessels. Since the existing wave-current interaction studies are not adequate to address the strong and complex interactions occurring in wave-forced river out flows, In locations such as a river inlet, an approach that can model the nonlinear effects is needed. Such work requires theoretical development on wave-current interaction which has been introduced in the work done by Dong (2016)(DK16 herein after). The

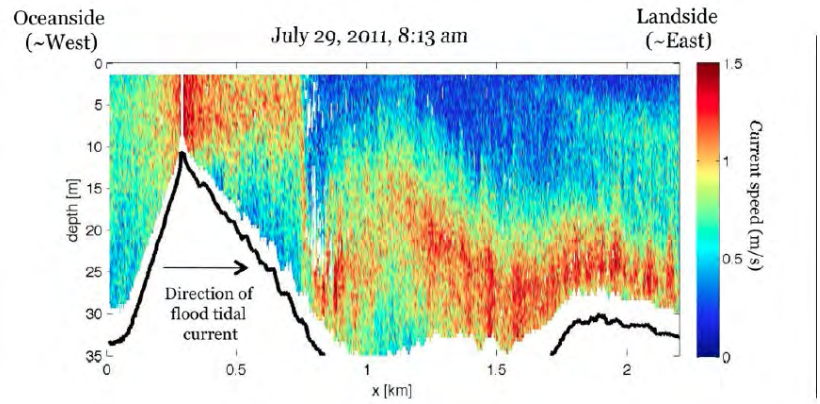

Figure 1.3: Flow velocities observed using ship-board ADCP with the ship track in along-strait direction. The incoming flood tide is accelerated over the sill and plunges underneath the lighter bay water about 700m after the sill. (Janssen & Herbers, 2014)

wave-current interaction theory has been applied in their work to a coupled system of NHWAVE and SWAN (NH$\overline{\text{WAVE}}$), with which our research starts.

1.3 Thesis Outline

The specific objectives of this study are (1) Finding possible ways to account for current shear effects in the wave action conservation equation in existing wave models such as SWAN and (2) Evaluating the performance of the model implementation presented by DK16 in NH$\overline{\text{WAVE}}$ coupled model against wave flume experiments.

After a preliminary presentation of the results of the wave-current interaction on strongly sheared mean flows theory presented by DK16 (Chapter 2), we will proceed in Chapters 3 and 4 by describing the work done to incorporate a better representation of frequency and direction-dependent group velocity and intrinsic frequency in the neighborhood of the spectral peak, thus improving the present practice of using quantities evaluated only at the spectral peak. Chapter 5 will give an introduction to the wave spectrum model SWAN and the wave-averaged non-hydrostatic model NHWAVE for nearshore and coastal ocean circulation followed by a test case to examine the validity of the model.

Chapter 2

WAVE CURRENT INTERACTION THEORY

In this chapter, we describe the procedure for separating wave and current motions using a multiple-scale expansion. We start with the Euler equations and decompose the motion into wave and current components. The current is treated as slowly varying motion with longer scales in time and space compared to waves. Thus mean flow dynamics can be separated from wave dynamics according to different scales. Following Phillips (1977), any variables such as velocity, pressure, surface elevation and vorticity can be separated into waves and current. We take ϕ for example. ϕ can be written as the superposition of currents and waves.

$$\phi = \overline{\phi} + \tilde{\phi} \tag{2.1}$$

where $\overline{\phi}$ represents mean flow variable and $\tilde{\phi}$ represents the wave variable. The mean flow is separated from oscillatory flows by applying wave-average $'' < \cdot > ''$ to the variable in Eulerian framework, which is defined as the average over the wave phase.

$$< \cdot >= \frac{k_0}{2\pi} \int_0^{\frac{2\pi}{k_0}} \cdot \, dx = \frac{\omega_0}{2\pi} \int_0^{\frac{2\pi}{\omega_0}} \cdot \, dt \tag{2.2}$$

Mean flow variables remain while the oscillatory variables are assumed to be removed after wave-averaging. This is an Eulerian mean method.

$$< \overline{\phi} >= \overline{\phi} \tag{2.3}$$

$$< \tilde{\phi} >= 0 \tag{2.4}$$

The linear wave solution can induce other harmonics of oscillation due to nonlinearity. We apply the WKB representation to the wave motion to include the these harmonics. In general, we expand all dependent variables in multiple scales. The Eulerian equations are then sorted into mean flow equations and wave equations.

2.1 Governing Equations

We consider incompressible, inviscid flow governed by the Euler equations. Due to current vertical shear, wave motions are not typically irrotational. A turbulence model and stratification effects can be added to our formulation later. We separate our problem into horizontal and vertical directions by defining the coordinates $(x, y, z, t) = (\mathbf{x}, z, t)$, velocity $\mathbf{q} = (u, v, w) = \mathbf{u} + w\mathbf{i}_z$ and gradient vector $\nabla = (\partial/\partial x, \partial/\partial y, \partial/\partial z) = (\nabla_h, \partial/\partial z)$. We use p for pressure, h for still water depth and η for instantaneous water surface elevation. The governing equations and boundary conditions are given by

$$\frac{\partial \mathbf{q}}{\partial t} + \mathbf{q}\cdot\nabla\mathbf{q} + \frac{1}{\rho}\nabla p + g\mathbf{i}_z = 0 \qquad -h \le z \le \eta \tag{2.5}$$

$$\nabla\cdot\mathbf{q} = 0; \qquad -h \le z \le \eta \tag{2.6}$$

$$w = -\mathbf{u}\cdot\nabla_h h; \qquad z = -h \tag{2.7}$$

$$w = \frac{\partial \eta}{\partial t} + \mathbf{u}\cdot\nabla_h \eta; \qquad z = \eta \tag{2.8}$$

$$p = 0; \qquad z = \eta \tag{2.9}$$

The curl of the momentum equation leads to a vorticity equation, which is used to describe the motion's vorticity dynamics.

$$\frac{\partial \mathbf{\Omega}}{\partial t} + (\mathbf{q}\cdot\nabla)\mathbf{\Omega} = (\mathbf{\Omega}\cdot\nabla)\mathbf{q}; \qquad -h \le z \le \eta \tag{2.10}$$

where vorticity is defined by $\mathbf{\Omega} = \nabla \times \mathbf{q}$, and may be written in terms of horizontal and vertical components as $(\boldsymbol{\xi}, \chi)$. In our problem, the motion consists of strong mean flows with long wave contributions and narrow-banded surface gravity waves. Weakly nonlinear surface gravity waves have small surface slope so that parameter

$\epsilon = k_0 a_0 \ll 1$, where k_0 is a representative wave number and a_0 is a representative wave amplitude. All the scaling in our problem is done based on parameter ϵ. The oscillatory wave motion is described using complex function $e^{i\Theta} = \cos\Theta + i\sin\Theta$, where $\Theta(\mathbf{x}, t)$ is the wave phase function, with wave number and absolute frequency defined by

$$\mathbf{k}(\mathbf{x}, t) = \nabla_h \Theta(\mathbf{x}, t)$$

$$\omega(\mathbf{x}, t) = -\frac{\partial \Theta}{\partial t}(\mathbf{x}, t)$$

$\mathbf{k}$ and ω are assumed to be slowly varying over horizontal and temporal scales. Wave number conservation is given by cross-differentiating Θ to obtain

$$\frac{\partial \mathbf{k}}{\partial t} + \nabla_h \omega = 0 \tag{2.11}$$

2.2 Multiple-scale Approach

In most cases, the spatial and temporal scales of variations of the current and of average properties of the wave field are much larger than the period and wavelength of individual waves. Thus the scales of wave and current variations may be treated separately. We introduce multiple-scale format in horizontal scale $\mathbf{x}$ and temporal scale t to describe the general modulations of variables,

$$\mathbf{x} = \mathbf{x} + \epsilon \mathbf{x} = \mathbf{x} + \mathbf{X} \tag{2.12}$$

$$t = t + \epsilon t = t + T \tag{2.13}$$

We assume that motions contain both fast scale and slow scale variations. The fast scales denoted by $(\mathbf{x}, z, t)$ are used to describe local wave-like behavior as well as vertical variation, while slow scales are used to illustrate the slowly varying features of the mean flow as well as properties of narrow-banded wave trains in horizontal space and time denoted by $(\mathbf{X}, T)$. The topography is also assumed to vary slowly in horizontal space as $h = h(\mathbf{X})$. In addition to the general multiple-scale approach, we apply a WKB

theory to wave motions to facilitate the isolation of problems at each order (n) for each harmonic frequency (m) as shown below, where n denotes ordering in ϵ and m denotes the harmonic number. We expand the variable ϕ, for instance, as

$$\begin{aligned}\phi &= \sum_{n=0}^{\infty} \epsilon^n \phi_n(\mathbf{x}, z, t, \mathbf{X}, T) \\ &= \sum_{n=0}^{\infty} \epsilon^n \sum_{m=-n}^{n} \phi_{n,m}(z, \mathbf{X}, T) E^m \end{aligned} \tag{2.14}$$

where $E = e^{i\Theta}$. We require $\phi_{n,-m} = \phi^*_{n,m}$, where ϕ is any physical variable and * denotes complex conjugation (*c.c.* thereafter), in order to obtain real-valued physical quantities. Specifically, the mean flow is represented by terms with $m = 0$, while linear waves are represented by $m = 1$. Quadratic waves appear in terms with $m = 2$ plus slow-scale derivatives of linear wave terms. We note that wave terms with $E^m (m \neq 0)$ are formally removed by wave-averaging. It is thus easy to identify current terms and waves terms in the expansion. According to

$$\overline{\phi} = \sum_{n=0}^{\infty} \epsilon^n \phi_{n,0} = \phi_{0,0}(\mathbf{X}, z, T) + \epsilon \phi_{1,0}(\mathbf{X}, z, T) + \epsilon^2 \phi_{2,0}(\mathbf{X}, z, T) + \cdots \tag{2.15}$$

$$\begin{aligned}\tilde{\phi} &= \sum_{n} \sum_{m \neq 0} \epsilon^n \phi_{n,m} E^m \\ &= \epsilon[\phi_{1,1}(\mathbf{X}, z, T)E + c.c.] + \epsilon^2[\phi_{2,1}(\mathbf{X}, z, T)E + \phi_{2,2}(\mathbf{X}, z, T)E^2 + c.c.] + \cdots \end{aligned} \tag{2.16}$$

The instantaneous surface elevation $\eta(\mathbf{x}, t)$ consists of the wave-averaged component $\overline{\eta}(\mathbf{X}, T)$ and the oscillatory component $\tilde{\eta}(\mathbf{x}, t, \mathbf{X}, T)$.

$$\eta = \overline{\eta} + \tilde{\eta} \tag{2.17}$$

The total mean water depth seen by waves is $d = h + \bar{\eta}$, hence we expand the surface boundary conditions in Taylor series about the slowly varying water surface level $z = \bar{\eta}$,

which is consistent with subsequent use of the theory in numerical models.

$$(\cdot)_{z=\eta} = (\cdot)_{z=\bar{\eta}} + \tilde{\eta}\frac{\partial}{\partial z}(\cdot)_{z=\bar{\eta}} + \frac{\tilde{\eta}^2}{2}\frac{\partial^2}{\partial z^2}(\cdot)_{z=\bar{\eta}} + O(\epsilon^3) \tag{2.18}$$

In addition, both fast and slow scale variations are involved in our problem. To simplify it, we use the relation between fast and slow scale coordinates $\mathbf{x} = \mathbf{X}/\epsilon, t = T/\epsilon$ and substitute for fast scale coordinates using slow scale coordinates. The horizontal slow scale gradient is defined as ∇_H. The local slow scale derivative is defined as $\partial/\partial T$. The phase function then becomes $\Theta(\mathbf{x}, t) = \Theta(\mathbf{X}, T)/\epsilon$, and wave number and frequency are defined as

$$\mathbf{k} = \nabla_h\Theta(\mathbf{x}, t) = \epsilon\nabla_H[\frac{1}{\epsilon}\Theta(\mathbf{X}, T)] = O(1)$$

$$\omega = \frac{\partial}{\partial t}\Theta(\mathbf{x}, t) = \epsilon\frac{\partial}{\partial T}[\frac{1}{\epsilon}\Theta(\mathbf{X}, T)] = O(1)$$

The governing equations are given with surface boundary conditions expanded at $z = \overline{\eta}$

$$\epsilon\frac{\partial \mathbf{u}}{\partial T} + \epsilon(\mathbf{u}\cdot\nabla_H)\mathbf{u} + w\frac{\partial \mathbf{u}}{\partial z} + \frac{\epsilon}{\rho}\nabla_H p = 0; \qquad -h \le z \le \overline{\eta} \tag{2.19}$$

$$\epsilon\frac{\partial w}{\partial T} + \epsilon(\mathbf{u}\cdot\nabla_H)w + w\frac{\partial w}{\partial z} + \frac{1}{\rho}\frac{\partial p}{\partial z} + g = 0; \qquad -h \le z \le \overline{\eta} \tag{2.20}$$

$$\epsilon\nabla_H\cdot\mathbf{u} + \frac{\partial w}{\partial z} = 0; \qquad -h \le z \le \overline{\eta} \tag{2.21}$$

$$w = -\epsilon\mathbf{u}\cdot\nabla_H h; \qquad z = -h \tag{2.22}$$

$$p + \epsilon\tilde{\eta}\frac{\partial p}{\partial z} + \frac{\epsilon^2\tilde{\eta^2}}{2}\frac{\partial^2 p}{\partial z^2} + \frac{\epsilon^3\tilde{\eta^3}}{6}\frac{\partial^3 p}{\partial z^3} = O(\epsilon^4); \qquad z = \overline{\eta} \tag{2.23}$$

$$w + \epsilon\tilde{\eta}\frac{\partial w}{\partial z} + \frac{\epsilon^2\tilde{\eta^2}}{2}\frac{\partial^2 w}{\partial z^2} + \frac{\epsilon^3\tilde{\eta^3}}{6}\frac{\partial^3 w}{\partial z^3} = \epsilon\frac{\partial \eta}{\partial T} + \epsilon(\mathbf{u} + \epsilon\tilde{\eta}\frac{\partial \mathbf{u}}{\partial z} + \frac{\epsilon^2\tilde{\eta^2}}{2}\frac{\partial^2 \mathbf{u}}{\partial z^2})\cdot\nabla_H\eta + O(\epsilon^4); \qquad z = \overline{\eta} \tag{2.24}$$

2.3 Wave-averaged Forces

With strong current and strong shear assumption, the current velocity can reach the same magnitude as the wave phase speed, $|\overline{\mathbf{u}}|/c_0 \sim O(1)$. The current vertical shear

is comparable to absolute wave frequency, $|\partial\overline{\mathbf{u}}/\partial z|/\omega_0 \sim O(1)$. The wave amplitude is assumed to be far less than wave length, or $a_0 k_0 = \epsilon \ll 1$. The non-dimensional wave variables are of order $O(\epsilon)$.

Dividing the motions into waves and current in the momentum equation and applying wave-averaging, we get the momentum equation for the mean flow alone, given by

$$\frac{\partial \overline{\mathbf{q}}}{\partial t} + \overline{\mathbf{q}}\cdot\nabla\overline{\mathbf{q}} + \frac{1}{\rho}\nabla\overline{p} + g\mathbf{i}_z = -\epsilon^2 < \tilde{\mathbf{q}}\cdot\nabla\tilde{\mathbf{q}} >; \qquad -h \le z \le \eta \tag{2.25}$$

The RHS term $- < \tilde{\mathbf{q}}\cdot\nabla\tilde{\mathbf{q}} >$ is the wave-averaged forcing. It can be interpreted either in terms of the radiation stress formalism or the C-L vortex force formalism. In this study, we adopt the vortex force formalism since it gives a clearer physical interpretation of the problem. Considering the relation $\mathbf{q}\cdot\nabla\mathbf{q} = \nabla(\mathbf{q}\cdot\mathbf{q})/2 - \mathbf{q}\times(\nabla\times\mathbf{q})$, we define

$$\kappa = \epsilon^2 < \frac{1}{2}(\tilde{\mathbf{q}}\cdot\tilde{\mathbf{q}}) > \tag{2.26}$$

$$(\mathbf{J}, K) = \epsilon^2 < \tilde{\mathbf{q}} \times (\nabla \times \tilde{\mathbf{q}}) > \tag{2.27}$$

where κ is Bernoulli head and $(\mathbf{J}, K)$ are vortex forces in horizontal and vertical directions, respectively. Therefore, the RHS term $- < \tilde{\mathbf{q}}\cdot\nabla\tilde{\mathbf{q}} >= -\epsilon^2(\nabla\kappa + \mathbf{J} + K\mathbf{i}_z)$. The body force is the combination of Bernoulli head gradient $\nabla\kappa$ and vortex force $(\mathbf{J}, K)$. The Bernoulli head gradient represents the wave-induced effects associated with wave set down. The vortex force represents wave refraction caused by the current field. The form of the vortex force above is slightly different from the Craik-Leibovich definition of vortex force, which is the distortion of current vorticity by the wave-induced Stokes drift. The theory indicates that the wave vorticity is directly related to the current vorticity and wave Stokes drift is derived from the wave orbital velocity $\tilde{w}$. Hence the present form finally leads to the Craik-Leibovich vortex force with wave solutions.

2.3.1 Leading order wave equation

The leading order wave equations (consistent with $(n = 1, m = \pm 1)$ in equation 2.15) are given as follows. As we can see, current vertical shear appears in wave momentum equation, which generates wave vorticity.

$$\frac{\partial \overline{\mathbf{q}}}{\partial z}\tilde{w} - i\sigma\tilde{\mathbf{q}} + \frac{i\mathbf{k}}{\rho}\tilde{p} = 0; \qquad -h \le z \le \overline{\eta} \tag{2.28}$$

$$-i\sigma\tilde{w} + \frac{1}{\rho}\frac{\partial \tilde{p}}{\partial z} = 0; \qquad -h \le z \le \overline{\eta} \tag{2.29}$$

$$\frac{\partial \tilde{w}}{\partial z} + i\mathbf{k}\cdot\tilde{\mathbf{q}} = 0; \qquad -h \le z \le \overline{\eta} \tag{2.30}$$

$$\tilde{w} = 0; \qquad z = -h \tag{2.31}$$

$$\tilde{w} = -i\sigma_s\tilde{\eta}; \qquad z = \overline{\eta} \tag{2.32}$$

To get the Rayleigh (or inviscid Orr-Sommerfeld) stability equation, we multiply Equation (2.28) by $\mathbf{k}$ and take its vertical derivative $\partial/\partial z$. After combining (2.29) - (2.30), we have the Rayleigh equation for the vertical component of wave velocity $\tilde{w}$, given by

$$\sigma\frac{\partial^2 \tilde{w}}{\partial z^2} - (\frac{\partial^2 \sigma}{\partial z^2} + k^2\sigma)\tilde{w} = 0; \qquad -h \le z \le \overline{\eta} \tag{2.33}$$

with combined surface boundary condition

$$\sigma_s^2\frac{\partial \tilde{w}}{\partial z} - (\sigma_s\frac{\partial \sigma}{\partial z} + gk^2)\tilde{w} = 0; \qquad z = \overline{\eta} \tag{2.34}$$

and bottom boundary condition (2.31). σ_s is the wave intrinsic frequency at mean surface. The horizontal orbital velocity $\tilde{\mathbf{q}}$ and pressure field amplitude $\tilde{p}$ are given in terms of $\tilde{w}$ by

$$\tilde{\mathbf{q}}(z) = -\frac{i}{\sigma}[\tilde{w}\frac{\partial \overline{\mathbf{q}}}{\partial z} - \frac{\sigma^2\mathbf{k}}{k^2}\frac{\partial}{\partial z}(\frac{\tilde{w}}{\sigma})] \tag{2.35}$$

$$\tilde{p}(z) = \frac{i\rho\sigma^2}{k^2}\frac{\partial}{\partial z}(\frac{\tilde{w}}{\sigma}) \tag{2.36}$$

The Rayleigh equation 2.33 has very few analytical solutions except for some

special cases. An approximate solution can be obtained using the perturbation solutions Kirby & Chen (1989), or by using a numerical approach following Fenton (1973). Hence, Dong (2016)(DK16 herein after) follow the work done by Kirby & Chen (1989) in terms of the perturbation solutions. The comparison between wave numerical solutions and perturbation solutions based on measured current velocity profiles is discussed in DK16 and results suggest that the perturbation solution up to $O(\epsilon)$ is a fairly good approximation to wave solutions for the real current velocity profile. Wave-averaged forces are provided with the perturbation solution instead of numerical solution to avoid extra computation time. The details of the wave perturbation solution will be provided further in section 2.4 along with the resulting wave forces. To obtain the wave forces for weak current in section 2.5, we will rescale the governing equations with weak current assumption, and reproduce part of the work done in McWilliams *et al.* (2004) (MLR04 hereinafter).

2.4 Wave Vortex Force formalism by DK16

A formulation for wave-induced Bernoulli head and vortex force is given by DK16 for the case of strong currents and strong shear. We intend to compare the vortex force formulation of DK16 with weak current with shear assumption to the vortex force formalism of McWilliams *et al.* (2004) in this chapter. Therefore we will present the forces up to $O(\epsilon^2)$ here which will be the leading order terms containing current shear terms. In addition, the slow time derivatives in horizontal vortex force are neglected since these terms are relatively small. The equations are rearranged as below.

As mentioned before, the forcing terms in DK16 are originally in terms of the wave vertical velocity $\tilde{w}$. Therefore in order to evaluate the forcing terms we need to seek wave solutions. We seek solutions for the vertical component of the wave orbital velocity

$$\tilde{w} = -i\sigma_s a F(z) \tag{2.37}$$

where a is the amplitude of the wave, $\sigma_s = \omega - \mathbf{k}\cdot\overline{\mathbf{u}}(0)$ is the intrinsic frequency at the mean water surface, and $F(z)$ has constraints $F(\overline{\eta}) = 1, F(-h) = 0$, defining the vertical structure of $\tilde{w}$

The equations governing mean flow in the vortex force formulation in Cartesian coordinates are given by

$$\frac{\partial \overline{\mathbf{u}}}{\partial t} + (\overline{\mathbf{u}}\cdot\nabla_H)\overline{\mathbf{u}} + \overline{w}\frac{\partial \overline{\mathbf{u}}}{\partial z} + \frac{1}{\rho}\nabla_H \overline{p} = -\nabla_H \kappa + \mathbf{J} \tag{2.38}$$

$$\frac{\partial \overline{w}}{\partial t} + (\overline{\mathbf{u}}\cdot\nabla_H)\overline{w} + \overline{w}\frac{\partial \overline{w}}{\partial z} + \frac{1}{\rho}\frac{\partial \overline{p}}{\partial z} + g = -\frac{\partial \kappa}{\partial z} + K \tag{2.39}$$

$$\nabla_H\cdot\overline{\mathbf{u}} + \frac{\partial \overline{w}}{\partial z} = 0 \tag{2.40}$$

$$\overline{w}|_{-h} + \overline{\mathbf{u}}|_{-h}\cdot\nabla_H h = 0 \tag{2.41}$$

$$\overline{w}|_{\overline{\eta}} - \frac{\partial \overline{\eta}}{\partial t} - (\overline{\mathbf{u}}\cdot\nabla_H)\overline{\eta} = \nabla_H\cdot\mathbf{U}^{st} \tag{2.42}$$

$$\overline{p}|_{\overline{\eta}} = P \tag{2.43}$$

Where $\mathbf{U}^{st}$ is the Stokes transport, which in turn is the depth integral of the Stokes drift as defined in 2.47 and 2.48. The divergence of the depth-integrated Stokes drift, $\nabla_H\cdot\mathbf{U}^{st}$, appears on the RHS of the kinematic surface boundary condition as a wave-induced mass source/sink term (Hasselmann, 1971). The wave-averaged forces consist of the gradient of Bernoulli head κ and vortex force $(\mathbf{J}, K)$. The depth-dependent continuity equation indicates the incompressibility of the flow with the wave part removed after wave-averaged. The mean water surface elevation $\overline{\eta}$ includes wave setup/setdown. P is the wave-averaged forcing term at $z = \overline{\eta}$.

With the wave solution given by 2.37 the wave forcing terms presented in DK16 can be rearranged as follows. (For more detailed derivation, see chapter 4 in DK16)

$$\kappa = \frac{{\sigma_s}^2 a^2}{4}\Big(\frac{{F_{,z}}^2}{k^2} + \left[1 + \frac{1}{\sigma^2(z)}\left(|\overline{\mathbf{u}}_{,z}|^2 - \frac{(\mathbf{k}\cdot\overline{\mathbf{u}}_{,z})^2}{k^2}\right)\right]F^2\Big) \tag{2.44}$$

$$\begin{aligned}\mathbf{J} &= \frac{{\sigma_s}^2 a^2}{4}\mathbf{i}_z \times \Big(\Big[-\frac{2F^2}{\sigma^2}\overline{\mathbf{u}}_{,z} + \frac{\sigma\mathbf{k}}{k^2}\Big(\frac{F^2}{\sigma^2}\Big)_{,z}\Big]\cdot\nabla_H\overline{\boldsymbol{\xi}} + \frac{\sigma\mathbf{k}}{k^2}\Big(\frac{F^2}{\sigma^2}\Big)_{,z}\overline{\chi}_{,z} \\ &+ \Big(\frac{2F^2}{\sigma^2}\overline{\xi}_{,z} + (\mathbf{k}\cdot\overline{\xi})\frac{\mathbf{k}}{k^2}\Big(\frac{F^2}{\sigma^2}\Big)_{,z}\Big)\cdot\nabla_H\overline{\mathbf{u}} - (\mathbf{k}\cdot\overline{\xi})\frac{\mathbf{k}}{k^2}\Big(\frac{F^2}{\sigma^2}\Big)_{,z}\nabla_H\cdot\overline{\mathbf{u}} \\ &+ \boldsymbol{\xi}^c\cdot\nabla_H\Big(\frac{F^2}{\sigma^2}\overline{\mathbf{u}}_{,z}\Big) + \frac{F^2}{\sigma^2}\boldsymbol{\xi}^c\cdot\nabla_H(\overline{\mathbf{u}}_{,z})\Big) \\ &- \mathbf{i}_z \times \frac{\overline{\boldsymbol{\xi}}}{\sigma}\cdot\nabla_H\Big(\frac{{\sigma_s}^2 a^2}{4}\frac{\sigma^2\mathbf{k}}{k^2}\Big(\frac{F^2}{\sigma^2}\Big)_{,z}\Big) - \mathbf{i}_z \times \mathbf{u}^{st}(z)\overline{\chi}\end{aligned} \tag{2.45}$$

$$K = \frac{{\sigma_s}^2 a^2}{4}\Big(\frac{2F^2}{\sigma^2}\overline{\mathbf{u}}_{,z}\times\overline{\boldsymbol{\xi}}_{,z} - \frac{\sigma}{k^2}\Big(\frac{F^2}{\sigma^2}\Big)_{,z}\mathbf{k}\times\Big(\overline{\mathbf{u}}_{,z}\frac{\mathbf{k}\cdot\overline{\boldsymbol{\xi}}}{\sigma} + \overline{\boldsymbol{\xi}}_{,z}\Big)\Big) \tag{2.46}$$

$$\mathbf{u}^{st} = \frac{{\sigma_s}^2 a^2}{4}\Big\{\Big[\frac{\sigma\mathbf{k}}{k^2}\Big(\frac{F^2}{\sigma^2}\Big)_{,z} - 2\frac{F^2}{\sigma^2}\overline{\mathbf{u}}_{,z}\Big]_{,z} + \Big(\frac{F^2}{\sigma^2}\Big)_{,z}\Big(\frac{\mathbf{k}}{k^2}\sigma_{,z} + \overline{\mathbf{u}}_{,z}\Big)\Big\} \tag{2.47}$$

$$\mathbf{U}^{st} = \frac{\sigma_s a^2}{4}\Big(\frac{\sigma\mathbf{k}}{k^2}\Big(\frac{F}{\sigma}\Big)_{,z} - \overline{\mathbf{u}}_{,z}\frac{F}{\sigma}\Big) + \frac{a^2}{4}\overline{\mathbf{u}}_{,z}(\overline{\eta}) \tag{2.48}$$

with the mean flow vorticity $\overline{\boldsymbol{\xi}}$ and $\overline{\chi}$

$$\overline{\boldsymbol{\xi}} = \mathbf{i}_z \times \overline{\mathbf{u}}_{,z} \tag{2.49}$$

$$\overline{\chi} = \nabla_H \times \overline{\mathbf{u}} \tag{2.50}$$

The dynamic surface boundary condition (2.43) is given by

$$\overline{p} = -<\tilde{\eta}\frac{\partial\tilde{p}}{\partial z}> = -\rho{\sigma_s}^2 a^2 F^2(\overline{\eta})\,/\,2 = -\rho{\sigma_s}^2 a^2\,/\,2; \qquad z = \overline{\eta} \tag{2.51}$$

2.5 Weak current assumption and comparison to wave vortex force formalism by McWilliams *et al.* (2004)

The weak current assumption is usually used in the modeling of wave-current interaction. In this section, we provide the wave-averaged forces for weak current with shear and compare them to the form presented in MRL04. The vortex force formulation with weak current assumption is implemented in our modeling approach in Chapter 5.

Two methods to obtain the wave forces for weak current are considered. One is

following MRL04 and formulates the problem by assuming weak current at the beginning. This will result in a reproduction of the work done in their 2004 paper. Instead of rescaling the governing equations with weak current assumption, we focus on the reduction of our wave-averaged forces based on perturbation solutions. The differences between the two methods are how to present current effects on wave solutions. The first method leads to the pure wave solutions at leading order and then presents the current effect at order $O(\epsilon^2)$ wave equations. The second method keeps current terms at leading order wave equations, leaving the order $O(\epsilon^2)$ wave equations current-free. Perturbation solutions to the leading order wave equations will include current effects. In this section, we adopt the second method. With weak current and weak shear assumption $|\overline{\mathbf{u}}|/c_0 \sim O(\epsilon)$, the wave-averaged forces in previous section are largely simplified as current related terms go at least one order higher. Following Kirby & Chen (1989) the perturbation wave solutions gives

$$
\begin{aligned}
w &= \sigma_s a \frac{f_0(z) + \epsilon f_1(z)}{f_0(0)} && (2.52)\\
f_0(z) &= \sinh k(h+z) && (2.53)\\
f_1(z) &= \frac{1}{2kc_0}[\tilde{I}_1(0) - \tilde{I}_1(z) - \frac{\tilde{I}_2(0)}{\tanh kh}]\sinh k(h+z)\\
&+ \frac{1}{2kc_0}\tilde{I}_2(z)\cosh k(h+z) && (2.54)\\
\tilde{I}_1(z) &= \int_{-h}^{z} \hat{\mathbf{k}}\cdot\overline{\mathbf{u}}_{,zz}(\xi)\sinh 2k(h+\xi)\,d\xi\\
\tilde{I}_2(z) &= \int_{-h}^{z} \hat{\mathbf{k}}\cdot\overline{\mathbf{u}}_{,zz}(\xi)(\cosh 2k(h+\xi) - 1)\,d\xi
\end{aligned}
$$

The wave-averaged forces can be reduced to

$$\begin{aligned}
\kappa &= \frac{{\sigma_s}^2 a^2}{4}\Big(\frac{\cosh 2k(h+z)}{\sinh^2 kd}+\frac{1}{kc_0\sinh^2 kd}\int_{-h}^{z}\hat{\mathbf{k}}\cdot\overline{\mathbf{u}}_{,zz}\sinh 2k(z-\xi)d\xi \\
&\quad+\frac{2\cosh 2k(h+z)}{c_0\sinh^2 kd}\Big[2k\int_{-h}^{0}\hat{\mathbf{k}}\cdot\overline{\mathbf{u}}\sinh 2k(h+\xi)d\xi-\frac{2k}{\tanh kd}\int_{-h}^{0}\hat{\mathbf{k}}\cdot\overline{\mathbf{u}}\sinh 2k(h+\xi)d\xi \\
&\quad+\hat{\mathbf{k}}\cdot\overline{\mathbf{u}}|_0+\hat{\mathbf{k}}\cdot\overline{\mathbf{u}}|_{-h}\Big]+\frac{\sinh 2k(h+z)}{kc_0\sinh^2 kd}(\hat{\mathbf{k}}\cdot\overline{\mathbf{u}}_{,z}|_{-h})\Big) \\
&\quad-\int_{-h}^{z}\mathbf{u}^{st}(\zeta)d\zeta\cdot\overline{\mathbf{u}}_{,z} \qquad (2.55)\\
\mathbf{J} &= -w^{st}\overline{\mathbf{u}}_{,z}-\mathbf{i}_z\times\mathbf{u}^{st}\chi^c-\nabla_H[\int_{-H}^{z}\mathbf{u}^{st}(\zeta)d\zeta\cdot\overline{\mathbf{u}}_{,z}] \qquad (2.56)\\
K &= -\int_{-h}^{z}\mathbf{u}^{st}(\zeta)d\zeta\cdot\mathbf{u}^c_{,zz}=\mathbf{u}^{st}\cdot\overline{\mathbf{u}}_{,z}-\frac{\partial}{\partial z}\Big(\int_{-h}^{z}\mathbf{u}^{st}(\zeta)d\zeta\cdot\overline{\mathbf{u}}_{,z}\Big) \qquad (2.57)
\end{aligned}$$

with

$$\begin{aligned}
\mathbf{u}^{st} &= \frac{a^2\sigma\mathbf{k}}{2\sinh^2 kd}\cosh 2k(z+h) \qquad (2.58)\\
\mathbf{U}^{st} &= \frac{a^2\sigma\mathbf{k}}{4k\sinh^2 kh}\sinh 2kd=\frac{E}{\rho c}\frac{\mathbf{k}}{k}=\frac{N}{\rho}\mathbf{k} \qquad (2.59)\\
w^{st}(z) &= -\nabla_H\cdot\int_{-h}^{z}\mathbf{u}^{st}dz' \qquad (2.60)
\end{aligned}$$

where E is the total wave energy and N is wave action. The last terms on the right hand sides of 2.56 and 2.57 are pure gradient terms,and thus can be combined with the Bernoulli head gradient, giving the final form of wave vortex force as

$$\begin{aligned}
\kappa &= \frac{{\sigma_s}^2 a^2}{4}\Big(\frac{\cosh 2k(h+z)}{\sinh^2 kd}+\frac{1}{kc_0\sinh^2 kd}\int_{-h}^{z}\hat{\mathbf{k}}\cdot\overline{\mathbf{u}}_{,zz}\sinh 2k(z-\xi)d\xi \\
&\quad+\frac{2\cosh 2k(h+z)}{c_0\sinh^2 kd}\Big[2k\int_{-h}^{0}\hat{\mathbf{k}}\cdot\overline{\mathbf{u}}\sinh 2k(h+\xi)d\xi-\frac{2k}{\tanh kd}\int_{-h}^{0}\hat{\mathbf{k}}\cdot\overline{\mathbf{u}}\sinh 2k(h+\xi)d\xi \\
&\quad+\hat{\mathbf{k}}\cdot\overline{\mathbf{u}}|_0+\hat{\mathbf{k}}\cdot\overline{\mathbf{u}}|_{-h}\Big]+\frac{\sinh 2k(h+z)}{kc_0\sinh^2 kd}(\hat{\mathbf{k}}\cdot\overline{\mathbf{u}}_{,z}|_{-h})\Big) \qquad (2.61)\\
\mathbf{J} &= -w^{st}\overline{\mathbf{u}}_{,z}-\mathbf{i}_z\times\mathbf{u}^{st}\overline{\chi} \qquad (2.62)\\
K &= -\int_{-h}^{z}\mathbf{u}^{st}(\zeta)d\zeta\cdot\mathbf{u}^c_{,zz}=\mathbf{u}^{st}\cdot\overline{\mathbf{u}}_{,z} \qquad (2.63)
\end{aligned}$$

with the dynamic surface boundary condition same as 2.51. Comparing the results to the widely used in ROMS/SWAN coupled model (Uchiyama *et al.*, 2010; Kumar *et al.*, 2012) the vortex forces are identical and the the second and third line in the bernoulli head equation 2.61 are additional terms compared to their Bernoulli head equation. The wave induced pressure is also different from that in Uchiyama *et al.* (2010), equation 9. These differences are thought to be due to different treatment of the surface boundary condition in the wave motion solution. Our f1(z) in equation 2.54 is equal to zero at the surface where the same treatment can not be seen in MRL04. The additional term added to $f1(z)$ adds the extra terms in our bernoulli equation while the value at the surface which is equal to zero will simplify our pressure to be equal to 2.51. Note that in MRL04 the combined contribution of Bernoulli head is separated in two parts of different order each. The higher order contribution is a quasi static balance between the mean pressure, mean surface elevation and the wave stresses, which is absorbed in the quasi static sea level component (Uchiyama *et al.*, 2010; Kumar *et al.*, 2012). This term results from subtracting 2.51 from the first term of 2.61 evaluated at the surface, which results in the quasi static sea level component as

$$\eta^{st} = -\frac{ka^2}{2\sinh 2kd} \tag{2.64}$$

The lower order quasi static balance is expressed as the Bernoulli head equal to the second term in 2.61 in (Uchiyama *et al.*, 2010; Kumar *et al.*, 2012) whereas by assuming weak current in DK16 vortex force formulation will result in five extra terms presented in the second and third line of equation 2.61.

Implementing the vortex force wave forcing in our coupled wave-current model $NH\overline{WAVE}$ will be discussed in Chapter 5.

Chapter 3

APPROXIMATION OF WAVE ACTION FLUX VELOCITY IN STRONGLY SHEARED MEAN FLOWS

The work presented in this chapter has been published in Ocean Modelling Volume-116, Pages 33-47.

https://doi.org/10.1016/j.ocemod.2017.06.002. Rights to this article are provided in Appendix E.

3.1 Introduction

Important theoretical advances have been made in the last several decades which have advanced our understanding of wave-current interaction in ocean circulation. Theories have been incorporated in numerical models with the main intent of including wind wave effects in ocean circulation without resolving surface gravity wave motions for computational efficiency. Within typical modeling systems, an ocean circulation model is coupled with a wave generation and propagation model in order to determine wave effects on currents and vice versa. The spectral wave models include the effect of the mean flow in the computation of wave action flux, and the ocean circulation models account for the wave-averaged wave forcing driving or modifying the mean flow.

Spectral wave models are usually based on the theory for waves in the presence of depth-uniform currents. In the real world, however, currents are usually vertically sheared to some degree. Recently, various studies (van der Westhuysen & Lesser, 2007; Ardhuin *et al.*, 2008) have suggested the use of a depth-weighted current $\tilde{U}(k)$ as the basis for the wave-current interaction in propagation models, where $\tilde{U}(k)$ is the first

order correction to the phase speed for an arbitrarily varying current $U(z)$ and is given by

$$\tilde{U}(k) = \frac{2k}{\sinh 2kh} \int_{-h}^{0} U(z) \cosh 2k(h+z)\, dz \tag{3.1}$$

where h is the water depth and k is the wave number (Skop, 1987; Kirby & Chen, 1989). In application, this approach is often further truncated by using $\tilde{U}(k_p)$ as the representative value of $\tilde{U}$ for all wave components, where k_p denotes the wavenumber at the spectral peak frequency. This procedure is now included as an option in widely used models such as Delft-3D and COAWST (Elias *et al.*, 2012; Kumar *et al.*, 2011, 2012). We remark here that the perturbation scheme of Kirby & Chen (1989), defined originally for the case of weak current, can be straightforwardly modified to cover the case of a strong current with weak additional shear. Assuming a fairly arbitrary split between a depth uniform and depth varying current

$$U(z) = U_0 + \alpha U_1(z); \quad \alpha \ll 1 \tag{3.2}$$

and repeating the procedure used to develop the solution in Kirby & Chen quickly establishes that the choice for leading order current speed is $U_0 = \tilde{U}$, with the details of the overall solution maintained up to second order. The parameter α represents the magnitude of current shear; a scaling analysis based on finite depth waves with horizontal and vertical length scales proportional to k^{-1}, leads naturally to an expression

$$\alpha = \frac{\Omega}{kU_s} \tag{3.3}$$

where Ω characterizes the maximum value of shear in the current profile, and U_s is the surface current speed. The expressions developed in both the perturbation solution and the analytic solution for constant shear discussed below are both easier to interpret using a slightly different expression

$$\alpha = \frac{\Omega h}{U_s} \tag{3.4}$$

which is used throughout the remainder of this chapter.

The purpose of this chapter is to demonstrate the inappropriateness of the use of the weighted current $\tilde{U}$ as the current component of the group velocity, and to examine the effect of using either the correct or incorrect estimate of the current speed evaluated only at the spectral peak frequency. We evaluate the accuracy of approximate solutions in comparison to analytical or numerical solutions for the full theory based on the Rayleigh stability equation. The theory described here is limited to unidirectional propagation on a following or opposing current, and so currents and wave numbers appear as scalars rather than vectors. General vector form will be further discussed in chapter (4). In section 3.2, the problem for a linear wave in a uniform domain with arbitrary current $U(z)$ is established. We then outline the common approximations for group velocity used in modeling and the errors resulting in these applications. In section 3.3, we evaluate the approximations for the analytic case of a wave on a current with constant vorticity, and establish the consistency of the expressions for group velocity derived from the perturbation solution of Kirby & Chen (1989). Section 3.4 examines comparable results of the numerical solution for a current profile measured at the mouth of the Columbia River (MCR) (Kilcher & Nash, 2010). In section 3.5, we evaluate the shortcomings of practical approximations in existing coupled circulation-spectral wave models, where it is typical to use only $\tilde{U}(k_p)$ as the current speed. Finally, in section 3.6 we describe a strategy for providing a compact but significantly more accurate representation of current advection velocity in SWAN or similar models, using a Taylor series expansion of the expression for the wavenumber-dependent current speed about the reference value at the peak frequency.

3.2 Theory and approximate expressions for the absolute group velocity C_{ga}

3.2.1 General theory

We consider the linearized wave motion of an incompressible, inviscid fluid, with wave number $\mathbf{k}$ and phase velocity $\mathbf{C_a} = \omega\mathbf{k}/k^2$, propagating on a stream of

velocity $\mathbf{U}(z)$ in finite water depth h. Current and depth variables are assumed to be uniform in horizontal directions (Figure 3.1). ω denotes the absolute wave frequency in a stationary frame of reference, which also fixes the value of $\mathbf{U}(z)$. We seek solutions for the vertical component of the wave orbital velocity

$$w(\mathbf{x}, z, t) = \tilde{w}(z)\mathrm{e}^{i(\mathbf{k}\cdot\mathbf{x}-\omega t)} \tag{3.5}$$

The problem for the vertical structure of plane waves in a spatially uniform domain, riding on a vertically sheared current $\mathbf{U}(z)$, is then given by an extension of the Rayleigh equation to allow for an oblique angle between wave and current direction as well as possible rotation of the current vector over depth

$$\begin{aligned} \sigma(z)(\tilde{w}'' - k^2\tilde{w}) - \sigma''(z)\tilde{w} &= 0; & -h \le z \le 0 \\ \sigma_s^2\tilde{w}' - [gk^2 + \sigma_s\sigma']\tilde{w} &= 0; & z = 0 \\ \tilde{w} &= 0; & z = -h \end{aligned} \tag{3.6}$$

where primes denote differentiation with respect to z and g is the gravitational constant. The quantity $\sigma(z) = \omega - \mathbf{k}\cdot\mathbf{U}(z)$ represents a depth-varying relative frequency, with σ_s denoting the value at the mean surface $z = 0$. The separate use of the kinematic surface boundary condition for a surface wave of form $\eta = a\exp i(\mathbf{k}\cdot\mathbf{x} - \omega\mathbf{t})$ gives $\tilde{w}(0) = -i\sigma_s a$.

The model (3.6) has been used in a number of studies of arbitrary or idealized velocity distributions; see reviews by Peregrine (1976), Jonsson (1990) and Thomas & Klopman (1997). For the general case of arbitrary $U(z)$, Voronovich (1976) has described the conservation law, in the geometric optics approximation, for an adiabatic invariant corresponding to the wave action density. Evaluation of these results requires knowledge of a solution to (3.6), however. Karageorgis (2012) has shown a method for constructing expressions for the dispersion relation for waves on a number of vertical vorticity distributions, but does not consider the further determination of the group

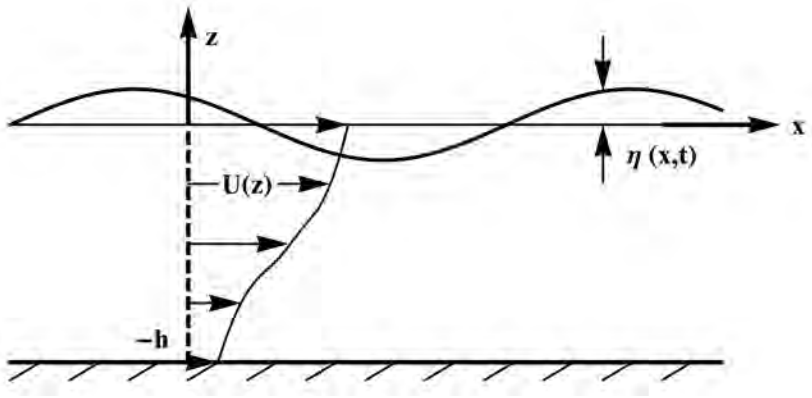

Figure 3.1: definition sketch

velocity.

For the case of weak shear, solutions to (3.6) may be obtained using a perturbation approach, described to leading order for deep water by Stewart & Joy (1974) and extended to finite depth by Skop (1987) and to second order by Kirby & Chen (1989). Considering deep water waves, Shrira (1993) has further demonstrated how series solutions may be extended to high order. Alternately, numerical solutions may be obtained using a shooting method due to Fenton (1973). In the following, we limit ourselves to the evaluation of the first and second-order solutions presented in Kirby & Chen (1989) and further limit ourselves to waves and currents propagating in the same direction (General form is discussed in chapter 4). For definiteness, we suppose that waves are propagating towards the right with $c > 0$ and $k > 0$, while the current can be propagating in either $\pm x$ direction.

3.2.2 Perturbation solution of Kirby & Chen (1989)

Following Kirby & Chen (1989), we assume that the steady current velocity is small relative to some measure of wave phase speed. Here, we use a Froude number based on the surface velocity $U_s = U(0)$ defined by

$$F = \frac{U_s}{\sqrt{gh}}; \qquad |F| \ll 1 \tag{3.7}$$

The wave phase speed is given by

$$C_a = \frac{\omega}{k} = C_0 + (F)C_1 + (F^2)C_2 + O(F^3) \tag{3.8}$$

where we indicate ordering w/r F schematically and retain dimensional expressions for now. C_0 is the usual result for linear waves on a stationary water column, and is given by

$$C_0 = \sqrt{\frac{g}{k}\tanh kh} \tag{3.9}$$

C_1 and C_2 arise from the current-induced Doppler shift, with $C_1 = \tilde{U}$ in (3.1) and C_2 given by

$$\begin{aligned} C_2 =& \frac{\tilde{U}}{2C_0}[4kI_1(0) - (1 + 2\cosh 2kh)\tilde{U}] \\ &+ \frac{k^2 C_0}{2gf_0^2(0)} \int_{-h}^{0} U^2(z)[1 + 2\cosh^2 k(h+z)]\, dz \\ &+ \frac{2k^3 C_0}{gf_0^2(0)} \int_{-h}^{0} [I_2(z)I_1'(z) - I_1(z)I_2'(z)]\, dz \end{aligned} \tag{3.10}$$

with

$$\begin{aligned} I_1(z) &= \int_{-h}^{z} U(\xi)\sinh 2k(h+\xi)\, d\xi \\ I_2(z) &= \int_{-h}^{z} U(\xi)\cosh 2k(h+\xi)\, d\xi \\ f_0 &= \sinh k(h+z) \end{aligned} \tag{3.11}$$

To $O(F^2)$, the absolute wave group velocity $\tilde{C}_{ga}$ determined from the perturbation solution is given by

$$\tilde{C}_{ga} = \frac{\partial\omega}{\partial k} = \frac{\partial(kC_a)}{\partial k} = \frac{\partial(kC_0)}{\partial k} + (F)\frac{\partial(k\tilde{U})}{\partial k} + (F^2)\frac{\partial(kC_2)}{\partial k} \tag{3.12}$$

The first, $O(F^0)$ term on the right hand side is the usual expression for the current-free

case, given by

$$C_{g0} = \frac{C_0}{2}(1+G); \qquad G = \frac{2kh}{\sinh 2kh} \tag{3.13}$$

The second component on the RHS of (3.12) gives the expression

$$\hat{U} = \tilde{U} + k\frac{\partial \tilde{U}}{\partial k} = (2 - G\cosh 2kh)\tilde{U} + \frac{4k^2}{\sinh 2kh}\int_{-h}^{0}(h+z)U(z)\sinh 2k(h+z)\,dz \tag{3.14}$$

which clearly differs from the apparent phase speed correction $\tilde{U}$ at $O(F)$. The remaining term at $O(F^2)$ is derived in sections 3 and 4 for the specific cases studied here.

It is clear that the expression

$$C_{ga} = C_{g0} + \tilde{U} \tag{3.15}$$

suggested for use by a number of authors, does not represent a consistent approximation for the current component of the group velocity at $O(F)$. This point was made in the original study of Kirby & Chen (1989), and we re-examine that conclusion in the context of two cases in 3.3 and 3.4. The result that $\hat{U}$ rather than $\tilde{U}$ is the correct leading-order estimate of current velocity for use in the wave action equation is the first main point of this study.

In the following sections, the validity of the first and second order perturbation approximation will be examined for two cases; (1) a linear shear current, where the analytical dispersion relation has been obtained from the Rayleigh equation by Thompson (1949), and (2) a current profile measured at the mouth of the Columbia River (Kilcher & Nash, 2010), where a numerical solution is found using a shooting method described in Dong & Kirby (2012).

3.3 Wave on a current with constant shear

The linear problem for waves riding on a horizontally-uniform current with constant vertical shear has an exact solution. For the case of co-linear wave and

current flow, the wave motion is described by a potential, and no vorticity is developed at the wave frequency (Thompson, 1949). Maïssa *et al.* (2016) examine the resulting expressions for group velocity in the co-linear case without and with surface tension, and consider blocking conditions for waves on an opposing stream, corresponding to the limit $C_{ga} \to 0$. For the case of waves propagating at an angle to the current direction, Constantin (2011) and others have shown that a flow with constant vorticity and irrotational wave motion does not exist. Ellingsen (2016) points out that this result simply implies that the waves are then described by a rotational flow with vorticity fluctuating at wave frequency. The resulting problem is completely described by (3.6) with additional work needed to develop an expression for the vorticity. Ellingsen (2016) considers the case of deep water and develops expressions for the resulting horizontal vorticity; the extension to finite water depth is described by DK16; see section 3.1.2.

We limit attention here to the co-linear case and let

$$U(z) = U_s + \Omega z = U_s(1 + \alpha \frac{z}{h}) \tag{3.16}$$

where U_s is the surface velocity, Ω is the constant current shear and α is the current shear parameter defined in (3.4). The exact dispersion relation, written in terms of the phase speed relative to surface velocity $C_{rs} = C_a - U_s$, is given by (Thompson, 1949)

$$C_{rs}^2 = (gh - \alpha U_s C_{rs}) \frac{\tanh kh}{kh} \tag{3.17}$$

The exact expression for the absolute group velocity $C_{ga}^e = \partial\omega/\partial k$ is found from (3.17) to be

$$C_{ga}^e = U_s + \left(\frac{g(1+G) - (\alpha U_s/h) C_{rs} G}{2g - (\alpha U_s/h) C_{rs}} \right) C_{rs} \tag{3.18}$$

Introducing the Froude number $F = U_s/\sqrt{gh}$, we normalize the group velocity and phase speed by $(gh)^{1/2}$ and obtain

$$\frac{C_{ga}^e}{\sqrt{gh}} = C_{ga}^{e*} = F + \frac{(1+G) - \alpha F G C_{rs}^*}{2 - \alpha F C_{rs}^*} C_{rs}^* \tag{3.19}$$

where $C^*_{rs} = C_{rs}/\sqrt{gh}$. Using (3.17) leads to

$$C^*_{rs} = \frac{1}{2}(\sqrt{4\mu + \alpha^2 F^2 \mu^2} - \alpha\mu F) \tag{3.20}$$

with μ defined as

$$\mu = \frac{\tanh kh}{kh} \tag{3.21}$$

Turning to the perturbation solution of Kirby & Chen (1989), we obtain results to $O(F^2)$ and compare them to the full solution to determine their range of validity. The dimensionless $O(1)$ phase speed and group velocity are given by

$$C^*_0 = \sqrt{\mu}; \quad C^*_{g0} = \frac{1}{2}\sqrt{\mu}(1+G) \tag{3.22}$$

At $O(F)$, the depth weighted current $\tilde{U}$ and it's derivative with respect to k are given in dimensionless form by

$$\tilde{U}^* = \frac{\tilde{U}}{\sqrt{gh}} = F(1 - \alpha\frac{\mu}{2}); \quad \frac{\partial \tilde{U}^*}{\partial k} = \alpha\frac{F}{2}\frac{\mu}{k}(1-G) \tag{3.23}$$

giving a leading order current contribution to the group velocity

$$\hat{U}^* = \frac{\hat{U}}{\sqrt{gh}} = F\left(1 - \frac{1}{2}\alpha\mu G\right) \tag{3.24}$$

Finally, at $O(F^2)$, the correction to the phase speed is given by

$$C^*_2 = \frac{1}{8}\alpha^2 F^2 \mu^{3/2} \tag{3.25}$$

The $O(F^2)$ correction to the group velocity is then

$$C^*_{g2} = \frac{1}{\sqrt{gh}}\frac{\partial(kC_2)}{\partial k} = \frac{1}{16}F^2\alpha^2\mu^{3/2}(3G-1) \tag{3.26}$$

The results for the complete expressions for group velocity are collected here for convenience:

$$Exact \qquad C^{e*}_{ga} = F + \frac{(1+G) - \alpha F G C^*_{rs}}{2 - \alpha F C^*_{rs}} C^*_{rs} \tag{3.27a}$$

$$O(F) \qquad \tilde{C}^*_{ga} = \frac{1}{2}\sqrt{\mu}(1+G) + F\left(1 - \frac{1}{2}\alpha\mu G\right) \tag{3.27b}$$

$$O(F^2) \qquad \tilde{C}^*_{ga} = \frac{1}{2}\sqrt{\mu}(1+G) + F\left(1 - \frac{1}{2}\alpha\mu G\right) + \frac{1}{16}F^2\alpha^2\mu^{3/2}(3G-1) \tag{3.27c}$$

It may be verified after some tedious algebra that the resulting expression $\tilde{C}^*_{ga}$ agrees with the expansion of the exact result (3.27a) truncated at either $O(F)$ or $O(F^2)$ as desired. The perturbation solution is thus consistent with the full solution to the order considered, with a clear indication that the commonly used $\tilde{U}$ is not the correct advection velocity to use in the wave action equation.

3.3.1 Following currents $F > 0$

The results for the first and second order perturbation solutions expressed in (3.27) are compared to the full theory in Figure 3.2 for various choices of α and for $F > 0$, corresponding to currents flowing in the direction of wave propagation. (Values of $0 \leq |F| \leq 1$ and $0 \leq \alpha \leq 1$ represent variation from weak to strong current and weak to strong shear, respectively. The values here are chosen purely for example). Both the first and second order perturbation solutions are quite good approximations to the full solution, with little indication that there is a need to use the $O(F^2)$ correction in practice.

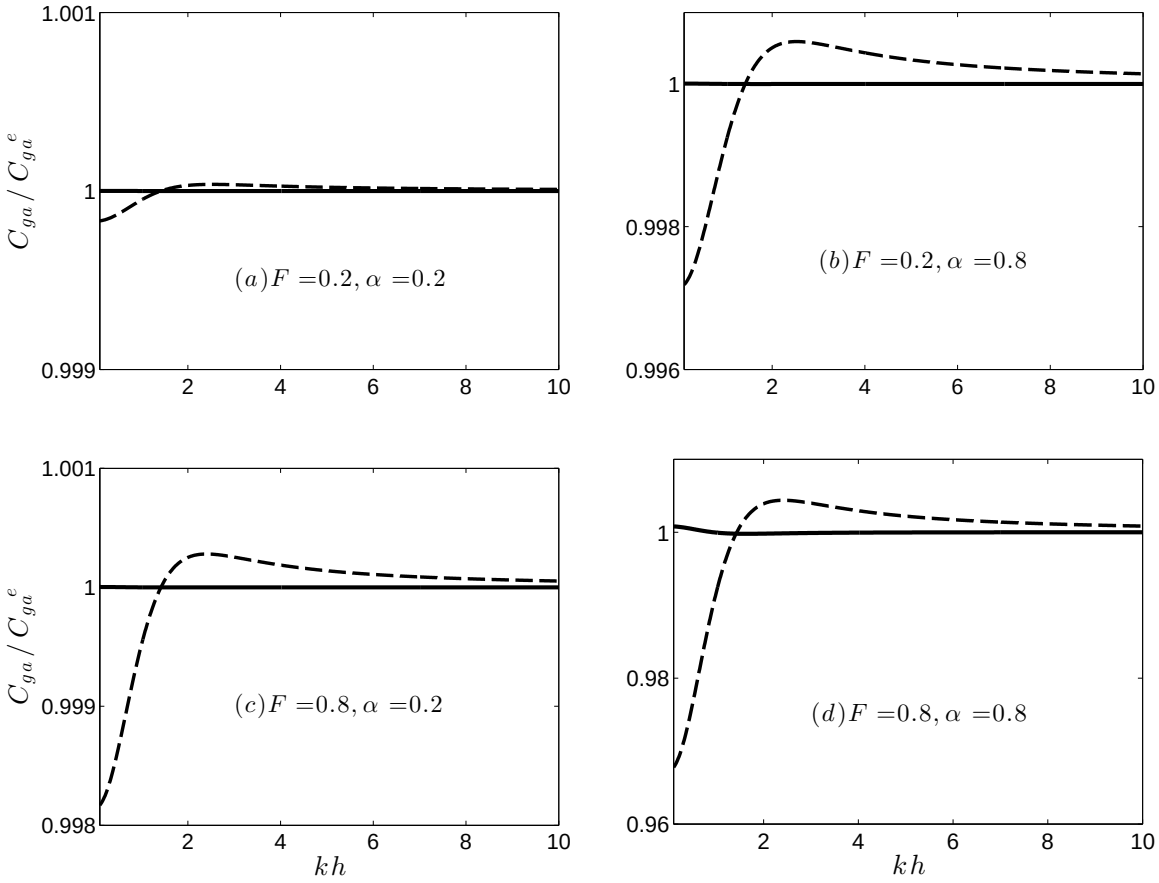

Figure 3.2: Wave group velocity comparison C_{ga}/C_{ga}^{e} vs relative depth kh: linear shear current. Solid lines indicate $O(F^2)$ approximation; dashed lines indicate $O(F)$ approximation.

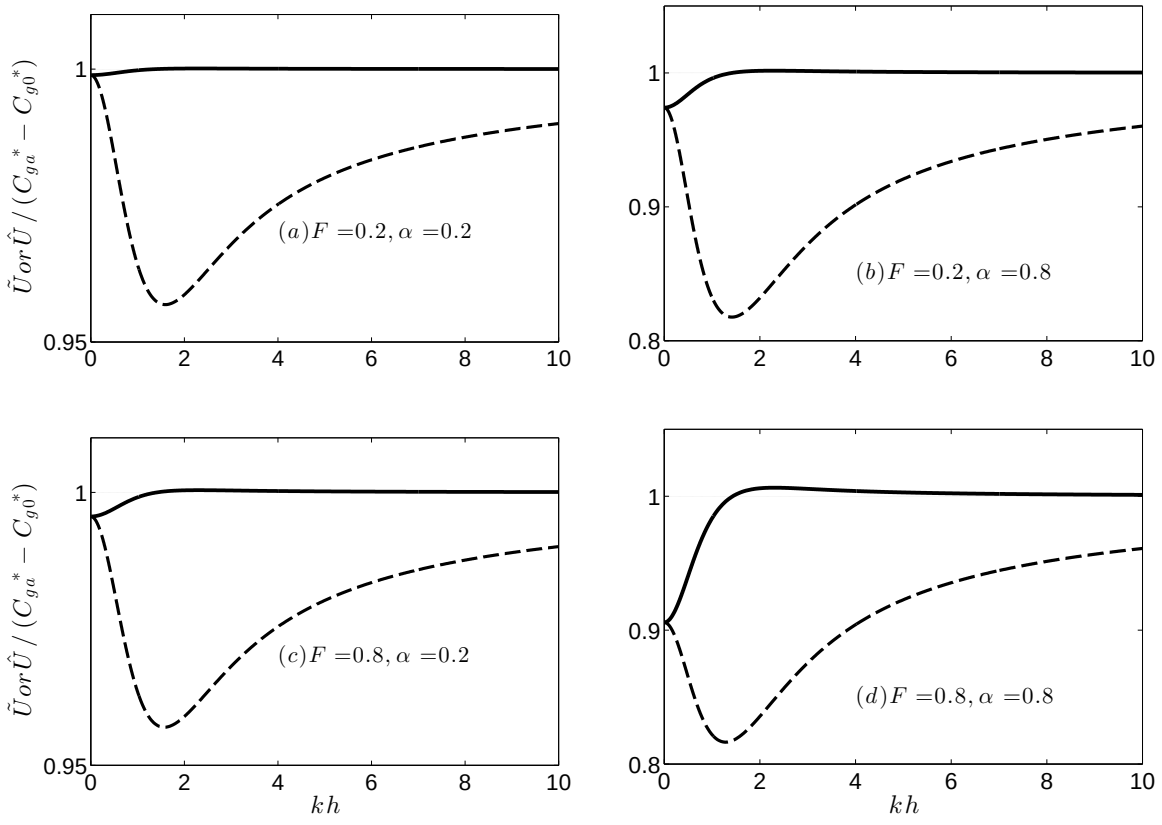

Figure 3.3: Ratio of first order approximations $\tilde{U}$ and $\hat{U}$ to the second order correction $(\hat{U}^* + C^*_{g2})$ for various choices of current shear α and Froude number F. Solid lines are for the consistent $O(F)$ contribution $\hat{U}^*$, while dashed lines are for the depth weighted current $\tilde{U}^*$, used inconsistently as the current component of the group velocity.

Figure 3.3 compares the first order approximations $\tilde{U}^*$ and $\hat{U}^*$ to the second order correction $(\hat{U}^* + C^*_{g2})$ for various choices of α and F. It can be seen that, as the current becomes more sheared, the error of neglecting the term $k\partial\tilde{U}/\partial k$ increases.

3.3.2 Opposing currents $F < 0$ and blocking

For the case of an opposing current with $F < 0$, the group velocity of the wave train is decreased by the current. When the current becomes strong enough to reduce the group velocity to zero (or $C_{ga} \to 0$), wave blocking occurs and waves are unable to transport energy in the direction of propagation. Results for the case of constant shear

are discussed in Maïssa *et al.* (2016). We investigate the validity of the perturbation solution in predicting the blocking current speed by setting the absolute group velocity to zero in each expression in (3.27). Using the exact expression (3.27a), we obtain the following nonlinear equation for blocking of waves

$$F^2\left(\alpha {C^*}_{rs}\right) + F\left(\alpha G {C^*_{rs}}^2 - 2\right) - (1+G)C^*_{rs} = 0 \tag{3.28}$$

which is solved numerically in MATLAB. The long wave limit for the exact solution is given by

$$kh \to 0: \qquad F_b = \frac{-1}{(1-\alpha)^{1/2}} \tag{3.29}$$

which is singular for $\alpha = 1$, where the current speed is reduced to zero at the bottom. This singularity results from the linearization of the problem with respect to the wave motions. A more complete examination of the critical Froude number F_c in a hydraulic flow with constant vertical shear yields the result $F_c = -1/(1-\alpha+\alpha^2/12)^{1/2}$, where criticality corresponds to blocking of upstream propagation of information by infinitesimal waves.) The $O(F)$ approximation, obtained from (3.27b), is given by

$$F_b = \frac{\mu^{1/2}(1+G)}{(\alpha\mu G - 2)} \tag{3.30}$$

with long wave asymptote $F_b = -1/(1-\alpha/2)$. This long wave limit is a valid leading order estimate for the exact result (3.30) only in the limit of small shear α; the source of this additional restriction is not immediately clear in the context of the small F restriction in the perturbation solution. It is noted that a re-ordering of the problem (3.6) to allow for $O(1)$ current speeds but with a small shear restriction recovers the same perturbation series to the order given here, and thus the small shear limitation is perhaps a better interpretation in the context of the large F values associated with blocking.

Results for the first order approximation are shown in Figure 3.4 in comparison to the full theory. Exact and $O(F)$ approximate solutions for the blocking current

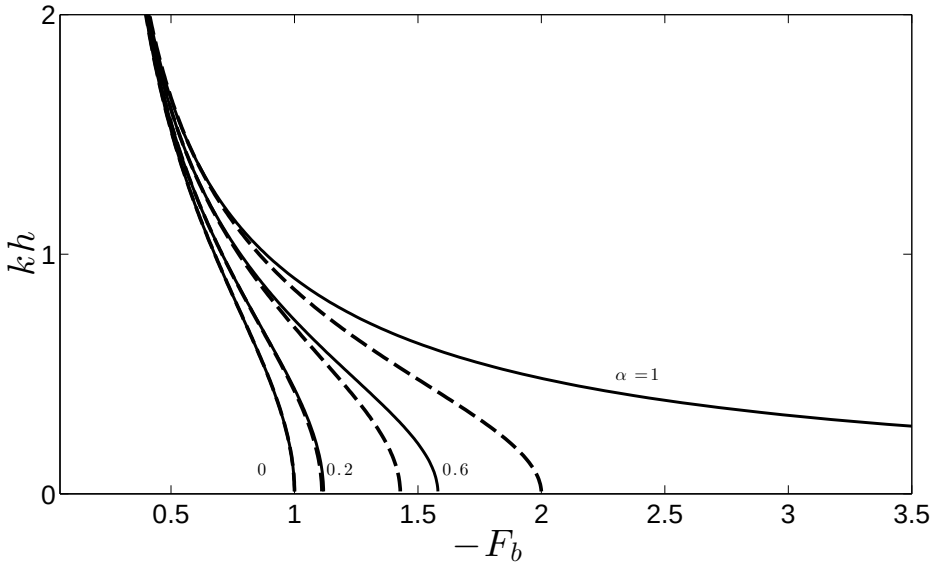

Figure 3.4: Blocking current Froude number vs corresponding relative depth kh for various choices of current shear α. (Solid lines) exact solution, (dashed lines) $O(F)$ approximation.

speed show significant deviations for values of $kh < 1$. For small values of α, (3.30) may be approximated by $F_b = -1/(1 - \alpha/2)$, in agreement with the perturbation solution.

At $O(F^2)$, solving the quadratic equation for F_b resulting from (3.27c) gives the expression

$$F_b = \frac{-B + [B^2 - 4AC]^{1/2}}{2A} \tag{3.31}$$

with

$$A = \alpha^2 \mu^{3/2}(3G - 1); \quad B = 16\left(1 - \frac{1}{2}\alpha\mu G\right); \quad C = 8\mu^{1/2}(1 + G) \tag{3.32}$$

Real-valued solutions for F_b only exist for positive values of the discriminant $B^2 - 4AC$. Since μ and G are both functions of kh, it is simpler to solve the equation $B^2 = 4AC$

for a critical shear α_c as a function of kh; doing so gives

$$\alpha_c = \frac{4\left[\left(\frac{3}{2}G^2 - G - \frac{1}{2}\right)^{1/2} - G\right]}{\mu\left(G^2 + 2G - 1\right)} \tag{3.33}$$

Using (3.33) in (3.31) then gives a critical blocking Froude number F_{bc} for each kh, given by

$$F_{bc} = \frac{-B}{2A} = -\frac{8\left(1 - \frac{1}{2}\alpha_c\mu G\right)}{\alpha_c^2\mu^{3/2}(3G-1)} \tag{3.34}$$

with the $O(F^2)$ solution for blocking breaking down for $\alpha > \alpha_c$ at each kh. The long wave results are given by

$$kh \to 0: \qquad \alpha_c = 2(\sqrt{2}-1) \approx 0.828; \qquad F_{bc} = -(2+\sqrt{2}) \approx -3.414 \tag{3.35}$$

with the solution breaking down at smaller current speeds with increasing kh and α, as indicated by the dash-dot curve in Figure 3.5.

Figure 3.6 compares the first and second order perturbation solutions to the exact solution for various choices of $F < 0$ and α. The solutions are compared for a range of kh values corresponding to unblocked waves range before the waves are blocked by the current. Both first and second order perturbation solutions are accurate predictors of group velocity for current speeds up to the blocking condition when shear α is small; however, as indicated above, the approximations become weak for long waves and values of dimensionless shear much in excess of $\alpha = 0.5$.

3.4 Columbia River velocity profile

In this section we compare the group velocities obtained from different approximations using a measured current profile from the mouth of the Columbia River (MCR). The Columbia River is well known for it's large freshwater discharge and the resulting development of a rapidly moving, buoyant plume during ebb tide conditions. Here, we select a sample velocity profile collected by a pole-mounted ADCP during the RISE (River Influences on Shelf Ecosystems) project (Kilcher & Nash, 2010). The profile,

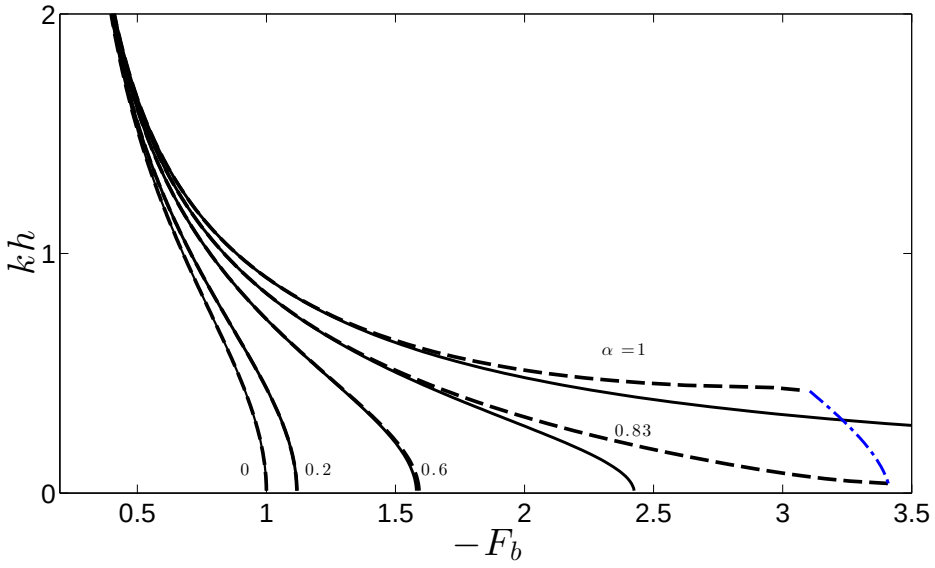

Figure 3.5: Blocking current Froude number F_b vs corresponding relative depth kh for various choices of current shear α. Solid lines show the exact solution, dashed lines are the $O(F^2)$ approximation. The dash-dot line shows the locus of F_{bc} values where the second order solution breaks down, as indicated in (3.31).

shown in Figure 3.7, represents a maximum ebb condition for the time frame covered by the file. The normalized shear parameter for this current profile is $\alpha \sim 8$ which indicates a strongly sheared current.

We consider the idealized case of wave propagating landward against the opposing current at Columbia river mouth. We follow a general procedure of fitting polynomials to either measured profiles or profiles taken from gridded model results in order to establish a basis for computing weighted current values. Expressions below are based on the form

$$U(z) = U_s \sum_{n=0}^{N} a_n (\frac{z}{h})^n \tag{3.36}$$

with current speed referenced to the surface value U_s and with dimensionless a_n's. The relative depth is assumed to be varying between $kh \sim 0.5$ to $kh \sim 3$. Calculations here are carried out using $N = 6$, with the fitted profile for the demonstration case also shown in Figure 3.7. Results for expressions for $\tilde{U}$, $\hat{U}$, C_2 and C_{g2} resulting

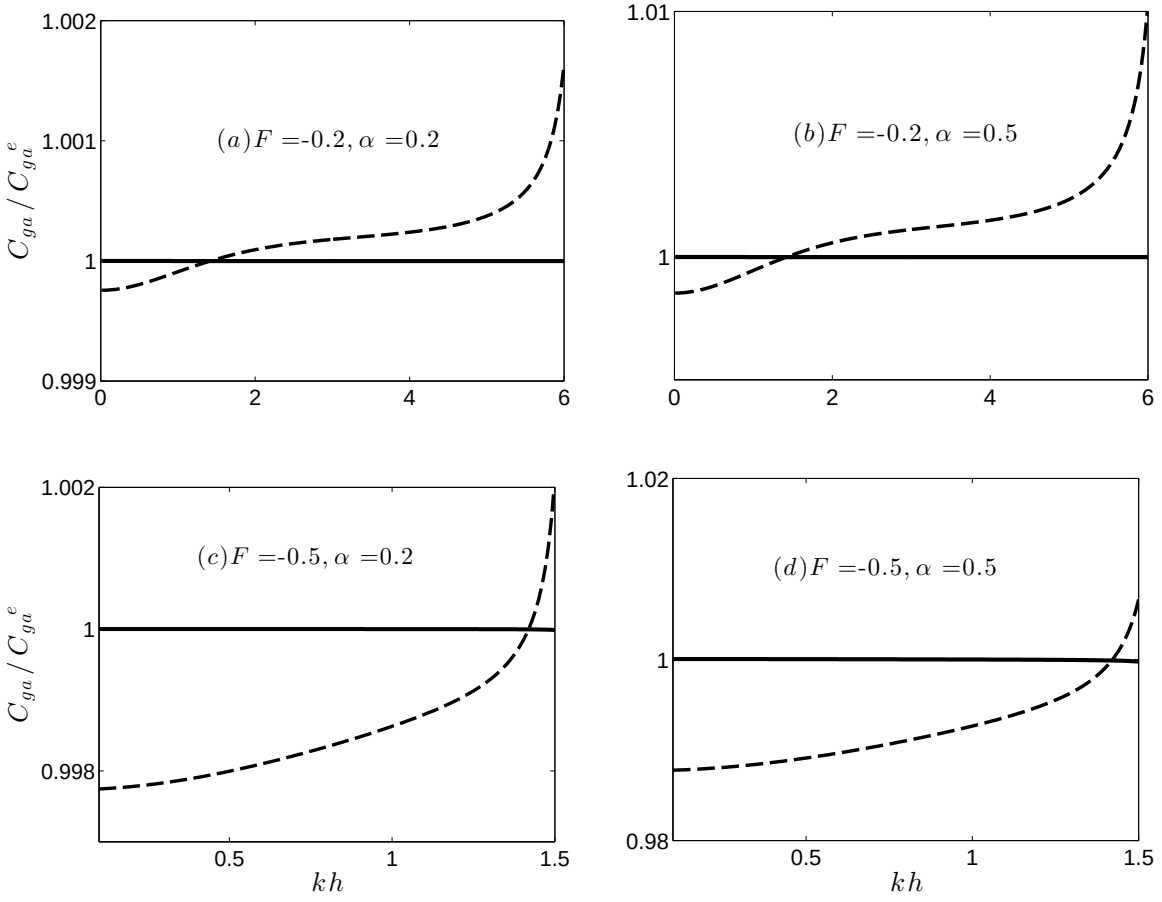

Figure 3.6: Wave group velocity comparison C_{ga}/C_{ga}^{e} vs relative depth kh for various choices of current shear α and Froude number F. Solid lines are $O(F^2)$ approximation and dashed lines are the $O(F)$ approximation.

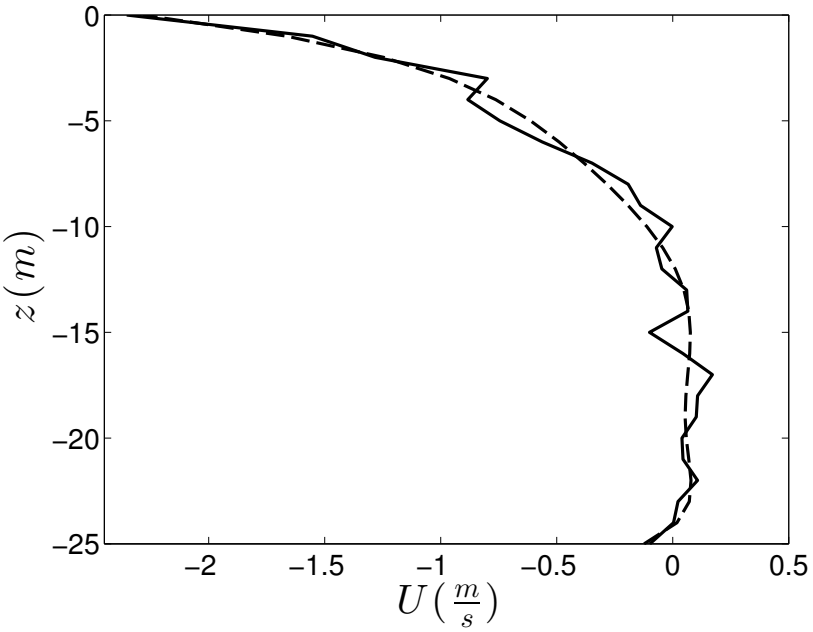

Figure 3.7: Columbia River current profile during ebb tide. Solid line is measured data (Kilcher & Nash, 2010) and the dashed line is a 6th order polynomial fit to the data.

from evaluating the perturbation solutions after introducing the expansion (3.36) are presented in Appendix A.

3.4.1 Numerical solution

In the absence of an analytic solution for the original problem (3.6), a numerical method is used to solve the Rayleigh equation. We first introduce normalized vertical shape functions $L(z) = \sigma(z)/\sigma_s$ for the relative frequency and $f(z) = \tilde{w}/(-i\sigma_s a)$, where a is wave amplitude. (3.6) becomes

$$\begin{aligned} f'' - (k^2 + \frac{L''}{L})f &= 0; \quad -h \le z \le 0 \\ f &= 0; \quad z = -h \\ f' &= (L' + \frac{gk^2}{\sigma_s^2})f; \quad z = 0 \end{aligned} \tag{3.37}$$

We then introduce a non-dimensional vertical coordinate $\hat{z} = z/h$ following

Fenton (1973) and define a new dependent variable

$$Q(\hat{z}) = \frac{f}{hf'} \tag{3.38}$$

The problem is then reduced to a Riccati equation

$$\begin{aligned} \frac{dQ}{d\hat{z}} =& 1 - \gamma^2 Q^2; \quad -1 \leq \hat{z} \leq 0; \\ \gamma^2(\hat{z}) =& (kh)^2 + \frac{L''}{L} \\ Q =& \frac{\sigma_s^2}{(gk^2h + L'\sigma_s^2)}; \quad \hat{z} = 0; \\ Q =& 0; \quad \hat{z} = -1 \end{aligned} \tag{3.39}$$

The Riccati equation is solved using a shooting method (Fenton, 1973; Kirby & Chen, 1989; Dong & Kirby, 2012), with the absolute frequency ω determined from the value of $Q(0)$. We then calculate the derivative of the absolute frequency w/r k using a central difference method to evaluate the group velocity C_{ga}^n numerically.

$$C_{ga}^n = \frac{\partial \omega}{\partial k} \approx \frac{\omega(k + \Delta k) - \omega(k - \Delta k)}{2\Delta k} \tag{3.40}$$

3.4.2 Comparison of numerical and perturbation results

Using the expressions in Appendix A, group velocity comparisons based on first and second order perturbation approximations are shown in Figure 3.8. The perturbation solutions are seen to be fairly good approximations. Figure 3.9 compares the incorrect first order approximation $\tilde{U}$ and the consistent first order approximation $\hat{U}$ to the second order correction $(\hat{U} + C_{g2})$. The neglected term $k\partial\tilde{U}/\partial k$ is shown to be as big as 40% of the second order perturbation correction, indicating the magnitude of the error involved in using $\tilde{U}$ instead of $\hat{U}$ as the estimate for current velocity in the wave model. At the same time, $\hat{U}$ provides a fairly accurate estimate of the current component of the group velocity when compared to the higher order $O(F^2)$ result.

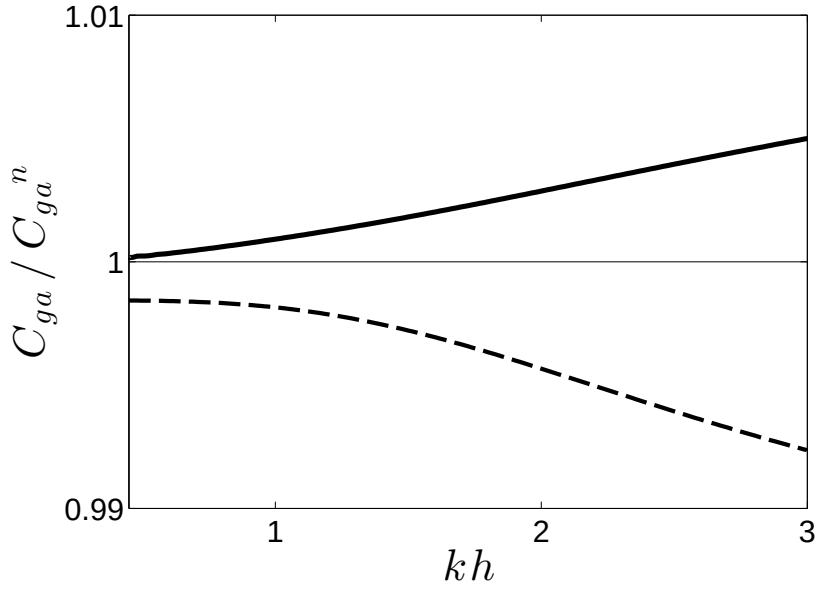

Figure 3.8: Wave group velocity comparison $C_{ga}/{C_{ga}}^{n}$ vs relative depth kh: Mouth of Columbia River (MCR). Solid line indicates $O(F^2)$ approximation and dashed line indicates $O(F)$ approximation.

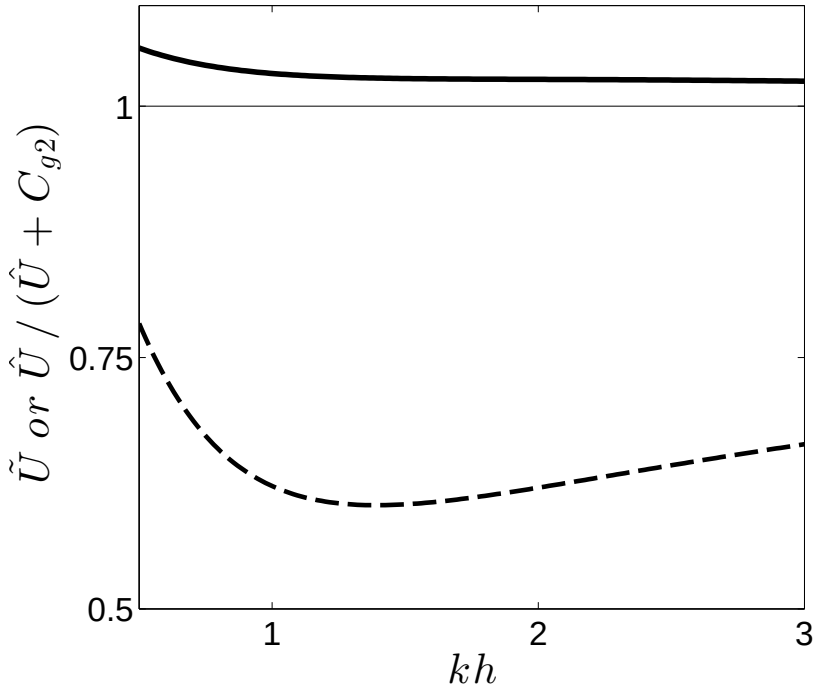

Figure 3.9: Ratio of first order approximations $\tilde{U}$ and $\hat{U}$ to the second order correction $(\hat{U}+C_{g2})$: Mouth of Columbia River (MCR). Solid line is $\hat{U}$ and dashed line is $\tilde{U}$

3.5 Common approximations in modeling

Choices for current values to be used in evaluating current effects on waves have historically included depth-averaged current $\overline{U}$ or surface current U_s. More recently, as discussed above, several investigators have suggested using the depth-weighted current $\tilde{U}$ as the choice for effective current (van der Westhuysen & Lesser, 2007; Ardhuin *et al.*, 2008; Warner *et al.*, 2010). Lesser (2009) introduced the procedure of using a single value $\tilde{U}(k_p)$ instead of the frequency dependent $\tilde{U}(k)$ to represent the current used for all frequency-directional components, where k_p is the wavenumber at peak frequency; this procedure is included as an option in Delft-3D (Lesser, 2009); see also discussions in Elias *et al.* (2012). The approach has also been introduced in ROMS (Warner *et al.*, 2010).

As has been mentioned above, direct use of $\tilde{U}$ as a replacement for depth averaged velocity incurs an error of $O(F)$ in action flux conservation. In this section, we examine the limitations of these approximations for both the analytic and numerical cases considered above. We also consider a fourth choice of $\hat{U}(k_p)$, the correct estimate of the advective current component to $O(F)$, but evaluated only at the peak frequency. We assume that the spectrum is narrow banded in the sense that $|k - k_p| \,/\, k_p \ll 1$ for any k within the energetic part of the spectrum and also select three peak wave numbers corresponding to $k_p h = 1, 2$ and 3. Figures 3.10, 3.11 and 3.12 compare the validity of these approximations for the linear shear current, while Figures 3.13,3.14 and 3.15 show the same comparison for the MCR current profile. It can be seen that although the depth weighted current $\tilde{U}(k_p)$ gives a better approximation compared to the choice of depth-average or surface current, the effect of neglecting the term $k\partial\tilde{U} \,/\, \partial k$ can still cause significant errors even at the peak frequency. It should also be noted that, despite the fact that $\hat{U}(k_p)$ is a more fundamentally accurate choice near the spectral peak, it still produces a comparable rate of deviation between modeled and true group velocity estimates with increasing Δk. This would indicate the potential need to represent frequency dependence in $\hat{U}$ in applications to broad-banded frequency spectra, unless a more advantageous strategy can be developed using values

computed at the peak frequency alone. We explore such an extension in the following section.

3.6 An improved approximation based on Taylor expansion about k_p

The comparisons of the group velocity approximations in previous sections have indicated that significant errors may be incurred by neglecting either the contribution of the term $k\partial\tilde{U}/\partial k$ to the group velocity at $O(F)$ or the wavenumber dependence of $\hat{U}$. For the remainder of this discussion, it should be clear that we advocate the use of the velocity $\hat{U}$ in place of $\tilde{U}$ in any coupled wave-current modeling system. In this section, we describe a possible strategy for additionally recovering wavenumber dependence in $\hat{U}$ using only values calculated at the peak wavenumber k_p, thereby minimizing the amount of additional information to be passed from the circulation model to the wave model.

The Taylor expansion of $\hat{U}(k)$ about the peak wavenumber k_p is given to leading order by

$$\hat{U}(k) = \hat{U}(k_p) + \frac{d\hat{U}}{dk}\Big|_{k_p}(\Delta k) + O(\Delta k^2) \tag{3.41}$$

$$\Delta k = k - k_p \tag{3.42}$$

Using the relation between $\hat{U}$ and $\tilde{U}$ indicated in (3.14), we obtain

$$\begin{aligned}\hat{U}(k) &= \tilde{U}(k_p) + k_p\frac{\partial\tilde{U}}{\partial k}\Big|_{k_p} + \Delta k\left[\frac{\partial\tilde{U}}{\partial k}\Big|_{k_p} + \frac{\partial\tilde{U}}{\partial k}\Big|_{k_p} + k\frac{\partial^2\tilde{U}}{\partial k^2}\Big|_{k_p}\right] + O(\Delta k)^2 \\ &= \tilde{U}(k_p) + \frac{\partial\tilde{U}}{\partial k}\Big|_{k_p}[2k - k_p] + k_p\frac{\partial^2\tilde{U}}{\partial k^2}\Big|_{k_p}\Delta k + O(\Delta k)^2 \end{aligned} \tag{3.43}$$

To $O(\Delta k)$, the group velocity is then given by

$$C_{ga} = \frac{C_0}{2}(1+G) + \hat{U}(k) \tag{3.44}$$

This procedure retains the effect of the wavenumber dependence of $\tilde{U}$ but requires the

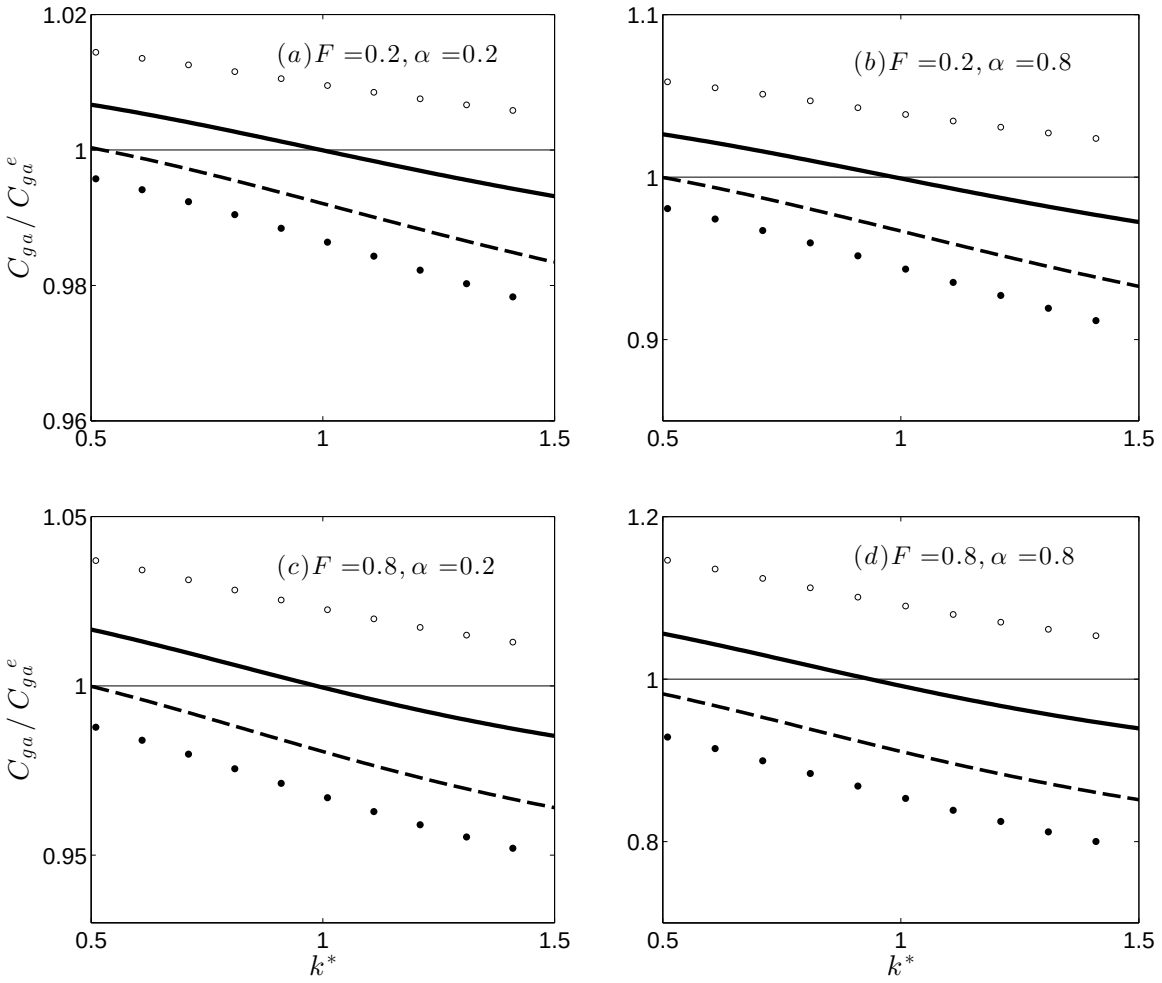

Figure 3.10: Wave group velocity comparison $C_{ga}\,/\,C^e_{ga}$ vs normalized wave number $k^* = k/k_p$, with $k_p h = 1$: linear shear flow. Solid lines are using $\hat{U}(k_p)$, dashed lines are based on $\tilde{U}(k_p)$, dots indicate the depth averaged approximation and the circles are only using the surface value U_s.

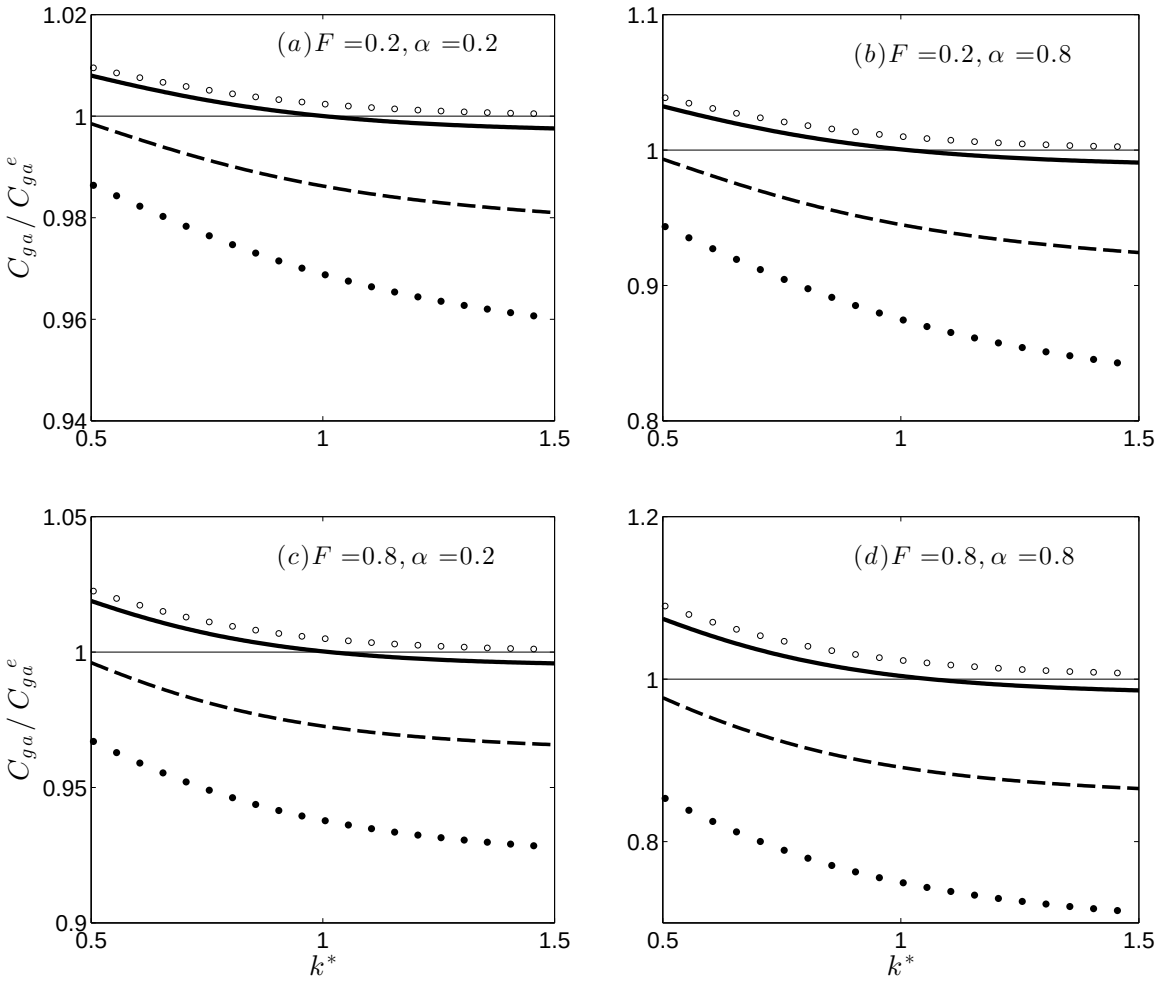

Figure 3.11: Wave group velocity comparison $C_{ga}\,/\,C^e_{ga}$ vs normalized wave number $k^* = k/k_p$, with $k_p h = 2$: linear shear flow. Solid lines are using $\hat{U}(k_p)$, dashed lines are based on $\tilde{U}(k_p)$, dots indicate the depth averaged approximation and the circles are only using the surface value U_s.

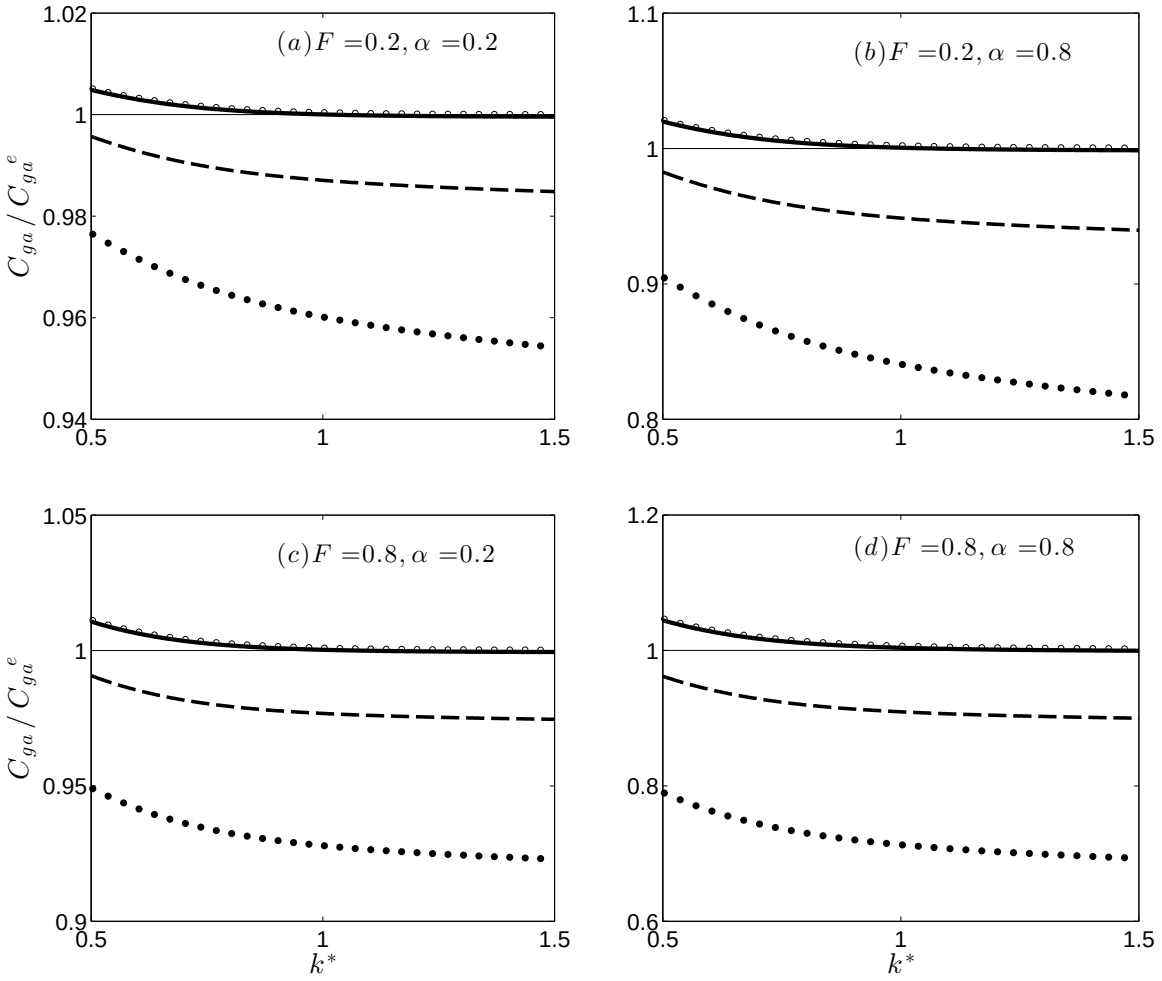

Figure 3.12: Wave group velocity comparison $C_{ga}\,/\,C^e_{ga}$ vs normalized wave number $k^* = k/k_p$,with $k_p h = 3$: linear shear flow. Solid lines are using $\hat{U}(k_p)$, dashed lines are based on $\tilde{U}(k_p)$, dots indicate the depth averaged approximation and the circles are only using the surface value U_s.

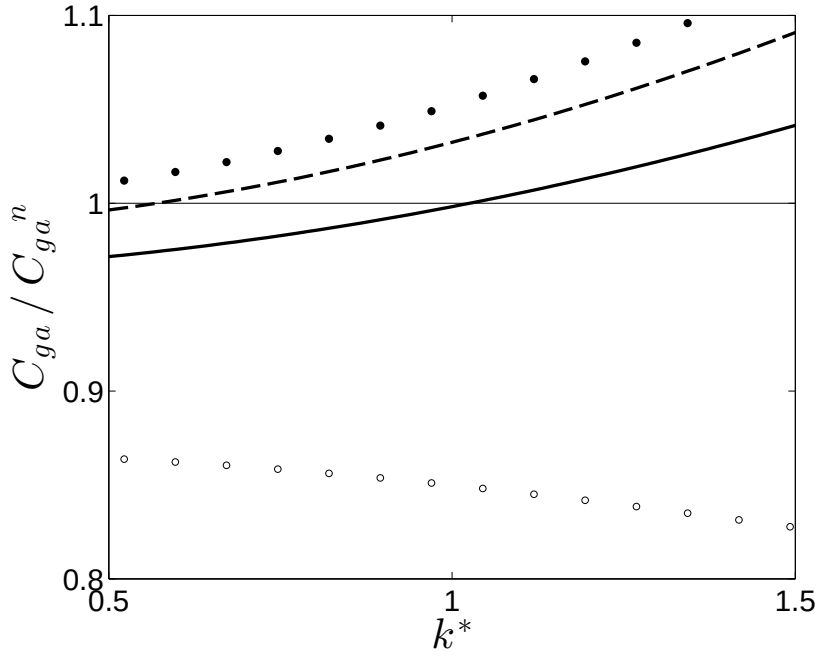

Figure 3.13: Wave group velocity comparison $C_{ga}\,/\,C_{ga}^{n}$ vs normalized wave number $k^* = k/k_p$,with $k_p h = 1$: MCR velocity profile. Solid lines are using $\hat{U}(k_p)$, dashed lines are based on $\tilde{U}(k_p)$, dots indicate the depth averaged approximation and the circles are only using the surface value U_s.

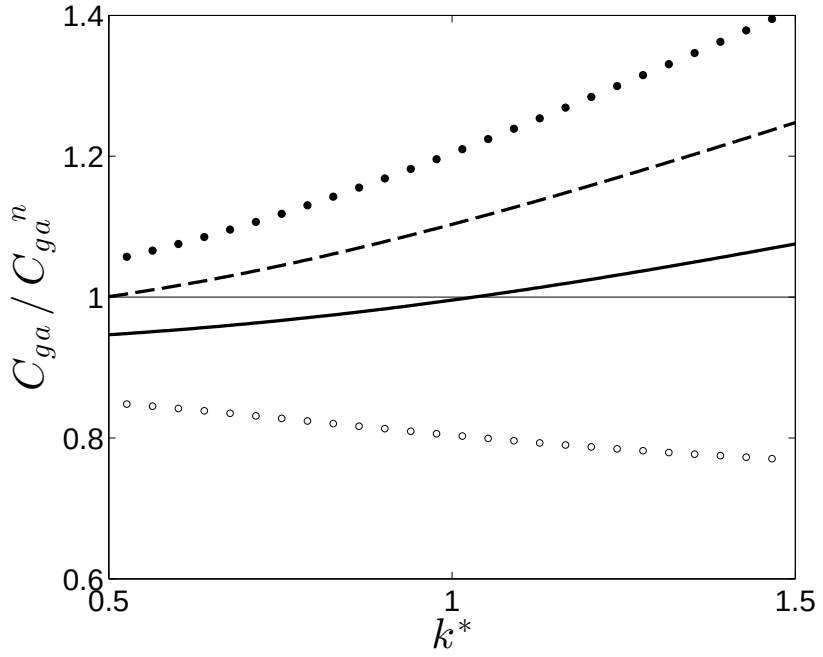

Figure 3.14: Wave group velocity comparison $C_{ga}\ /\ C_{ga}^{n}$ vs normalized wave number $k^* = k/k_p$,with $k_p h = 2$: MCR velocity profile. Solid lines are using $\hat{U}(k_p)$, dashed lines are based on $\tilde{U}(k_p)$, dots indicate the depth averaged approximation and the circles are only using the surface value U_s.

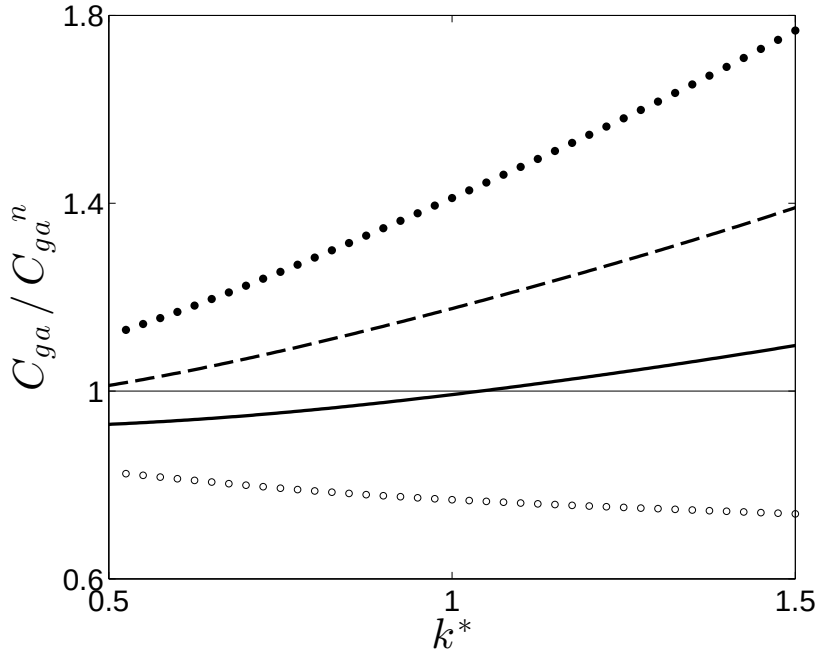

Figure 3.15: Wave group velocity comparison $C_{ga}\,/\,C_{ga}^{n}$ vs normalized wave number $k^* = k/k_p$, with $k_p h = 3$: MCR velocity profile. Solid lines are using $\hat{U}(k_p)$, dashed lines are based on $\tilde{U}(k_p)$, dots indicate the depth averaged approximation and the circles are only using the surface value U_s.

passage of only one or two additional coefficients to the wave model, depending on whether expressions based on $\hat{U}$ or $\tilde{U}$ are employed. The extra data can then be used in the wave model to compute frequency and direction-dependent current values for use with each component wave.

The accuracy of the approximation is compared to prediction of group velocity using $\hat{U}(k)$ evaluated only at the peak wavenumber as

$$\hat{U}(k_p) = \tilde{U}(k_p) + k_p \frac{\partial \tilde{U}}{\partial k}\Big|_{k_p} \tag{3.45}$$

For the linear shear case, the Taylor series coefficients are given by

$$\begin{aligned} \frac{\partial \tilde{U}}{\partial k} &= \alpha \frac{U_s}{2} \frac{\mu}{k}(1 - G) \\ \frac{\partial^2 \tilde{U}}{\partial k^2} &= \alpha \frac{U_s}{2} \frac{\mu}{k^2}[G^2(\cosh 2kh - 1) + 2G - 2] \end{aligned} \tag{3.46}$$

For the numerical case, the first two derivatives of $\tilde{U}$ are obtained from (A.9) and (A.27).

Comparisons for both analytic and numerical cases are shown in Figures 3.16-3.18 and 3.19 -3.21 for three different cases of $k_p h = 1, 2$ and 3. Considering a narrow-banded spectrum in frequency or wave number, it is seen that the Taylor series approach provides a good estimate of the group velocity while including the first order correction to the group velocity, as explained in (3.9), and evaluating it for just one peak wavenumber shows rapid deviation from the exact solution. The Taylor series approximation could thus be used as the basis for estimating frequency-dependent current values, with the wave model being able to construct a reasonable estimate of the group velocity using a minimal set of additional information.

3.7 Discussion and Conclusions

The main aims of the present work have been to emphasize that the depth-weighted current value $\tilde{U}$ in (3.1) is not the appropriate leading-order estimate for

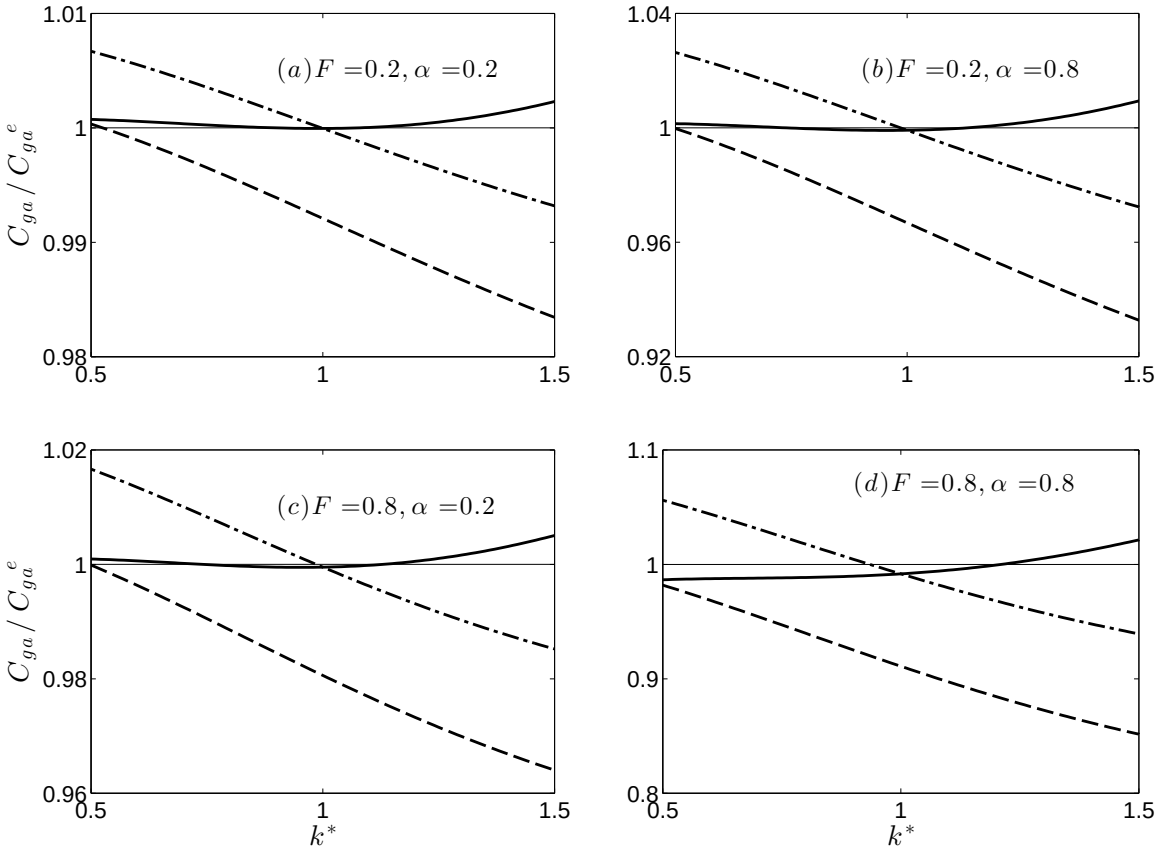

Figure 3.16: Comparison of absolute group velocity $C_{ga}\ / C^e_{ga}$ vs normalized wave number $k^* = k/k_p$,with $k_p h = 1$: linear shear flow. Solid lines are based on the Taylor series expansion of $\hat{U}(k)$ about k_p, dashed-dotted lines are based on $\hat{U}(k_p)$ and dashed line is using $\tilde{U}(k_p)$.

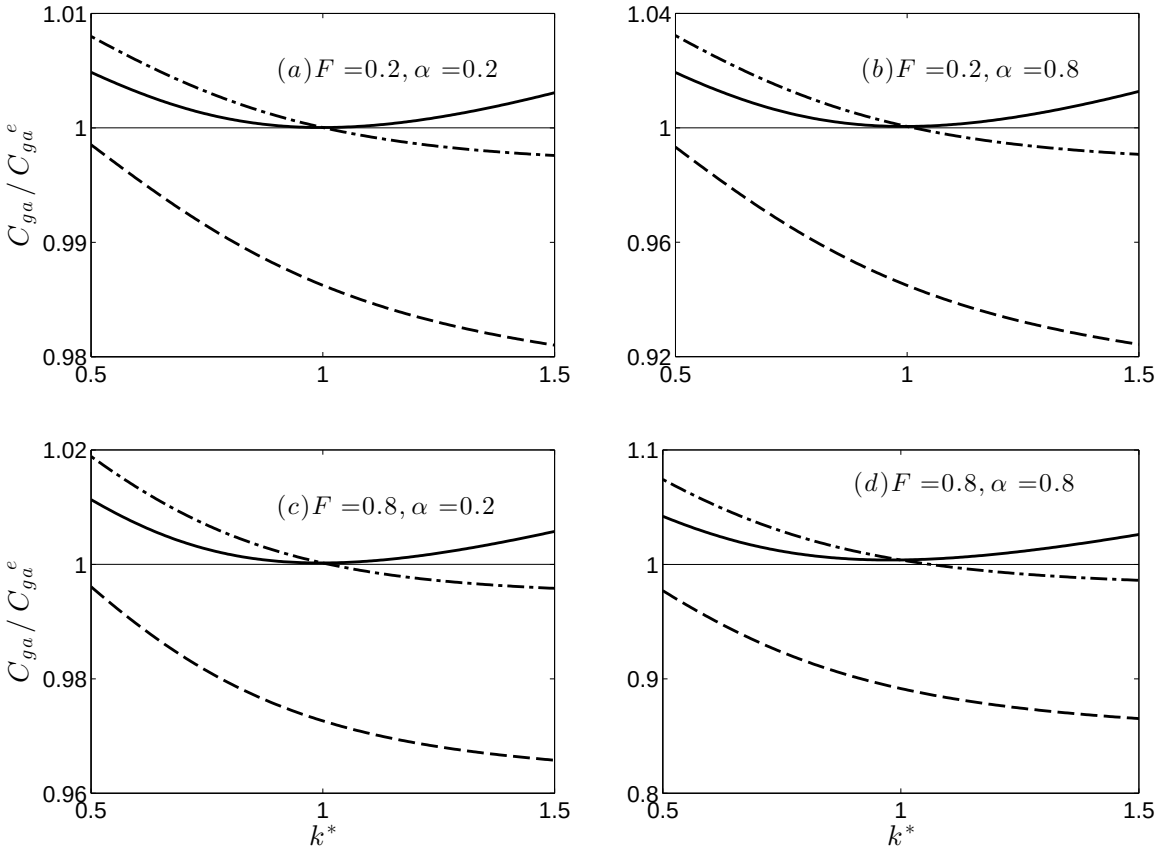

Figure 3.17: Comparison of absolute group velocity $C_{ga}\ / C^e_{ga}$ vs normalized wave number $k^* = k/k_p$,with $k_p h = 2$: linear shear flow. Solid lines are based on the Taylor series expansion of $\hat{U}(k)$ about k_p, dashed-dotted lines are based on $\hat{U}(k_p)$ and dashed line is using $\tilde{U}(k_p)$.

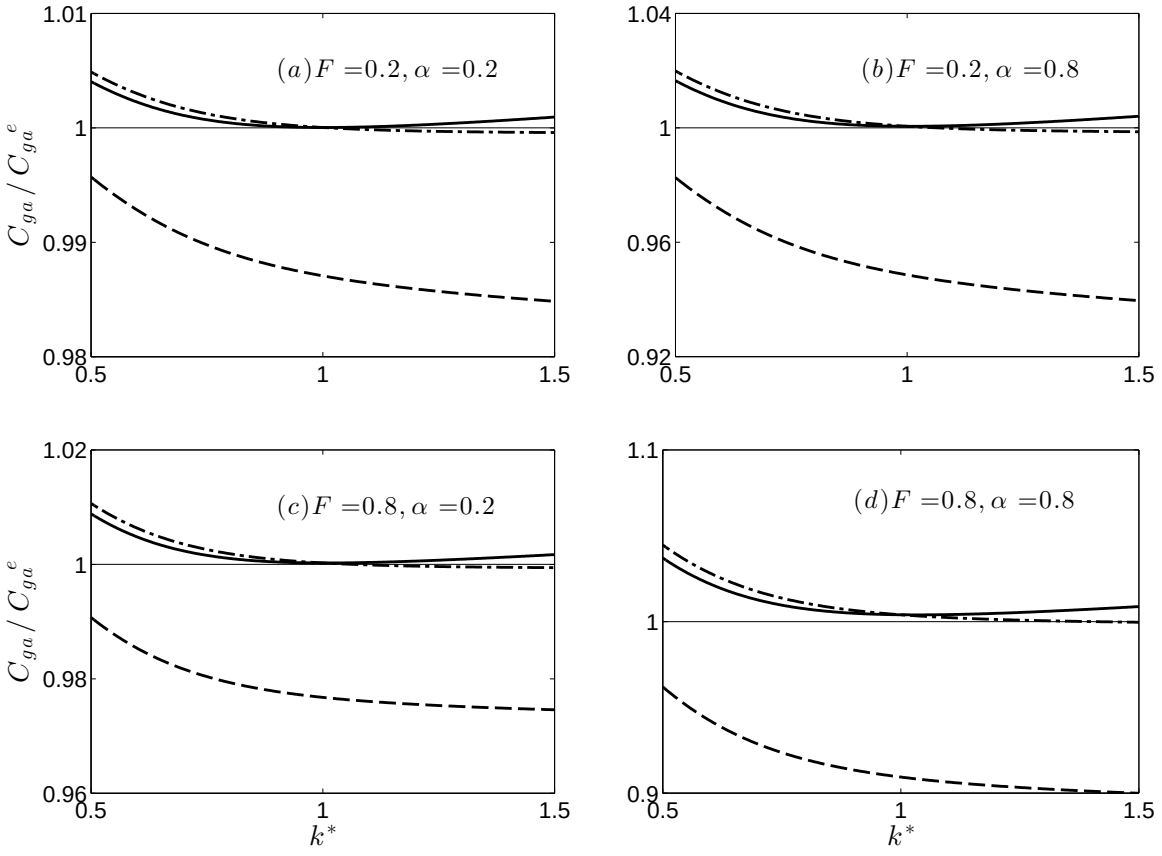

Figure 3.18: Comparison of absolute group velocity $C_{ga}\ / C^e_{ga}$ vs normalized wave number $k^* = k/k_p$,with $k_p h = 3$: linear shear flow. Solid lines are based on the Taylor series expansion of $\hat{U}(k)$ about k_p, dashed-dotted lines are based on $\hat{U}(k_p)$ and dashed line is using $\tilde{U}(k_p)$.

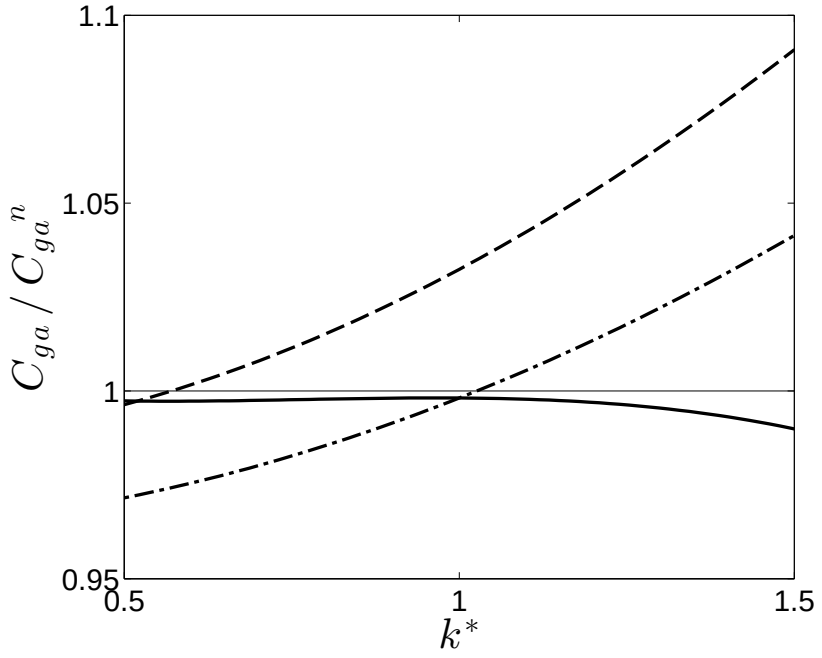

Figure 3.19: Comparison of absolute group velocity $C_{ga}\ / C_{ga}^{n}$ vs normalized wave number $k^* = k/k_p$,with $k_p h = 1$: Mouth of Columbia River (MCR). Solid lines are based on the Taylor series expansion of $\hat{U}(k)$ about k_p, dashed-dotted lines are based on $\hat{U}(k_p)$ and dashed line is using $\tilde{U}(k_p)$.

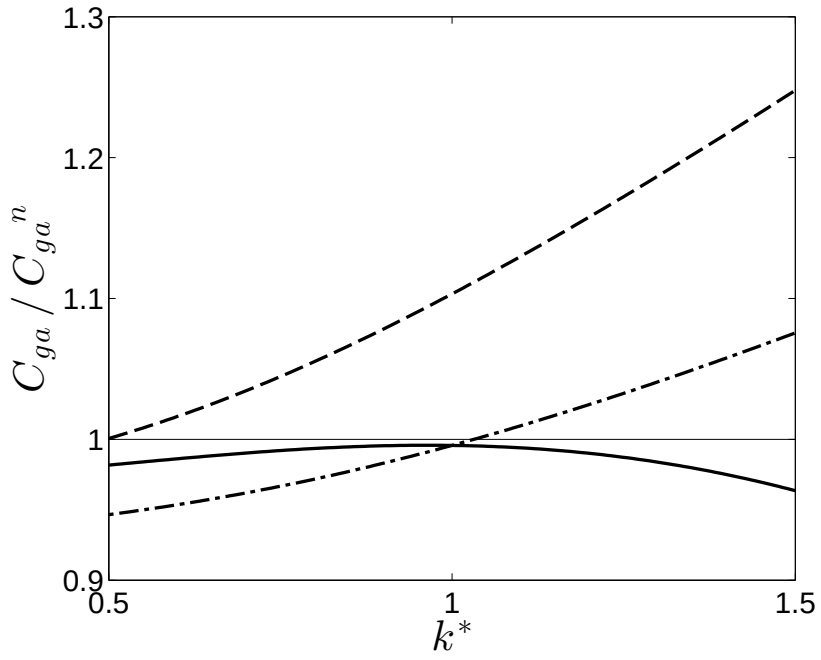

Figure 3.20: Comparison of absolute group velocity $C_{ga}\ /\,C_{ga}^{n}$ vs normalized wave number $k^* = k/k_p$,with $k_p h = 2$: Mouth of Columbia River (MCR).Solid lines are based on the Taylor series expansion of $\hat{U}(k)$ about k_p, dashed-dotted lines are based on $\hat{U}(k_p)$ and dashed line is using $\hat{U}(k_p)$.

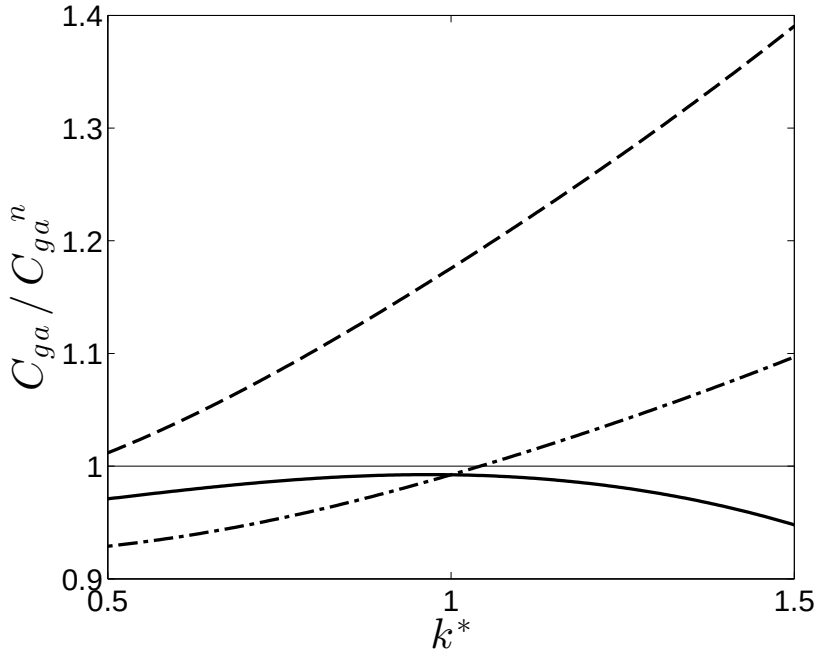

Figure 3.21: Comparison of absolute group velocity $C_{ga}\ / C_{ga}^{n}$ vs normalized wave number $k^* = k/k_p$,with $k_p h = 3$: Mouth of Columbia River (MCR). Solid lines are based on the Taylor series expansion of $\hat{U}(k)$ about k_p, dashed-dotted lines are based on $\hat{U}(k_p)$ and dashed line is using $\tilde{U}(k_p)$.

current velocity in expressions for group velocity, and that the use of velocity evaluated at peak frequency can lead to rapid accumulation of error at frequencies away from the peak. The first point has been demonstrated by showing that the retention of wavenumber dependence in $\tilde{U}$ when differentiating the approximate dispersion relation to obtain group velocity leads to results which are consistent with an exact solution in the case of waves on a current with constant shear, and with a numerical solution computed using a candidate, strongly sheared current profile from MCR.

In order to illustrate the effect of an incorrect choice of current on wave predictions, we end with an example of a shoaling calculation based monochromatic waves propagating in constant depth against an increasingly strong opposing flow. We take the MCR current profile shown in Figure 3.7 as reference $U(x_m, z)$ and construct a current distribution

$$U(x,z) = U(x_m,z)\frac{x - x_0}{x_m - x_0} \tag{3.47}$$

where x_0 represents an offshore starting point and the wave shoals in the interval $x_0 \leq x \leq x_m$. Using wave action conservation for waves on a depth uniform current then gives a wave height distribution

$$\frac{H(x)}{H_0} = \sqrt{\frac{C_{g0}}{C_g(x)}\frac{\sigma(x)}{\sigma_0}} \tag{3.48}$$

where subscripts 0 denote initial values at x_0 and H is waveheight, with energy density $E = 1/8\rho g H^2$. Figure 3.22 shows results for cases with C_g and σ evaluated using current values $\tilde{U}, \hat{U}, \overline{U}$ and U_s. The relative accuracy of the result based on $\hat{U}$ has been established in Section 4 and is used here as the reference for the three remaining choices. Results are shown for incident waves with periods ranging from 6 to 12 seconds. As would be expected, the prediction based on $\hat{U}$ deviates the most from the value based on depth-averaged current $\overline{U}$ for shorter waves, where the influence of the larger currents near the surface is enhanced, and from the value based on surface current U_s the most for longer waves, where the weighting over depth becomes more uniform.

The prediction based on $\tilde{U}$ is always closer to the correct answer than predictions made using surface or depth-averaged values, but errors are still significant and can be corrected using the proper expression $\hat{U}$.

The second point is cautionary in nature, and we have proposed a method for extending the range of model accuracy without imposing a massive increase in required data exchange between circulation and wave models.

The results here are limited to an examination of the group velocity C_{ga} and do not address the corresponding approximations for wave action density. In particular, it is important to determine whether the action density can be approximated using a simple form $N = E_0/\sigma^*$, with $E_0 = 1/2\rho g a^2$ based on depth-uniform currents and $\sigma^* = \omega - kU^*$ with U^* related to the available weighted forms of U in some simple manner. This problem has also been recently considered Quinn *et al.* (2017).

In the next Chapter, Using a modification of Kirby & Chen (1989)'s perturbation solution for weakly-sheared currents, where the basic flow is allowed to be a strong current with waves propagating at an arbitrary angle to the surface current direction, we develop approximate expressions for the wave action density and action flux in terms of a weighted integral over depth of the arbitrary current profile.

Further, the theory described in this Chapter was limited to unidirectional propagation on a following or opposing current, and so currents and wave numbers appear as scalars rather than vectors. The expressions for depth-weighted currents given here are extended to two horizontal dimensions for use in modeling, and the Taylor series expansion about peak wavenumber similarly has been developed in full vector form. These extensions have been developed and utilized in an extension of the SWAN wave model, which will be further discussed in Chapter 5.

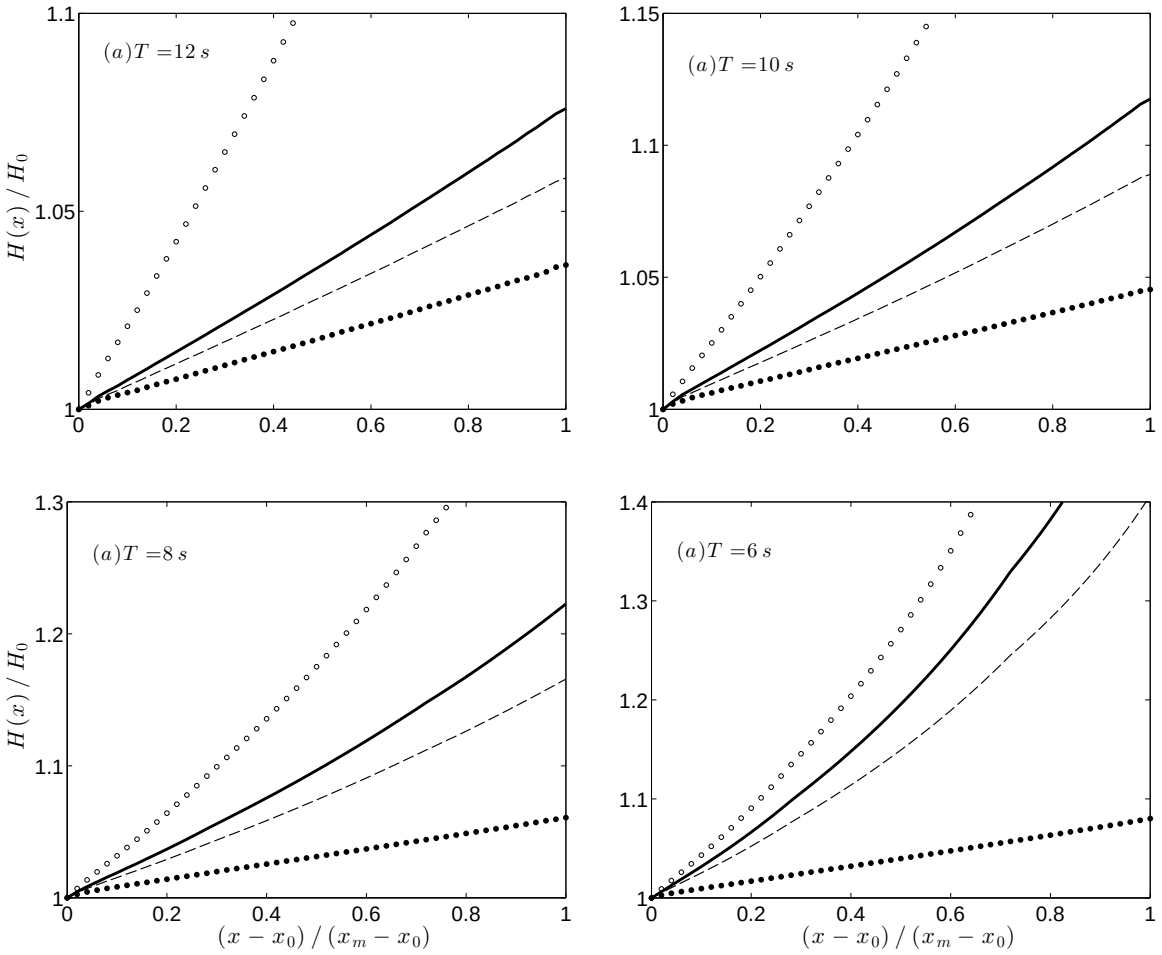

Figure 3.22: Wave shoaling $H(x)/H_0$ for waves on an opposing current of the form shown in Figure 3.7. Results are shown for four choices of current values, each used as a representation of depth-uniform current in determining wave action. $\hat{U}$: solid line; $\tilde{U}$: dashed line; $\overline{U}$: dots; U_s: circles.

Chapter 4

APPROXIMATION OF WAVE ACTION CONSERVATION IN VERTICALLY SHEARED MEAN FLOWS

The work presented in this chapter has been published in Ocean Modelling Volume 143, 101460.

https://doi.org/10.1016/j.ocemod.2019.101460.

We develop asymptotic expressions for wave action density and action flux, using an extension of Kirby & Chen (1989)'s perturbation solution for weakly-sheared currents allowing for a basic flow with Froude number $F = U/\sqrt{gh} = O(1)$ but with weak vertical shear. The accuracy of the expressions for action density and flux are established by comparison to analytic results for a current with constant shear, and to numerical results for a field case involving a buoyant ebb-tidal plume with strong vertical shear and for a case involving a numerically determined profile for a wind-driven current. We compare our results to those from recent work of Quinn *et al.* (2017), and find unresolved discrepancies in that prior work. We provide additional suggestions for efficiently implementing the required extensions in coupled wave/circulation models using a Taylor series expansion based on conditions at peak frequency and direction. These results generalize the previous work of Banihashemi *et al.* (2017) to motions in two horizontal dimensions, and cover the determination of the wave action.

4.1 Introduction

Significant advances have been made in the numerical modeling of wave-current interaction in recent decades. An important component in these advances has been the

recognition of wave action as the fundamental conserved quantity expressing the wave-averaged energy of a slowly-varying wave train. The simplest description is typically based on the underlying dynamics for monochromatic waves, governed by the wave action balance of Bretherton & Garrett (1968) and given by

$$\mathcal{N}_{,t} + \nabla_h \cdot \boldsymbol{\mathcal{F}} = 0 \tag{4.1}$$

where subscripted commas denote partial differentiation. For the case of depth uniform mean current $\mathbf{U}$, action density $\mathcal{N} = E/\sigma$ and action flux $\boldsymbol{\mathcal{F}} = \mathcal{N}\mathbf{c}_{ga}$, where E is energy density, $\sigma = \omega - \mathbf{k}\cdot\mathbf{U} = \sqrt{gk\tanh kh}$ is intrinsic frequency, h and $k = |\mathbf{k}|$ are depth and wavenumber, and $\mathbf{c}_{ga} = \omega_{,\mathbf{k}} = \sigma_{,\mathbf{k}} + \mathbf{U}$ is the absolute group velocity vector in stationary coordinates.

Phase-averaged spectral wave models typically calculate wave properties based on the linear theory for waves superposed on depth-uniform currents. However, currents in the field are occasionally strongly sheared over the vertical, leading to the need for a treatment of the rotationality or shear in the flow field. An approximate treatment for the effect of current shear may be based on a perturbation approach that has been developed through a sequence of papers (Stewart & Joy, 1974; Skop, 1987; Kirby & Chen, 1989; Ellingsen & Li, 2017), with Kirby & Chen (1989, hereafter referred to as KC89) providing a solution to second order for the finite depth case for currents that are assumed to deviate only weakly from depth-uniformity.

The main utility of the approximate solution has been the specification of a depth-weighted current $\tilde{\mathbf{U}}$, specified by Skop (1987) and KC89 and given by (4.12) below, as a representative depth-uniform current for determining intrinsic frequency and action density in spectral wave models (van der Westhuysen & Lesser, 2007; Ardhuin *et al.*, 2008). As pointed out in the original study of KC89 and recently elaborated on by Banihashemi *et al.* (2017, hereafter BKD17), the depth weighted current $\tilde{U}$ does not represent a consistent approximation for the current contribution to the group velocity $\mathbf{c}_{ga}$ at leading order. BKD17 demonstrate the inappropriateness of the use

of the weighted current $\tilde{\mathbf{U}}$ as the current speed in the expression for absolute group velocity, and establish the accuracy of the alternate value $\hat{\mathbf{U}}$ which follows naturally from consideration of the dependence of $\tilde{\mathbf{U}}$ on wavenumber k when differentiating the dispersion relation to get group velocity. The accuracy of this result provides a target for determining appropriate expressions for the group velocity for use in estimating wave action flux.

Models for spectral wave conditions more commonly solve for $\mathcal{N}(\mathbf{x}, t, \sigma, \theta)$ using a spectral action balance equation, which, for Cartesian coordinates, is given by (Hasselmann, 1973)

$$\mathcal{N}_{,t} + \nabla_h \cdot (\mathcal{N}\mathbf{c}_{ga}) + (c_\sigma \mathcal{N})_{,\sigma} + (c_\theta \mathcal{N})_{,\theta} = \frac{S}{\sigma} \tag{4.2}$$

where the third and forth terms represent transport in spectral space (σ, θ). Expressions for these propagation speeds are taken from linear wave theory (Whitham, 1974; Dingemans, 1997) for waves superimposed on depth-uniform currents. The right hand side of the equation represents source and sink terms associated with wave generation, dissipation and nonlinear wave-wave interactions. The introduction to each source term included in SWAN, for example, can be found in Booij *et al.* (1999). In applications using wave models which take as input a single Eulerian current vector at each grid point from the circulation model, this approach, based on a wavenumber-dependent current speed, is often simplified by using the current value at the peak wave frequency or wavenumber, $\tilde{U}(\mathbf{k}^p)$ (for example, Elias *et al.*, 2012), or at some weighted-average wavenumber value. BKD17 further examine the effect of using either the correct or incorrect estimate of the current speed evaluated only at the spectral peak frequency. The study suggested an alternate strategy, involving a Taylor series expansion of the depth-weighted current about the peak frequency, which significantly extends the range of accuracy of current information available to the wave model with minimal additional transfer of data between wave and circulation models.

In this study, the change in the estimate of action density and action flux due to

current shear is investigated, using asymptotic approximations of the Voronovich (1976) action balance equation obtained using a strong-current extension of the KC89 perturbation solution. In section 4.2, the problem for a linear wave in a horizontally-uniform domain with arbitrary current $\mathbf{U}(z)$ is established. In section 4.3 and B, KC89's perturbation solution for weakly-sheared currents is modified to allow for steady currents which are strong and oriented at arbitrary angles to the wave propagation direction. Approximate expressions for the wave action density and action flux are then developed following a procedure described in Appendix B. The approach is similar to that of Quinn *et al.* (2017), although our results differ significantly. In section 4.4, we evaluate the approximations for the analytic case of a wave on a current with constant vorticity, and establish the consistency of the expressions for action and action flux derived from the perturbation solution of KC89. Section 5 considers an application to a field case involving a strongly sheared vertical profile measured in the Mouth of the Columbia River (Kilcher & Nash, 2010). In Section 6, we extend the proposed Taylor series expansion of the expressions for the wavenumber-dependent approximations about the reference value at the peak frequency, originally presented in BKD17, to include wave directionality and the variation in intrinsic frequency appearing in the denominator of the action density. The differences between our results and those of Quinn *et al.* (2017) are discussed in section 4.7, along with suggestions for further work. A Supplement provides a number of plots comparing action density and flux estimates based on the usual depth-uniform current expressions and using the surface or depth-averaged currents as the representative values.

4.2 General theory

We consider the linearized problem for periodic surface waves in an incompressible, inviscid fluid, with wave number $\mathbf{k}$ and phase velocity $\mathbf{c}_a = (\omega/k)\hat{\mathbf{k}}$, propagating on a stream of velocity $\mathbf{U}(z)$ in finite water depth h. Here, ω denotes the absolute wave frequency in a stationary frame of reference, which also fixes the value of $\mathbf{U}(z)$. A unit vector pointing in the direction of wave propagation is defined as $\hat{\mathbf{k}} = \mathbf{k}/k$. The

problem is formulated in terms of the vertical component of the wave orbital velocity, written in complex form as

$$w(\mathbf{x}, z, t) = \frac{w(z)}{2} \mathrm{e}^{i(\mathbf{k}\cdot\mathbf{x}-\omega t)} + c.c. \tag{4.3}$$

where $c.c$ denotes the complex conjugate. The problem for the vertical structure of plane waves in a spatially uniform domain is then given by an extension of the Rayleigh equation to allow for an oblique angle between wave and current direction as well as possible rotation of the current vector over depth,

$$\begin{aligned} \sigma(z)(w_{,zz} - k^2 w) &= \sigma_{,zz}(z) w; \quad -h \le z \le 0 && \text{(4.4a)} \\ \sigma^2(0) w_{,z}(0) - [gk^2 + \sigma(0)\sigma_{,z}(0)] w(0) &= 0 && \text{(4.4b)} \\ w(-h) &= 0 && \text{(4.4c)} \end{aligned}$$

where g is the gravitational constant. The quantity $\sigma(z) = \omega - \mathbf{k} \cdot \mathbf{U}(z)$ represents a depth-varying relative frequency. We subsequently denote the values of current $\mathbf{U}(0)$ and intrinsic frequency $\sigma(0)$ at the mean surface $z = 0$ by $\mathbf{U}_s$ and σ_s, respectively. The amplitude of w may be related to surface displacement amplitude a through the kinematic surface boundary condition linearized w/r the fluctuating motion, given by

$$\eta_{,t} + \mathbf{U}_s \cdot \nabla_h \eta = w(0) \tag{4.5}$$

with η given by

$$\eta(\mathbf{x}, t) = \frac{a}{2} \mathrm{e}^{i(\mathbf{k}\cdot\mathbf{x}-\omega t)} + c.c, \tag{4.6}$$

leading to the relation $w(0) = -i\sigma_s a$. This result can be extended to cover the full water depth by introducing a dimensionless shape function $f(z)$ according to

$$w(z) = -i\sigma_s a f(z); \quad f(-h) = 0, \quad f(0) = 1 \tag{4.7}$$

The form of (4.4a) is intended to indicate that the problem is simply solvable for the case of current profiles without curvature, or $\sigma_{,zz} = 0$. The model (4.4a)-(4.4c) has been used in a number of studies of arbitrary or idealized velocity distributions; see reviews by Peregrine (1976), Jonsson (1990) and Thomas & Klopman (1997). For the general case of arbitrary $\mathbf{U}(z)$, Voronovich (1976) derived a conservation law, in the geometric optics approximation, for an adiabatic invariant corresponding to the wave action density, with $\mathcal{N}$ and $\boldsymbol{\mathcal{F}}$ in (4.1) given by

$$\mathcal{N} = -\frac{\rho}{4}\int_{-h}^{0}\frac{1}{\sigma^2k^2}\sigma_{,zz}|w|^2dz + \rho\left[\left(\frac{g}{2\sigma^3}+\frac{1}{4\sigma^2k^2}\sigma_{,z}\right)|w|^2\right]_{z=0} \tag{4.8a}$$

$$\begin{aligned}\boldsymbol{\mathcal{F}} = {} & \frac{\rho}{4}\int_{-h}^{0}\left(-\frac{\mathbf{U}}{\sigma^2k^2}\sigma_{,zz}+\frac{1}{\sigma k^2}\mathbf{U}_{,zz}-\frac{2\mathbf{k}}{k^2}\right)|w|^2dz \\ & +\left\{\rho\left[\mathbf{U}\left(\frac{g}{2\sigma^3}+\frac{1}{4\sigma^2k^2}\sigma_{,z}\right)-\frac{1}{4\sigma k^2}\mathbf{U}_{,z}+\frac{g\mathbf{k}}{2\sigma^2k^2}\right]|w|^2|\right\}_{z=0}.\end{aligned} \tag{4.8b}$$

These results may be written in more compact form using the substitution (4.7), giving

$$\mathcal{N} = \frac{E_0}{\sigma_s}\left[1+\frac{\sigma_s}{2gk^2}\left(\sigma_{,z}(0)-\sigma_s^2\int_{-h}^{0}\sigma^{-2}\sigma_{,zz}f^2dz\right)\right] \tag{4.9a}$$

$$\begin{aligned}\boldsymbol{\mathcal{F}} = {} & \frac{E_0}{\sigma_s}\left[\mathbf{U}_s+\mathbf{c}_{rs}\left(1-\frac{\sigma_s^2}{g}\int_{-h}^{0}f^2dz\right)\right. \\ & \left.+\frac{\sigma_s}{2gk^2}\left(-\mathbf{A}(0)+\sigma_s^2\int_{-h}^{0}\sigma^{-2}\mathbf{A}_{,z}f^2dz\right)\right]\end{aligned} \tag{4.9b}$$

where $E_0 = (1/2)\rho g a^2$ is the energy density for a wave on a depth-uniform current, $\mathbf{c}_{rs} = (\sigma_s/k)\hat{\mathbf{k}}$ is the wave phase velocity relative to the surface current, and

$$\mathbf{A}(z) = \sigma(z)\mathbf{U}'(z) - \sigma'(z)\mathbf{U}(z) \tag{4.10}$$

The adiabatic invariant $\mathcal{N}$ in (4.8a) or (4.9a) is not clearly in the form of wave energy divided by frequency, as expected from the work of Bretherton & Garrett (1968), but takes on this form in cases where analytic results for $\tilde{w}$ are available, such as the special case of waves on a current with constant vertical shear (Jonsson *et al.*, 1978).

Additionally, the flux vector $\boldsymbol{\mathcal{F}}$ in (4.8b) or (4.9b) isn't clearly in the form of action density times group velocity, $\mathcal{N}\mathbf{c}_{ga}$, but can also be shown to be in this form for the constant shear case.

Analytic solutions for progressive waves for the problem (4.4a)-(4.4c) are limited to the cases of currents with constant vertical shear, including the uniform-over-depth limit of zero shear. For more complex profiles, results may be obtained using perturbation solutions due to Stewart & Joy (1974) for deep water or Skop (1987) for finite depth, with solutions extended to second order by KC89. Shrira (1993) has further demonstrated how series solutions for deep water may be extended to high order. Ellingsen & Li (2017) have extended the basis for perturbation solutions to include currents with constant shear in the leading order solution. Alternately, numerical solutions may be obtained using a variety of methods, including shooting methods (Fenton, 1973; Dong & Kirby, 2012) or an iterative approach to the boundary value problem described by Li & Ellingsen (2019), used below in Section 4.5.

4.3 Approximate solution and analysis of action and action flux expressions

KC89 considered the propagation of a wave train which was colinear with the mean current, and assumed that $F = U/c \ll 1$, where F represents a Froude number for the mean flow, U describes the current magnitude, and c is a reference phase speed, usually taken to be $\sqrt{gh}$. Here, we consider the case of arbitrary orientation of wave and current, and allow for strong currents $F = O(1)$, in which case the current enters the wave dispersion relation at leading order. This generalization of the results of Skop (1987) and KC89 has also been described previously by Dong & Kirby (2012) and Ellingsen & Li (2017). The results are repeated here as a basis for discussion of the approximate forms for action density and flux. We also modify the treatment of the surface boundary condition for $f(z)$ from prior studies in order to simplify numerical applications.

4.3.1 Scaling framework and series solution

An appropriate scaling of the problem and the resulting perturbation solution is described in B, and leads to a problem characterized by parameters F (describing the strength of the current), ϵ (characterizing the magnitude of current shear), and μ (characterizing the ratio of water depth to wavelength). Here, we consider the case of $\mu, F = O(1)$ and $\epsilon \ll 1$, which allows for the development of a formally ordered expansion in powers of ϵ. The solution to the resulting problem is carried out to $O(\epsilon)$ in B. In particular, the intrinsic frequency σ is approximated by

$$\sigma(z) = \omega - \mathbf{k}\cdot\mathbf{U}(z) = (\omega - \mathbf{k}\cdot\tilde{\mathbf{U}}) - \epsilon\mathbf{k}\cdot\mathbf{U}_1(z) = \tilde{\sigma} + \epsilon\sigma_1(z) \tag{4.11}$$

where

$$\tilde{\mathbf{U}} = \frac{2k}{\sinh 2kh}\int_{-h}^{0}\mathbf{U}(z)\cosh 2k(h+z)dz \tag{4.12}$$

and $\mathbf{U}_1(z) = \mathbf{U}(z) - \tilde{\mathbf{U}}$. The vertical velocity w is given to $O(1)$ by

$$w(z) = -i\tilde{\sigma}af_0(z) \tag{4.13}$$

with

$$f_0(z) = \frac{\sinh k(h+z)}{\sinh kh} \tag{4.14}$$

and the dispersion relation

$$\tilde{\sigma}^2 = gk\tanh kh \tag{4.15}$$

The leading-order correction to the vertical shape function f is given by

$$f_1(z) = \frac{1}{2\tilde{\sigma}}\left[I_1(0) - I_1(z) - (I_2(0)/\tanh kh)\right]f_0(z) + \frac{I_2(z)}{2k\tilde{\sigma}}f_{0,z}(z) \tag{4.16}$$

where, in contrast to KC89 or Quinn *et al.* (2017), we retain the homogeneous part of the solution for $f_1(z)$ in order to specify a boundary condition $f_1(0) = 0$, as discussed

in B. The integrals in (4.16) are given by

$$\begin{aligned} I_1(z) &= \sinh^{-1} kh \int_{-h}^{z} \hat{\mathbf{k}} \cdot \mathbf{U}_{,\xi\xi}(\xi) \sinh 2k(h+\xi)\, d\xi \\ I_2(z) &= \sinh^{-1} kh \int_{-h}^{z} \hat{\mathbf{k}} \cdot \mathbf{U}_{,\xi\xi}(\xi) (\cosh 2k(h+\xi) - 1)\, d\xi \end{aligned} \tag{4.17}$$

The solution for w up to $O(\epsilon)$ is then given by

$$\tilde{w} = -i\sigma_s a[f_0(z) + f_1(z)] \tag{4.18}$$

with $\sigma_s = \tilde{\sigma} + \sigma_1(0) = \tilde{\sigma} - \mathbf{k} \cdot \mathbf{U}_1(0) = \tilde{\sigma} - \mathbf{k} \cdot (\mathbf{U}_s - \tilde{\mathbf{U}})$. For later use, the depth dependent intrinsic frequency $\sigma(z)$ can also be written as

$$\sigma(z) = \sigma_s - \mathbf{k} \cdot (\mathbf{U}(z) - \mathbf{U}_s) \tag{4.19}$$

4.3.2 Approximate expressions for action density and flux

Results presented here favor a framework where quantities are defined primarily in a frame moving with the velocity $\tilde{\mathbf{U}}$, with associated intrinsic frequency $\tilde{\sigma}$. This choice is not unique, and is often replaced by representations based on conditions at the water surface. A particular example is that of Quinn *et al.* (2017), who developed asymptotic expressions for $\mathcal{N}$ and $\boldsymbol{\mathcal{F}}$ by starting from (4.8a) and (4.8b) and introducing expansions for w, σ (or phase speed C), and for the amplitude of their w relative to surface wave amplitude a.

Here, we pursue a different approach starting from (4.9a) and (4.9b), where the original expressions have been simplified using the transformation (4.7) and the known properties of the problem prior to expansion. This transformation and the simplified expressions (4.9a) and (4.9b) are still an exact description of the original problem. In order to assess the difference between the two choices of reference frames, we develop a generic approximation which specifies neither, and then specialize it to the two frames of interest. The basic development of the framework is described in C, and leads to

(C.4) and (C.18) for action density $\mathcal{N}_0$ and flux $\boldsymbol{\mathcal{F}}_0$ in which a final choice of reference frame velocity and leading order dispersion relation has not been made. As in Quinn *et al.* (2017), the choice of surface conditions as a reference leads to an expression for action density containing an $O(\epsilon)$ component, where ϵ here is basically similar to ϵ_5 in Quinn *et al.* The expression is given here by (C.19) or

$$\mathcal{N}^* = \frac{E_0}{\sigma_s}\left[1 + \epsilon\frac{(\sigma_s - \tilde{\sigma})}{\sigma_s}\right] \tag{4.20}$$

This expression is similar in form to (4.2) in Quinn *et al.* (2017), but the $O(\epsilon)$ components in the two studies do not appear to have a close correspondence. This is discussed further in section 4.7.1. In contrast, the approximation resulting from the choice of the depth-weighted current reference frame gives the estimate (C.20) or

$$\tilde{\mathcal{N}} = \frac{E_0}{\tilde{\sigma}} + O(\epsilon^2) \tag{4.21}$$

This result was suggested by KC89 based on an analysis of the constant shear case of Section 4.4, but was not formally established there as a general result. We note that the two formulas (4.20) and (4.21) are asymptotically equivalent to within the accuracy of the approximation, which can easily be established by substituting between σ_s and $\tilde{\sigma}$. However, actual numerical values from the two expressions are seen to diverge in particular examples, as will be shown for a linear shear profile in section 4.4 and for a wind driven current in section 4.7.1.

It is clear, from these results, that a formulation in terms of $\tilde{\sigma}$ and $\tilde{\mathbf{U}}$ is a more compact version of the approximation. Similar treatment for the action flux (C.18) leads to the expressions

$$\boldsymbol{\mathcal{F}}^* = \frac{E_0}{\sigma_s}\left[\hat{\mathbf{U}} + \mathbf{c}_{grs} + \epsilon\left(\frac{\mathbf{U}_s}{\sigma_s} + \frac{\hat{\mathbf{k}}}{k}(1-G)\right)(\sigma_s - \tilde{\sigma})\right] + O(\epsilon^2) \tag{4.22}$$

and

$$\tilde{\boldsymbol{\mathcal{F}}} = \frac{E_0}{\tilde{\sigma}} \left[\hat{\mathbf{U}} + \tilde{\mathbf{c}}_{gr} \right] + O(\epsilon^2) \tag{4.23}$$

We note the striking result that both versions of the approximate action flux identify $\hat{\mathbf{U}} = \tilde{\mathbf{U}} + \hat{\mathbf{k}}(\mathbf{k} \cdot \tilde{\mathbf{U}}_{,k})$ as the correct current advection velocity. The appearance of $\hat{\mathbf{U}}$ results from the treatment of the integral of the product of the zeroth and first order shape functions f_0 and f_1; see (C.13) - (C.17). The current $\hat{\mathbf{U}}$ is the vector form of the advection velocity suggested by KC89 and discussed recently by BKD17. This result may be obtained directly from the definition of group velocity,

$$\begin{aligned} \mathbf{c}_{ga} &= \omega_{,\mathbf{k}} = (\sigma + \mathbf{k} \cdot \tilde{\mathbf{U}})_{,\mathbf{k}} \\ &= \hat{\mathbf{k}}\sigma_{,k} + \tilde{\mathbf{U}} + \hat{\mathbf{k}} \left(\mathbf{k} \cdot \tilde{\mathbf{U}}_{,k} \right) \\ &= \mathbf{c}_{gr} + \hat{\mathbf{U}} \end{aligned} \tag{4.24}$$

Unlike the expressions (4.20) and (4.21) for $\mathcal{N}$, the expressions for $\boldsymbol{\mathcal{F}}$ do not appear to be consistent with each other to the order of approximation considered. An attempt to rearrange (4.22) to the form of (4.23) to within cancellation of $O(\epsilon^2)$ terms leads to the result

$$\boldsymbol{\mathcal{F}}^* = \frac{E_0}{\tilde{\sigma}} \left[\hat{\mathbf{U}} + \tilde{\mathbf{c}}_{gr} + \epsilon \frac{\hat{\mathbf{k}}}{k} (1 - G)(\sigma_s - \tilde{\sigma}) \right] \tag{4.25}$$

where the remaining term at $O(\epsilon)$ results from the treatment of the I_4 integral in (C.11) (or the first occurrence of $(1 - G)$ in (C.18)), where no $O(\epsilon)$ expansion term occurs in the surface-oriented expression, whereas the $O(\epsilon)$ expansion term occurring in the $\tilde{\mathbf{U}}$-oriented expression cancels the second $(1 - G)$ term contributed by the integral I_5 in (C.17). A similar attempt to work from (4.23) to (4.22) also leaves an $O(\epsilon)$ residual which differs from the one in (4.22).

The results (4.20) and (4.22) for $\mathcal{N}^*$ and $\boldsymbol{\mathcal{F}}^*$ are expected to be far accurate representations of action density and flux than simple constructs based on surface or depth-averaged currents, but the relative accuracy of the two asymptotic approaches

remains to be examined. We will take up this question again in sections 4.4 and 4.7.1.

4.4 Waves on currents with constant mean-flow shear

In this section, we examine the accuracy of the asymptotic expressions for $\mathcal{N}$ and $\boldsymbol{\mathcal{F}}$ for the case of waves on a current with constant vertical shear. This case has been studied extensively, with the basic solution described for co-linear propagation in one horizontal dimension (Thompson, 1949) and subsequently extended to two horizontal dimensions for waves oblique to the current (Craik, 1968; Ellingsen, 2016, among others). Ellingsen (2016) provides a clear description of the influence of wave orbital motion on the vorticity field for the case of oblique waves. Jonsson *et al.* (1978) gave expressions for the action density and flux for the 1D case of co-linear wave and current; the extension to the general case is given below based on the theory of Voronovich (1976). In this section, we determine the accuracy of the approximate expressions in a space covering variations of kh, F, θ (representing the angle between the wave direction and the surface current), and a shear parameter α defined below. Consider a current profile with constant shear (and possible rotation) given by

$$\mathbf{U}(z) = \mathbf{U}_s + \boldsymbol{\Omega} z \tag{4.26}$$

The current shear $\boldsymbol{\Omega}$ does not have to be collinear with either $\mathbf{U}_s$ or $\mathbf{k}$ (Figure 4.1). In this case, the BVP (4.4a-4.4c) simplifies and is given by

$$\begin{aligned} \sigma(w_{,zz} - k^2 w) &= 0; \qquad -h \le z \le 0 \\ \sigma_s^2 w_{,z}(0) - (gk^2 - \sigma_s \mathbf{k}\cdot\boldsymbol{\Omega}) w(0) &= 0 \\ w(-h) &= 0 \end{aligned} \tag{4.27}$$

The possibility of $\sigma(z)$ taking on a value of zero at a critical level is not typically of interest in surface wave dynamics; see also Ellingsen & Li (2017). The solution to

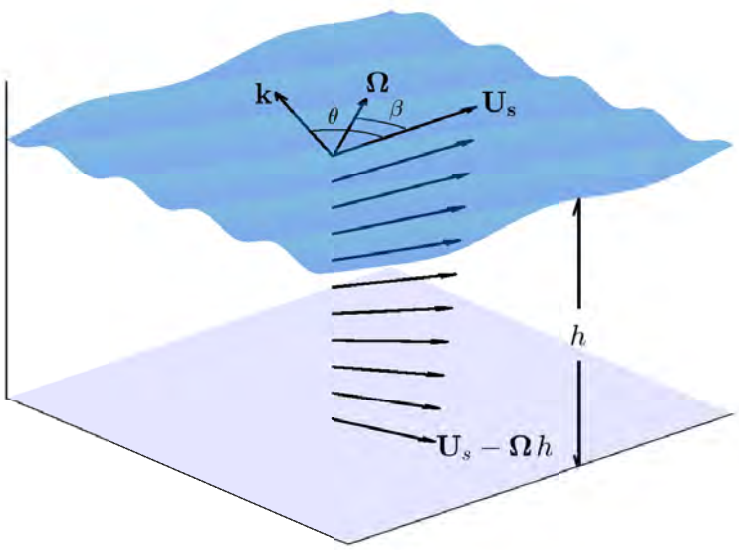

Figure 4.1: Definition sketch for linear shear current. The angle between the surface velocity and wave direction is θ while the angle between the surface current and current vertical shear is β

(4.27) is given by

$$w(z) = -i\sigma_s a f(z) \tag{4.28}$$

$$\mathbf{u}(z) = \sigma_s a \left(\frac{1}{\sigma}(\hat{\mathbf{k}}(\hat{\mathbf{k}} \cdot \boldsymbol{\Omega}) - \boldsymbol{\Omega}) f(z) + \frac{\hat{\mathbf{k}}}{k} f_{,z}(z) \right) \tag{4.29}$$

$$p(z) = \frac{\rho \sigma_s a}{k} \left((\hat{\mathbf{k}} \cdot \boldsymbol{\Omega}) f(z) + \frac{\sigma}{k} f_{,z}(z) \right) \tag{4.30}$$

with vertical shape function

$$f(z) = \frac{\sinh k(h+z)}{\sinh kh} \tag{4.31}$$

and with dispersion relation

$$\sigma_s^2 = (gk - \sigma_s \hat{\mathbf{k}} \cdot \boldsymbol{\Omega}) \tanh kh \tag{4.32}$$

Constant current shear affects the vertical structure of wave orbital velocity and wave pressure by modifying the dispersion relation and twisting wave horizontal velocity in the current shear direction. Absolute and relative phase speed vectors are related by

$$\mathbf{c}_a = \mathbf{c}_{rs} + \hat{\mathbf{k}}(\hat{\mathbf{k}} \cdot \mathbf{U}_s) \tag{4.33}$$

where $\mathbf{c}_a = c_a \hat{\mathbf{k}} = (\omega/k)\hat{\mathbf{k}}$ and $\mathbf{c}_{rs} = c_{rs}\hat{\mathbf{k}} = (\sigma_s/k)\hat{\mathbf{k}}$, with subscripts s denoting values at the SWL $z = 0$. From (4.32), an expression for c_{rs} is given by

$$c_{rs} = \frac{1}{2k} \left[\pm (4gk \tanh kh + (\hat{\mathbf{k}} \cdot \boldsymbol{\Omega} \tanh kh)^2)^{1/2} - \hat{\mathbf{k}} \cdot \boldsymbol{\Omega} \tanh kh \right] \tag{4.34}$$

Inserting the wave solutions in (4.9a) and (4.9b) gives exact expressions for the action density and flux, given by

$$\mathcal{N} = \frac{E_0}{\sigma_s} \left(1 - \frac{\hat{\mathbf{k}} \cdot \boldsymbol{\Omega} c_{rs}}{2g} \right) \tag{4.35}$$

and

$$\boldsymbol{\mathcal{F}} = \mathcal{N}\mathbf{c}_{ga}; \qquad \mathbf{c}_{ga} = \mathbf{U}_s + \mathbf{c}_{grs} \tag{4.36}$$

The relative group velocity $\mathbf{c}_{grs}$ is given by

$$\mathbf{c}_{grs} = \sigma_{s,\mathbf{k}} = \frac{\hat{\mathbf{k}}[g(1+G)c_{rs}] + [\hat{\mathbf{k}}(\hat{\mathbf{k}}\cdot\boldsymbol{\Omega})(1-G) - \boldsymbol{\Omega}]c_{rs}^2}{2g - (\hat{\mathbf{k}}\cdot\boldsymbol{\Omega})c_{rs}} \tag{4.37}$$

Turning to the perturbation solution of Section 4.3, we obtain results to $O(\epsilon)$ in the $\tilde{\mathbf{U}}$ reference frame and compare them to the full solution to determine their range of validity. The weighted current $\tilde{\mathbf{U}}$ is given by

$$\tilde{\mathbf{U}} = \mathbf{U}_s - \boldsymbol{\Omega}\frac{\tanh kh}{2k} \tag{4.38}$$

and the corresponding flux advection velocity $\hat{\mathbf{U}}$ is then given by

$$\hat{\mathbf{U}} = \tilde{\mathbf{U}} + \hat{\mathbf{k}}(\mathbf{k}\cdot\tilde{\mathbf{U}}_{,k}) = \mathbf{U}_s - \frac{\tanh kh}{2k}\Big(\boldsymbol{\Omega} - \hat{\mathbf{k}}(\hat{\mathbf{k}}\cdot\boldsymbol{\Omega})(1-G)\Big) \tag{4.39}$$

with action $\tilde{\mathcal{N}}$ and action flux $\tilde{\boldsymbol{\mathcal{F}}}$ determined by (4.21) and (4.23).

The % error $100(1-\tilde{\mathcal{N}}/\mathcal{N})$ for the first order perturbation approximation of the action density (4.21) compared to the exact result from (4.35) is shown in Figure 4.2 for $0.1 < kh < 10$, $-\pi/2 < \theta < \pi/2$, relative angle $\beta = 0$ and for different choices of current strength and shear. Additional results for $\beta = \pi/4$ and $\pi/2$ are provided as Figures D1 and D2 in the Supplement, Appendix D. (Angles θ and β represent the orientation of $\mathbf{k}$ and $\boldsymbol{\Omega}$ relative to the surface current U_s, as indicated in Figure 4.1. Current strength is represented through a Froude number based on surface current speed, $F = |\mathbf{U}_s|/\sqrt{gh}$, while shear is represented by dimensionless parameter $\alpha = h|\boldsymbol{\Omega}|/|\mathbf{U}_s|$.

The results show a considerably improved accuracy in the predicted action density, compared to values constructed using other common approaches, such as using the surface velocity $\mathbf{U}_s$, with $\mathcal{N}$ given by $\mathcal{N}_s = E_0/\sigma_s$; Figures D3 - D5 in Supplement)

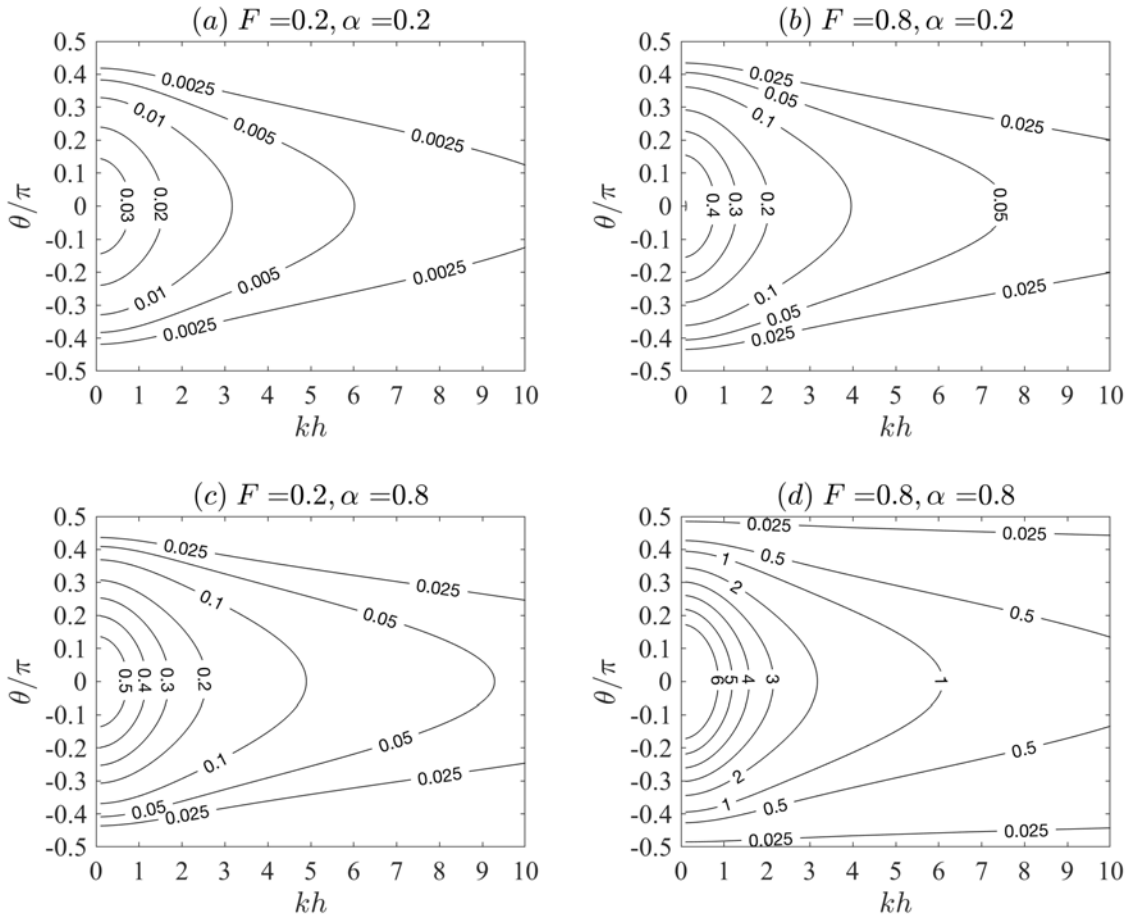

Figure 4.2: % error in wave action density $100(1-\tilde{\mathcal{N}}/\mathcal{N})$: linear shear with variation of kh and θ, first order perturbation approximation, $\beta = 0$.

or depth-averaged velocity $\overline{\mathbf{U}}$, with $\mathcal{N}$ given by $\overline{\mathcal{N}} = E_0/\overline{\sigma}$, $\overline{\sigma} = \omega - \mathbf{k}\cdot\overline{\mathbf{U}}$; Figures D6 - D8 in Supplement). Opposing currents require a more complex calculation of blocking conditions; this limit is not crucial to the development here and deserves it's own treatment in connection with wave propagation near buoyant plumes and other frontal features; see BKD17 for examples of the relative magnitudes of errors in those cases.

An extensive comparison of the correct and approximate action flux velocities for the 1D case has been discussed in BKD17. Figure 4.3 shows the composite error of $|\tilde{\boldsymbol{\mathcal{F}}}|$ as a function of kh and θ for $\beta = 0$ using the first order perturbation approximation,

with additional results for $\beta = \pi/4$ and $\pi/2$ in Figures D9 and D10 in the Supplement. Results for the same range of parameters using the surface and depth-average current values are shown in Figures D11 - D16 in the Supplement.

As mentioned is section 4.3.2, the relative accuracy of the two asymptotic approaches in the frame of reference based on the surface current and the depth weighted current remains to be examined. Figure 4.4 and 4.5 provide a simple comparison of equations (4.20) vs (4.21), and (4.22) vs (4.23). The comparison is done for a linear shear profile with variation of α, F and kh, with $\theta = 0$ and $\beta = 0$. The gain in accuracy provided by the estimates $\tilde{\mathcal{N}}$ and $\tilde{\boldsymbol{\mathcal{F}}}$ is shown, in spite of the two expressions being asymptotically equivalent within the accuracy of the approximation.

4.5 Columbia River velocity profile

In this section, we compare the action densities obtained from different approximations using a measured current profile from the Mouth of the Columbia River (MCR), where fresh riverine water meets salty seawater and the current becomes strongly sheared due to stratification and tidal effects. Here, we select a sample velocity profile collected by a pole-mounted ADCP during the RISE project (Kilcher & Nash, 2010). The profile, shown in Figure 4.6, was also used in BKD17, and represents a maximum ebb condition for the time frame covered by the file. The water depth is $h = 25\,m$, the normalized shear parameter for this current profile is $\alpha \sim 8$, which indicates a strongly sheared current, while the Froude number is $F \sim 0.15$. The current profile is assumed to be unidirectional.

We consider the case of waves propagating landward against the opposing current. We follow a general procedure of fitting polynomials to either measured profiles or profiles taken from gridded model results in order to establish a basis for computing weighted current values. Expressions below are based on the form

$$\mathbf{U}(z) = |\mathbf{U}_s| \sum_{n=0}^{N} \mathbf{a}_n (\frac{z}{h})^n \tag{4.40}$$

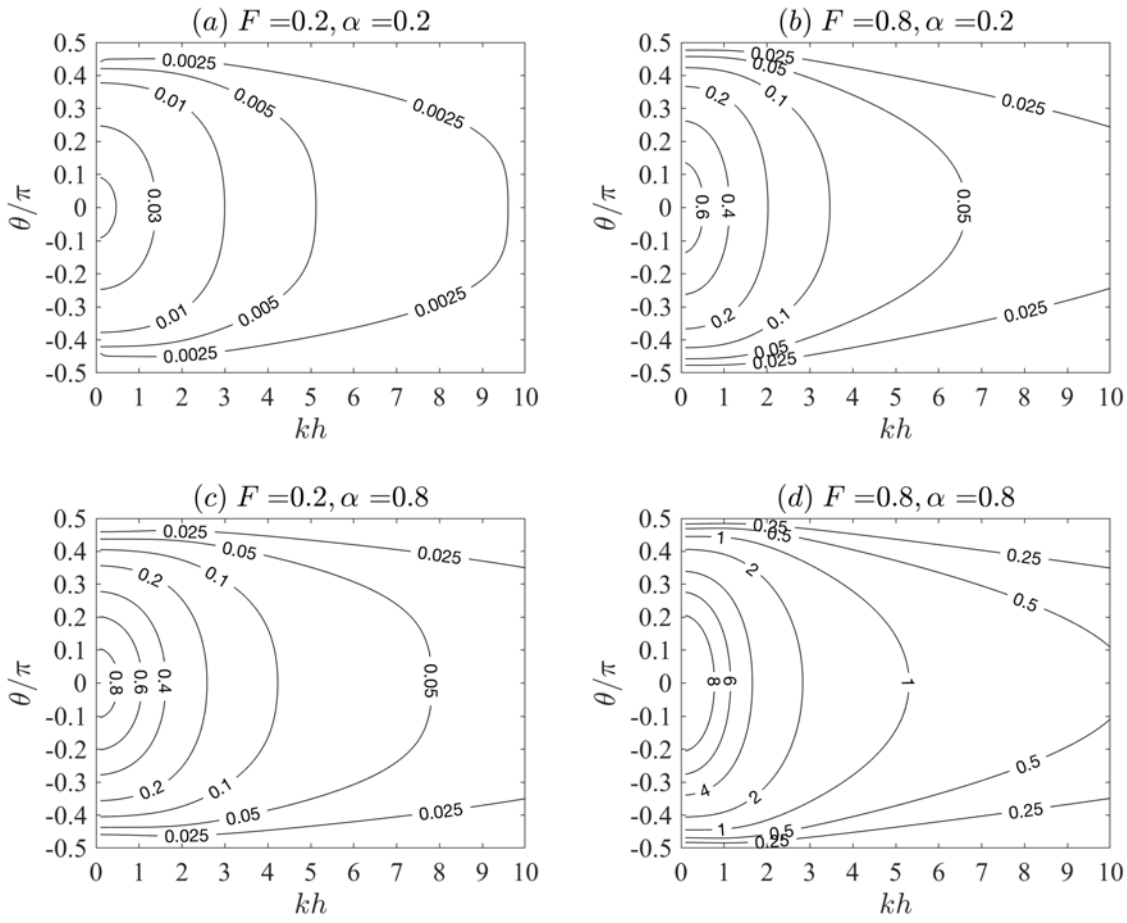

Figure 4.3: % error in wave action flux $100(1 - |\tilde{\boldsymbol{\mathcal{F}}}|/|\boldsymbol{\mathcal{F}}|)$: linear shear with variation of kh and θ, first order perturbation approximation, $\beta = 0$.

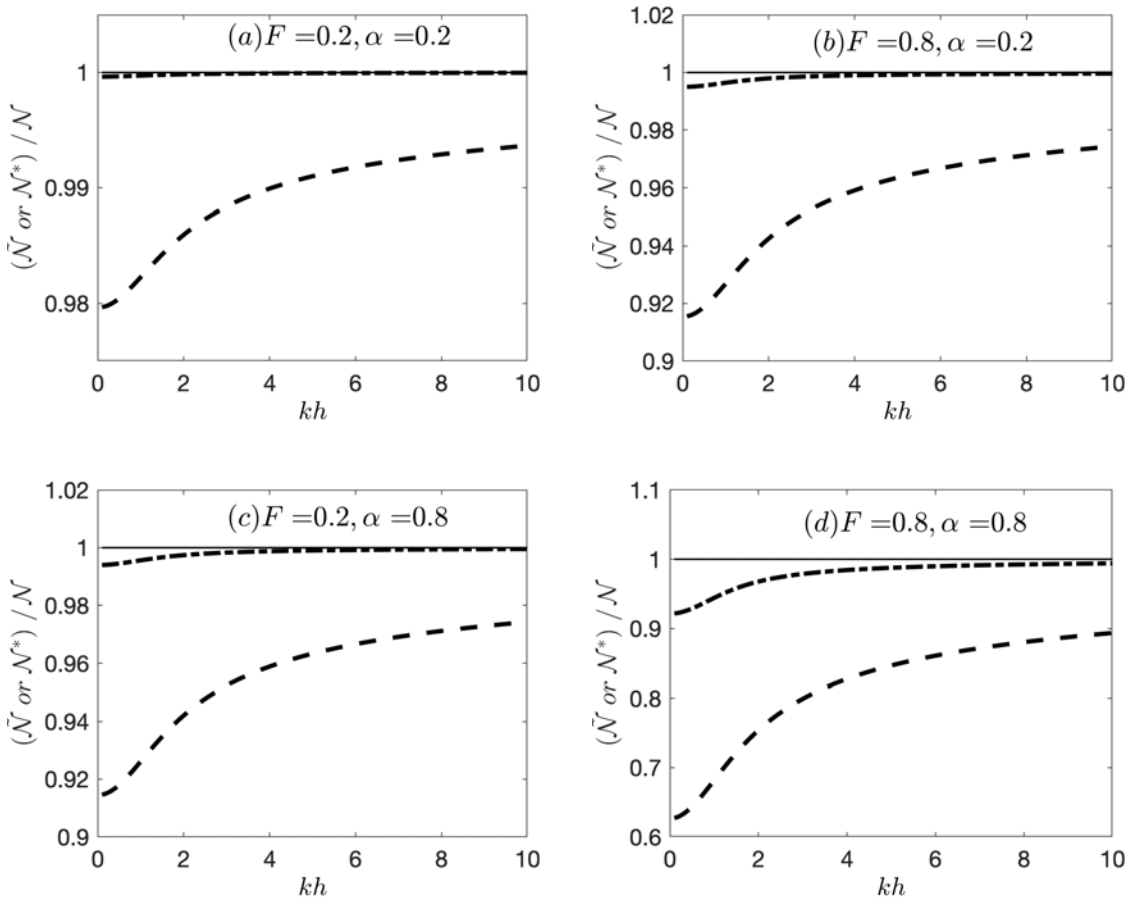

Figure 4.4: Comparison of action density estimates: linear shear with variation of kh, with $\theta = 0$ and $\beta = 0$. Dashed dotted lines indicate $\tilde{\mathcal{N}}/\mathcal{N}$ using the asymptotic expression (4.21) in the frame of reference based on the depth weighted current, dashed lines indicate $\mathcal{N}^*/\mathcal{N}$ using the asymptotic expression (4.20) in the frame of reference based on the surface current.

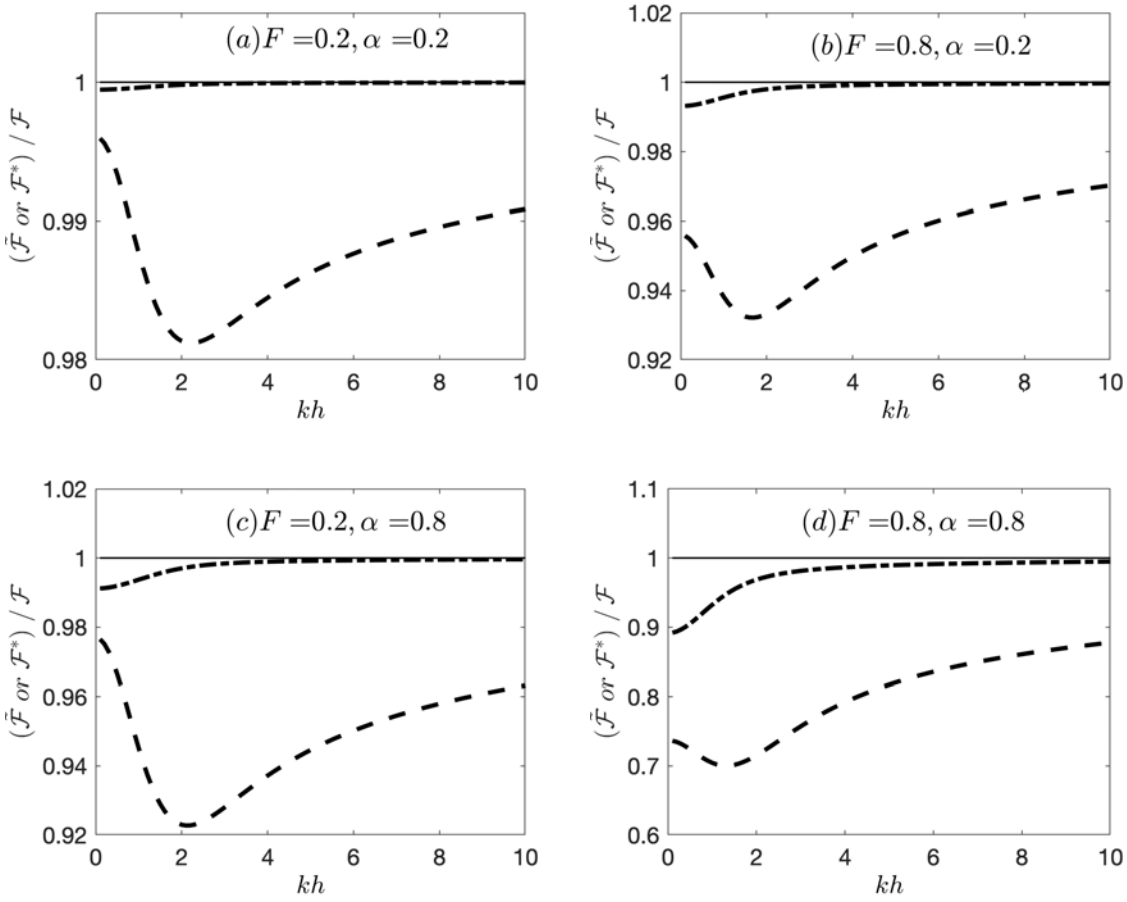

Figure 4.5: Comparison of action flux: linear shear with variation of kh with $\theta = 0$ and $\beta = 0$. Dashed dotted lines indicate $\tilde{\boldsymbol{\mathcal{F}}}/\boldsymbol{\mathcal{F}}$ using the asymptotic expression (4.23) in the frame of reference based on the depth weighted current, dashed lines indicate $\boldsymbol{\mathcal{F}}^*/\boldsymbol{\mathcal{F}}$ using the asymptotic expression (4.22) in the frame of reference based on the surface current.

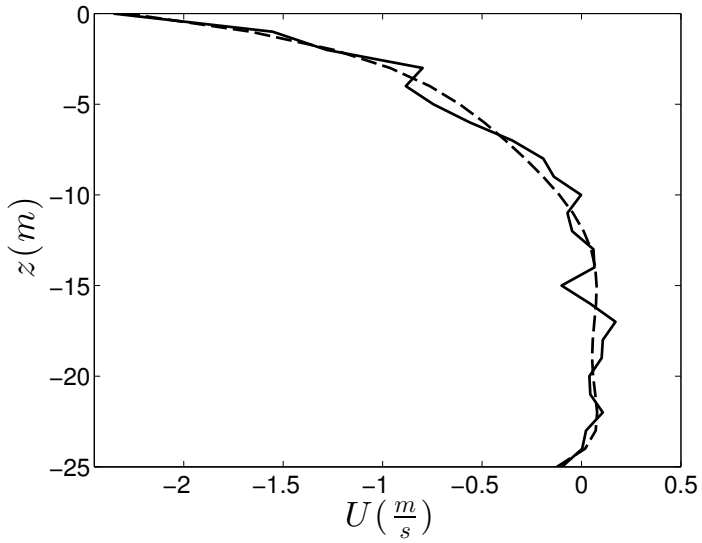

Figure 4.6: Columbia River current profile during ebb tide. The solid line is measured data (Kilcher & Nash, 2010) and the dashed line is a 6th order polynomial fit to the data.

with current speed referenced to the surface value U_s and with dimensionless a_n's. (Note that $a_0 = 1$ due to the normalization by the surface current velocity, while $a_1 = \Omega_s h/U_s \sim \alpha$, where Ω_s is the current shear at the surface.) Calculations here are carried out using $N = 6$, with the fitted profile for the demonstration case also shown in Figure 4.6. For the given profile the coefficients in (4.40) are then given by

$$\begin{aligned} U(z) &= -2.28\left(1 + 8.22\frac{z}{h} + 40.26(\frac{z}{h})^2 + 120.52(\frac{z}{h})^3 \right. \\ &\quad \left. +197.04(\frac{z}{h})^4 + 160.36(\frac{z}{h})^5 + 50.85(\frac{z}{h})^6\right) \end{aligned} \tag{4.41}$$

In the absence of an analytic solution, a numerical method is used to solve the Rayleigh equation. In BKD17 the procedure used by Dong & Kirby (2012) was considered to solve the boundary value problem. The vertical velocity $w(z)$ was found by solving a Riccati equation using a shooting method due to Fenton (1973), also discussed in KC89. Here, we use the Direct Integration Method (DIM) presented by Li & Ellingsen (2019) which is faster and easier to parallelize than the shooting method.

The method starts by rewriting (4.4a) - (4.4c) with the substitution (4.7) as

$$(f_{,zz} - k^2 f) = \frac{\sigma_{,zz}(z)}{\mathbf{k}\cdot\Delta\mathbf{U} - kc_{rs}} f; \quad -h \le z \le 0 \tag{4.42a}$$

$$c_{rs}^2 - c_{rs} I_c(c_{rs}) - {c_0}^2 = 0 \tag{4.42b}$$

where c_{rs} is the relative wave phase speed at the surface and

$$\begin{aligned} I_c(c_{rs}) &= \frac{\mathbf{k}\cdot\mathbf{U}_{,z}(0)\tanh kh}{k^2} \\ &\quad + c_{rs}\int_{-h}^{0} \frac{\mathbf{k}\cdot\mathbf{U}_{,z}(z) f(z)\sinh k(z+h)}{k(\mathbf{k}\cdot\Delta\mathbf{U} - kc_{rs})\cosh kh}\, dz \end{aligned} \tag{4.43a}$$

$${c_0}^2 = \frac{g}{k}\tanh kh \tag{4.43b}$$

$$f(z) = w(z)/w(0) \tag{4.43c}$$

$$\Delta\mathbf{U} = \mathbf{U}(z) - \mathbf{U}_s \tag{4.43d}$$

The DIM method treats equations (4.42a) and (4.42b) as two coupled equations with f and c_{rs} as the unknowns, and then obtains the numerical solution to the set of equations. The results are used in (4.8a) and (4.8b) to obtain numerical values for wave action density and flux, which are taken to be the reference "exact" solutions.

The accuracy of the first order perturbation approximation of the wave action density $\tilde{\mathcal{N}}$ and wave action flux $\tilde{\boldsymbol{\mathcal{F}}}$ relative to the numerical solution obtained from the DIM is shown in Figure 4.7. The results are plotted against a parameter kz_0 instead of kh where z_0 is specifically defined assuming a linear profile down from the surface until the current falls to zero at depth z_0. In this case the z_0 would be $z_0 = U_s/U_s'(0) \sim 3m$.

Similar to the linear shear case, the results show improved accuracy in the estimate of action density compared to the common approaches using depth averaged or surface current values, displayed as Figures C17 - C20 in the Supplement.

4.6 Taylor series expansion of $\tilde{\mathcal{N}}(\mathbf{k})$ and $\tilde{\boldsymbol{\mathcal{F}}}(\mathbf{k})$ about $\mathbf{k}^p$.

The use of the first order correction to the group velocity $\hat{U}$ and the more simplified procedure of using a single value $\hat{U}(k^p)$ instead of the frequency dependent

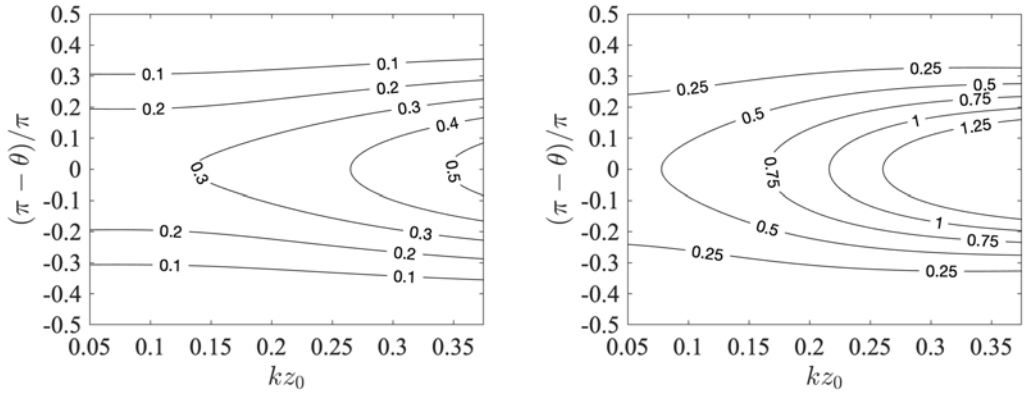

Figure 4.7: % error in wave action density $100(1-\tilde{\mathcal{N}}/\mathcal{N})$ (left) and wave action flux $100(1-|\tilde{\boldsymbol{\mathcal{F}}}|/|\boldsymbol{\mathcal{F}}|)$ (right): MCR current profile with variation of kz_0 and θ, first order perturbation approximations (4.21) and (4.23).

form has been investigated in BKD17 for the case of co-linear waves and current. BKD17 suggested an alternate strategy, involving a Taylor series expansion about the peak frequency, which should significantly extend the range of accuracy of current information available to the wave model with minimal additional data transfer between wave and circulation models. Writing the components of the effective advection velocity as $\hat{\mathbf{U}} = (\hat{U}_i, \hat{U}_j)$, the Taylor expansion in component form is given by

$$\hat{U}_{Ti}(\mathbf{k}) = \hat{U}_i(\mathbf{k}^p) + (\mathbf{k}-\mathbf{k}^p)\cdot\frac{\partial \hat{U}_i}{\partial \mathbf{k}}\Big|_{k^p} + O(|\mathbf{k}-\mathbf{k}^p|^2) \tag{4.44}$$

where subscript T denotes the value obtained from the truncated series. Using the relation between $\hat{\mathbf{U}}$ and $\tilde{\mathbf{U}}$ gives

$$\begin{aligned}\frac{\partial \hat{U}_i}{\partial \mathbf{k}} &= \frac{\partial \tilde{U}_i}{\partial \mathbf{k}} + \frac{\partial}{\partial \mathbf{k}}\left(\frac{k_i}{k}\mathbf{k}\cdot\frac{\partial \tilde{\mathbf{U}}}{\partial k}\right) \\ &= \hat{\mathbf{k}}\frac{\partial \tilde{U}_i}{\partial k} + \frac{k_i}{k}\left(\frac{\partial \tilde{\mathbf{U}}}{\partial k}\right) + \hat{\mathbf{k}}\left[\frac{k_i}{k}\left(\mathbf{k}\cdot\frac{\partial^2 \tilde{\mathbf{U}}}{\partial k^2}\right)\right]\end{aligned} \tag{4.45}$$

The Taylor series expansion in component form is then given by

$$\begin{aligned}\hat{U}_{Ti}(\mathbf{k}) &= \tilde{U}_i(\mathbf{k}^p) + \frac{k_i^p}{k}(\mathbf{k}\cdot\frac{\partial\tilde{\mathbf{U}}}{\partial k})\Big|_{\mathbf{k}^p} + \frac{\mathbf{k}^p}{k}\cdot(\mathbf{k}-\mathbf{k}^p)\frac{\partial\tilde{U}_i}{\partial k}\Big|_{k^p} \\ &+ \frac{k_i^p}{k}(\mathbf{k}-\mathbf{k}^p)\cdot\frac{\partial\tilde{\mathbf{U}}}{\partial k}\Big|_{k^p} \\ &+ \frac{k_i^p}{k}\frac{\mathbf{k}^p}{k}\cdot(\mathbf{k}-\mathbf{k}^p)\big(\mathbf{k}^p.\frac{\partial^2\tilde{\mathbf{U}}}{\partial k^2}\Big|_{k^p}\big) \end{aligned} \tag{4.46}$$

The same approach is used to calculate the intrinsic frequency relative to the value at the peak wave number as

$$\tilde{\sigma}_T(\mathbf{k}) = \omega - \mathbf{k}\cdot\tilde{\mathbf{U}}\Big|_{k_p} - \frac{\mathbf{k}^p}{k}\cdot(\mathbf{k}-\mathbf{k}^p)(\mathbf{k}\cdot\tilde{\mathbf{U}}_{,k}\Big|_{k_p}) \tag{4.47}$$

where we take advantage of the fact that the local value of ω is known for each frequency component.

Returning to the case of a current with constant shear, we show results for the accuracy of the action density $\tilde{\mathcal{N}}_T$ for three peak wave numbers corresponding to $k^p h = 1, 2$ and 3 in Figures 4.8-4.10, with the peak direction $\theta^p = 0$, the current non-rotational over depth ($\beta = 0$) and a range of directions of $\pm\pi/3$. Figures C21 - C23 in the Supplement compare the action flux approximation $\tilde{\boldsymbol{\mathcal{F}}}_p$ for the same cases. Corresponding results for action density $\tilde{\mathcal{N}}$ for the MCR current profile are provided in Figure 4.11 for $k_p h = 1\,,\, 2$ and the directional spreading of $\pi/5$, while the comparison for the action flux $\tilde{\boldsymbol{\mathcal{F}}}_T$ is shown in Figures C24 and C25 in the Supplement.

Overall, it is seen that the Taylor series approach provides a robust estimate for action density and action flux, using only information about the depth-weighted current velocity at the spectral peak frequency. These expressions should be relatively simple to implement in spectral wave models, but implementation would require the calculation of $\tilde{\mathbf{U}}(\mathbf{k}_p)$, $\tilde{\mathbf{U}}_{,k}(\mathbf{k}_p)$ and $\tilde{\mathbf{U}}_{,kk}(\mathbf{k}_p)$ in the circulation model using the 3D velocity field available there, and the passage of the three vector quantities at each grid point, rather than the passage of as single current velocity vector as presently

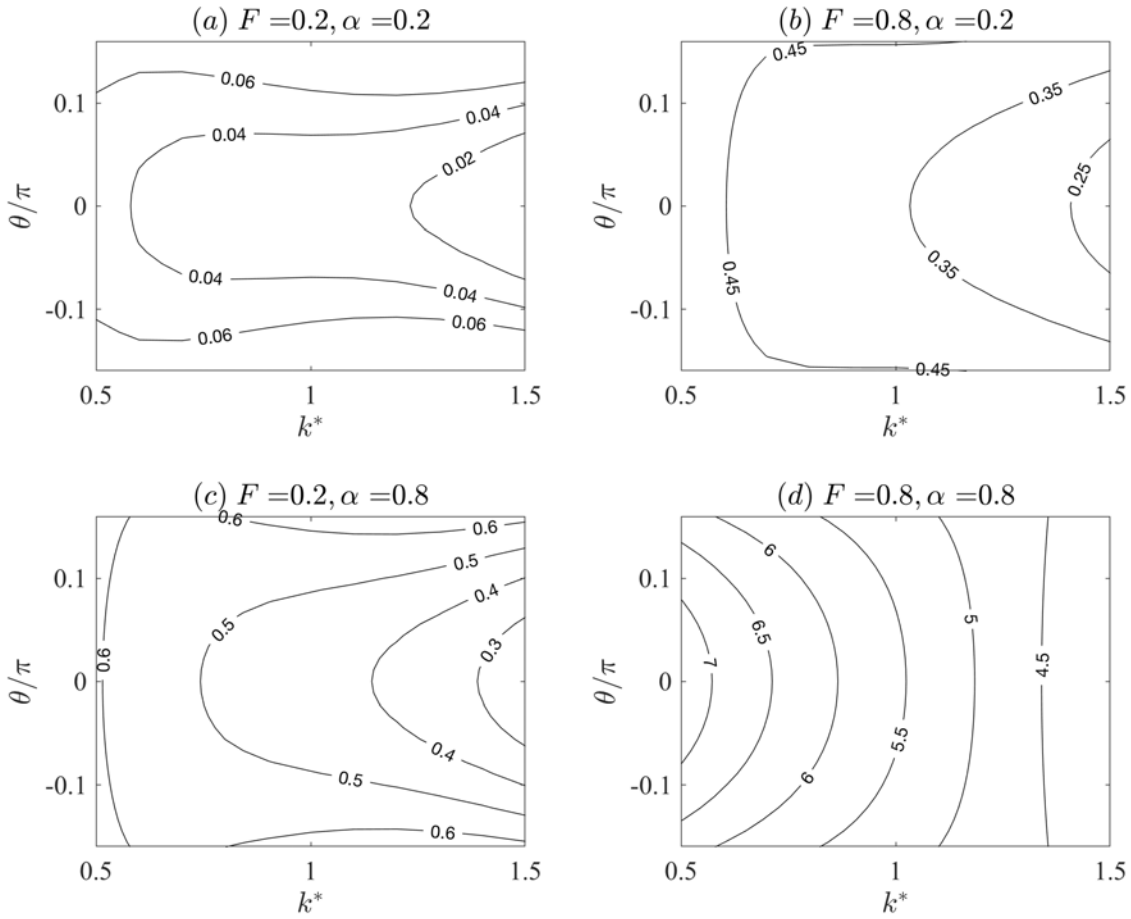

Figure 4.8: % error $100(1 - \tilde{\mathcal{N}}_T/\mathcal{N})$ in wave action density $\tilde{\mathcal{N}}_T$ for the Taylor series expansion about the peak wavenumber $\mathbf{k}^p$ with $k^* = k/k^p$: Constant shear current, $k^p h = 1$, $\beta = 0$.

implemented.

4.7 Discussion and Conclusions

4.7.1 Comparison to results of Quinn *et al.* (2017)

Despite the similarity in approach to developing approximations for action density and flux in this study and that of Quinn *et al.* (2017), the results are significantly different, as revealed in a comparison of the two results for the analytic case of a current with constant shear. For this case, $\mathbf{U}'' = 0$ simplifies the result for action density

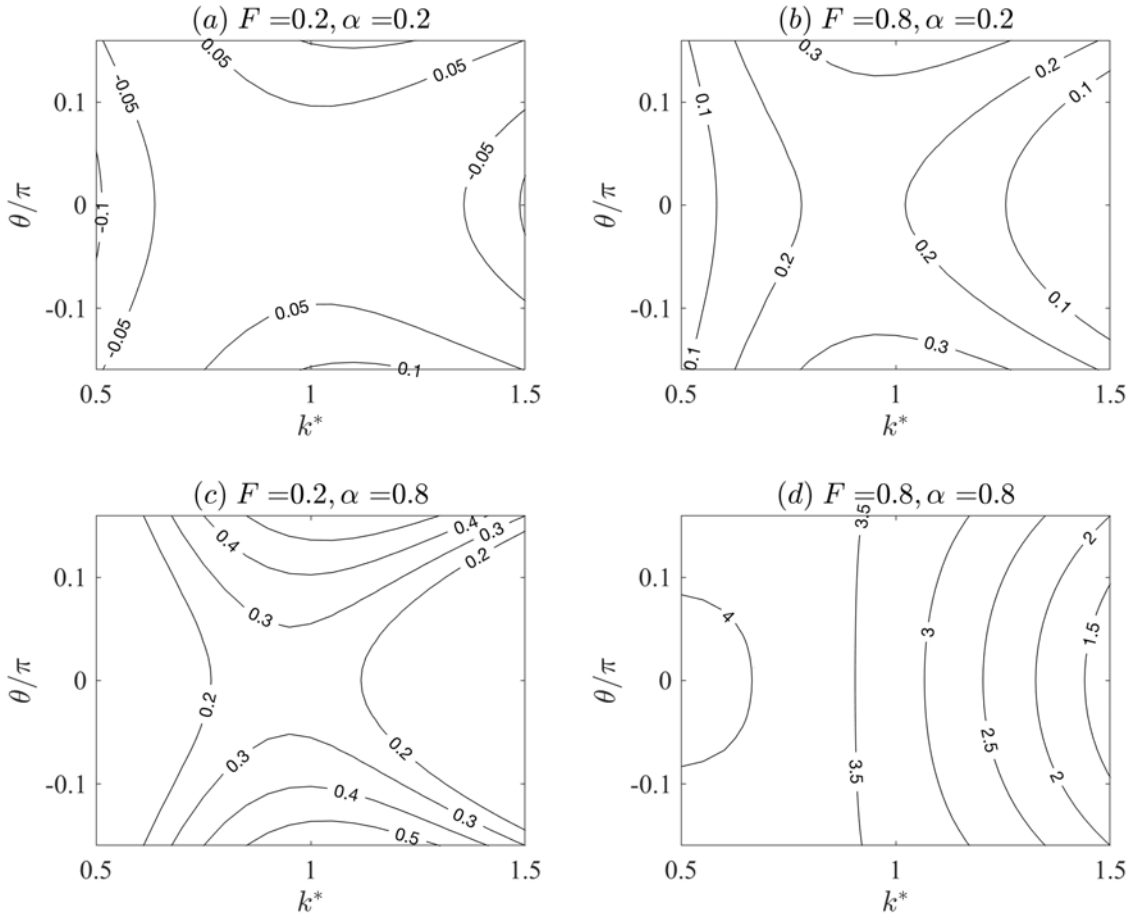

Figure 4.9: As in Figure 4.8: Constant shear current, $k^p h = 2$, $\beta = 0$.

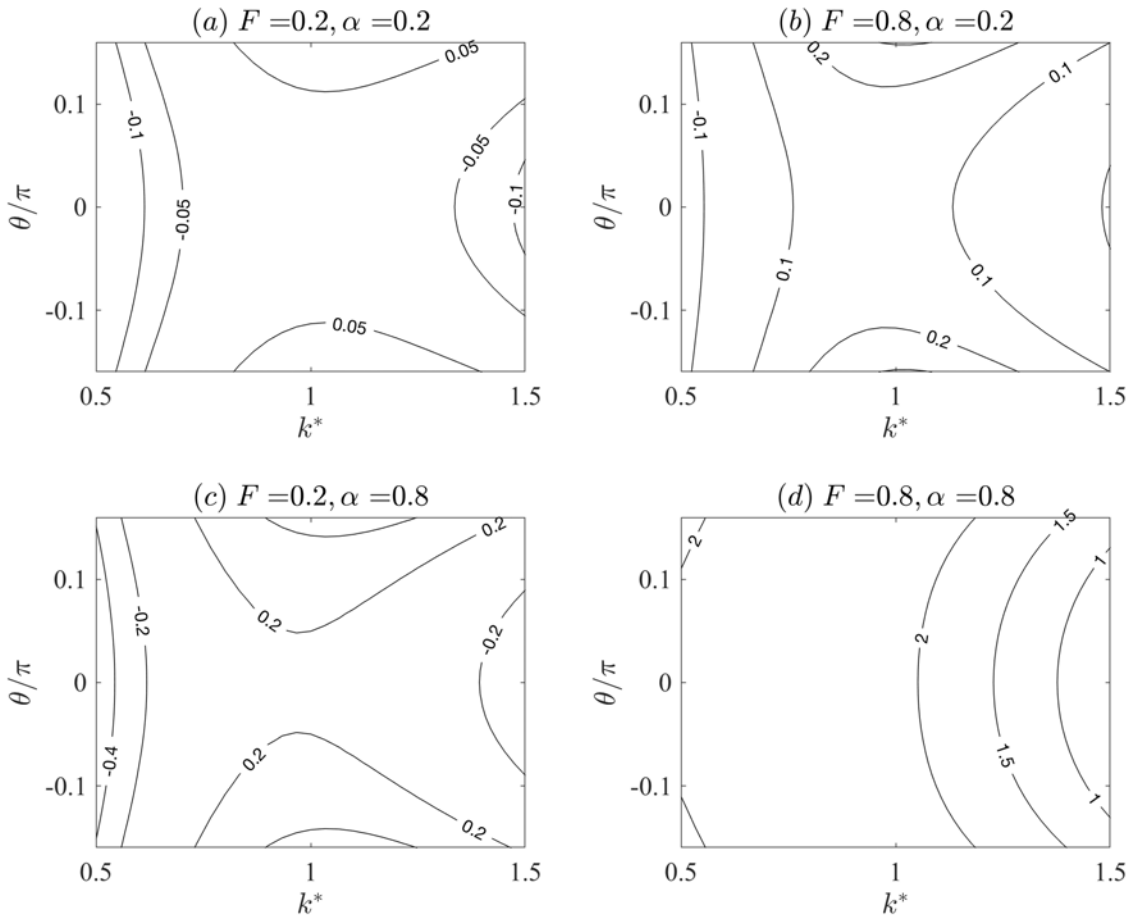

Figure 4.10: As in Figure 4.8: Constant shear current, $k^p h = 3$, $\beta = 0$.

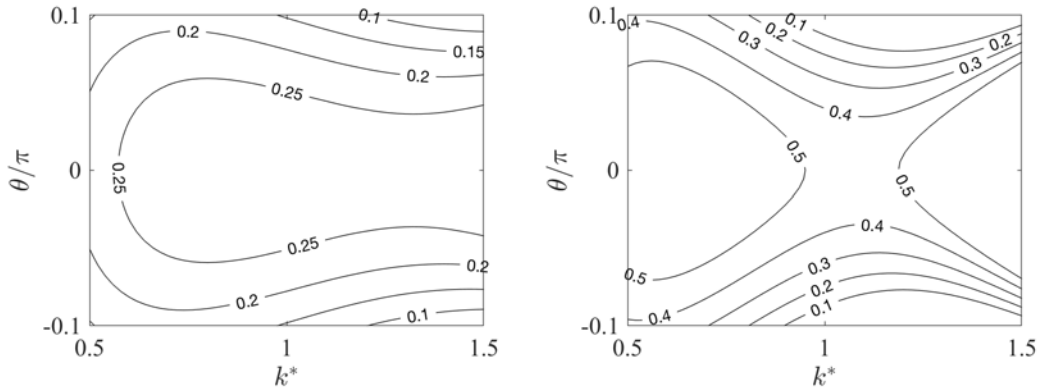

Figure 4.11: As in Figure 4.8: MCR current profile, $k^p h = 1$ (left) and $k^p h = 2$ (right), $\beta = 0$.

(4.2) in Quinn *et al.*. Their general result for action density is given by

$$\mathcal{N}^{Q17} = \frac{E_0}{\sigma_s}(1+\epsilon_5\mathcal{R}_1); \quad \mathcal{R}_1 = -2\mathcal{I}_2 \sinh kh - \frac{1}{c_0}\left(\frac{2}{\sinh 2kh}\mathcal{I}_3 + c_1\right) \tag{4.48}$$

we see that $\mathcal{I}_2 = 0$ from (4.4). Both terms $2\mathcal{I}_3(0)/\sinh 2kh$, evaluated directly and c_1 in the bracketed expression in $\mathcal{R}_1$ are equivalent to an expression $\hat{\mathbf{k}}\cdot\tilde{\mathbf{U}}$ as used here

For $z = 0$, it is also apparent that the first term in parentheses is the projection of the weighted average velocity, $\hat{\mathbf{k}}\cdot\tilde{\mathbf{U}}$, which follows directly from the definition (4.12) here and the expression for $\mathcal{I}_3$ as given in Quinn *et al.*'s (4.4). The evaluation of c_1 from (C.7) is more ambiguous. If $\mathcal{I}_1$ is interpreted as usual as the starting point for the definition of $\tilde{\mathbf{U}}$ after two integrations, then c_1 also is equal to $\hat{\mathbf{k}}\cdot\tilde{\mathbf{U}}$. This would then give an expression for $\mathcal{N}$ in our notation as

$$\mathcal{N}^{Q17} = \frac{E_0}{\sigma_s}\left[1 - \frac{2\mathbf{k}\cdot\tilde{\mathbf{U}}}{\tilde{\sigma}} + O(\epsilon^2)\right] \tag{4.49}$$

On the other hand, if the expression is taken literally for the constant shear case under development, then c_1 evaluates to $c_1 = \hat{\mathbf{k}}\cdot(\mathbf{U}_s - (c_0^2/2g)\mathbf{U}_{,z}(0))$, which referring to (4.38), is again the depth-weighted current for this special case, giving the expression (4.49) again. It is clear that this expression cannot be correct, as $\mathcal{N}^{Q17}$ would have to reduce to E_0/σ_s in the limit of a depth-uniform current, where $\tilde{\mathbf{U}} = \mathbf{U}_s$. We are thus not able to explain the discrepancies between our results written in terms of surface values, and the expressions provided by Quinn *et al.* (2017).

In contrast, the result obtained in the present study can be written as

$$\tilde{\mathcal{N}} = \frac{E_0}{\sigma_s}\left[1 - \frac{\mathbf{k}}{\tilde{\sigma}}\cdot(\mathbf{U}_s - \tilde{\mathbf{U}}) + O(\epsilon^2)\right] \tag{4.50}$$

Quinn *et al.* go on to suggest (below their (4.4)) that using the surface current in the estimate of action instead of depth-averaged current would be a reasonable no-cost extension in existing models. This suggestion corresponds to the results for $\mathcal{N}_s$ and

$\boldsymbol{\mathcal{F}}_s$ shown in the Supplement, Appendix C. From the results there, it is clear that the increase in accuracy afforded by using surface current instead of depth average current is apparent only for relatively short waves, whereas the proper use of the perturbation solution, or expansions based on that solution, is advantageous at all water depths.

In order to examine the relative predictions of the asymptotic forms (4.20) + (4.22) vs. (4.21) + (4.23), and to establish a basis for comparing our error estimates to a case examined by Quinn *et al.* (2017), we have repeated their analysis of a current profile given by Wu & Tsanis (1995) and presented in their Section 5 and Figures 1-4. The current profile is given by

$$U(z) = Au_* \ln(1 + \frac{z}{z_s}) + Bu_* \ln(1 - \frac{z}{z_b + h}) \tag{4.51}$$

in which

$$\begin{aligned} A &= \frac{q_2}{p_1 q_2 - q_1 p_2}; \qquad B = -\frac{q_1}{p_1 q_2 - q_1 p_2} \\ q_1 &= (1 + z_s/h)\ln(1 + h/z_s) - 1; \quad q_2 = z_s/h \ln(1 + h/z_b) - 1 \\ p_1 &= \gamma z_s/h; \qquad p_2 = \gamma z_s/z_b \end{aligned} \tag{4.52}$$

where z_b and z_s are characteristic viscous sublayer thicknesses at the bottom and surface respectively, and γ is a constant to characterize the intensity of the turbulence. The origin of the z-coordinate is located at the bottom for this velocity profile and the direction is upward. A lengthscale δ_s is taken to be the depth at which the current velocity falls to zero, and is used as the basis for a relative wavelength parameter $k\delta_s$ used in plots presented below and by Quinn *et al.*.

Figure 4.12 shows errors for action density $\tilde{\mathcal{N}}$ and flux $\tilde{\boldsymbol{\mathcal{F}}}$ using the asymptotic expressions (4.21) and (4.23) with variation of $k\delta_s$ and Froude number U_s/c_0. The axis has been modified to be in the same format as Quinn *et al.* (2017) figure 2 for comparison, however our Froude number is for a larger range $0 < U_s/c_0 < 1$, while they have only provided results for $0 < U_s/c_0 < 0.3$. Profile parameters are given

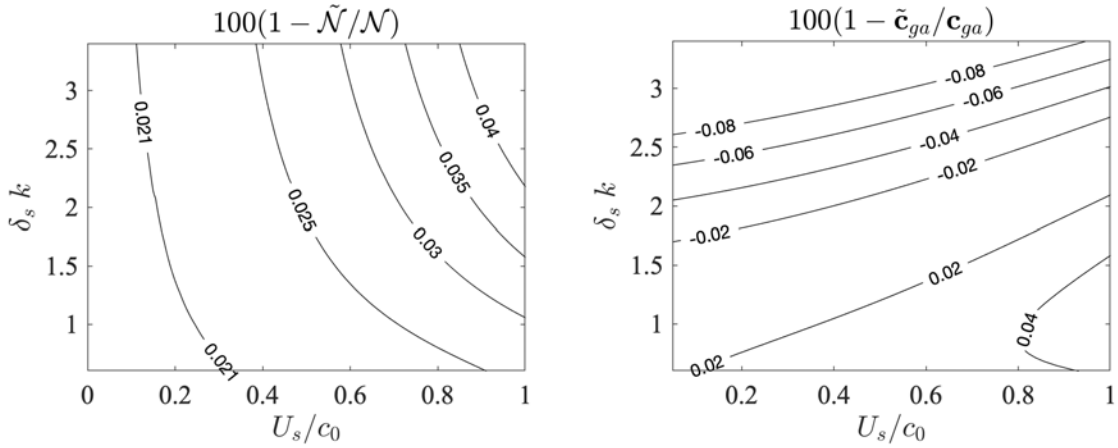

Figure 4.12: % error in estimates in action density $\tilde{\mathcal{N}}$ (left) and group velocity $\tilde{c}_{ga}$ (right), estimates for the case of Wu & Tsanis (1995) profile using the asymptotic expressions (4.21) and (4.23) in the frame of reference based on the depth-weighted current $\tilde{\mathbf{U}}$.

by $z_s = 2.2 \times 10^{-}4\, h$, $z_b = 1.4 \times 10^{-}4\, h$, $\gamma = 0.35$ and $h = 100\, m$. The thickness of the upper layer is $\delta_s = 0.34\, h$ in this case. Comparison between the results and the plots presented in their figure 2(a) and 2(d) demonstrate the accuracy gain in our approximation. Corresponding plots for our estimates $\mathcal{N}^*$ and $\mathbf{c}^*_{ga} = \boldsymbol{\mathcal{F}}^* / \mathcal{N}^*$ based on (4.20) and (4.22) are provided in Figure 4.13, and show a marked decrease in accuracy compared to the values $\tilde{\mathcal{N}}$ and $\tilde{\mathbf{c}}_{ga} = \tilde{\boldsymbol{\mathcal{F}}} / \tilde{\mathcal{N}}$ in spite of the demonstrated asymptotic equivalence of $\tilde{\mathcal{N}}$ and $\mathcal{N}^*$, with errors based on $\tilde{\mathcal{N}}$ and $\tilde{\boldsymbol{\mathcal{F}}}$ being up to 100 times smaller. We also note that our estimates for $\mathcal{N}^*$ and $\boldsymbol{\mathcal{F}}^*$ in the frame of reference based on the surface current is by far more accurate than the results shown in Quinn *et al.* (2017).

4.7.2 Conclusions

The results here clearly show that leading order asymptotic expressions for action density and flux are both more compact and more accurate numerically when written in terms of a depth-weighted current $\tilde{\mathbf{U}}$ and corresponding intrinsic frequency $\tilde{\sigma}$. The asymptotic expressions written in the form of (4.21) and (4.23), repeated here

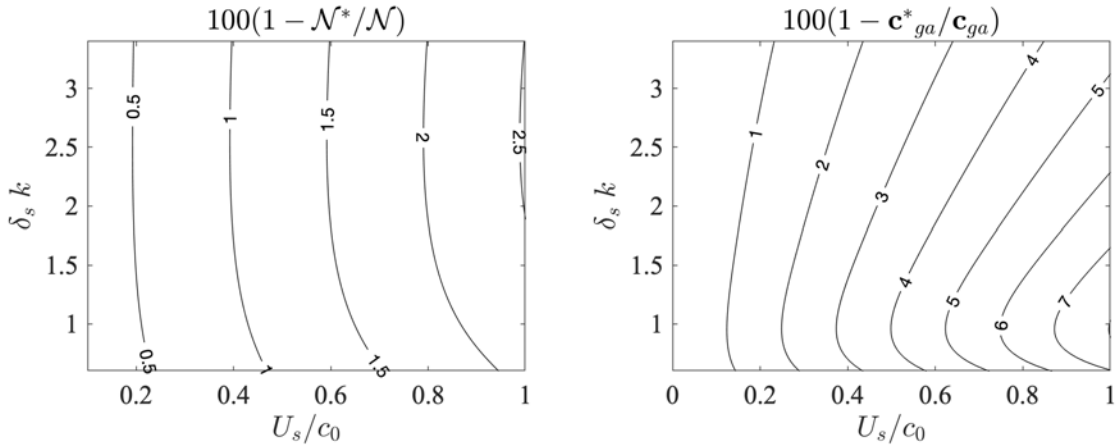

Figure 4.13: % error in estimates of action density $\mathcal{N}^*$ (left) and group velocity c^*_{ga} (right), estimates for the case of Wu & Tsanis (1995) profile using the asymptotic expressions (4.20) and (4.22) in the frame of reference based on the surface current.

as

$$\tilde{\mathcal{N}} = \frac{E_0}{\tilde{\sigma}} + O(\epsilon^2); \qquad \tilde{\boldsymbol{\mathcal{F}}} = \tilde{\mathcal{N}}(\hat{\mathbf{U}} + \tilde{c}_{gr}) + O(\epsilon^2) \tag{4.53}$$

defer the appearance of terms which are not in the standard form for action and flux to second order in the small parameter ϵ characterizing the weak shear in the depth-varying current profile. They provide a relatively more accurate estimate of the quantities in question than corresponding asymptotic forms (4.21) and (4.23) based on surface current U_s when compared to "exact" values obtained analytically or numerically, as shown for the analytic example of a current with constant shear in section 4, and for the strongly sheared profile of Wu & Tsanis (1995) in section 4.7.1.

We have further extended the suggestion of BKD17 to represent current information using a Taylor expansion around the peak wave number in a modeled spectrum, with extensions covering the specification of action, flux and intrinsic frequency as well as an extension to a general 2D horizontal setting. These results provide an avenue for calculating wave action and action flux in spectral wave models, using a compact set of information about the current field evaluated at the spectral peak wave number. The coupling would require that the wave model accept the values $\tilde{\mathbf{U}}, \hat{\mathbf{U}}$ and $\hat{\mathbf{U}}_{,k}$ at

each grid point, and corresponding changes would need to be made to the specification of action density and group velocity as a function of frequency and direction within the wave model formulation. These are not huge changes, and hopefully can be implemented in the near future. The corresponding effects on model source terms, such as the representation of nonlinear interactions, is still an open area for research.

Chapter 5

THE COUPLED NHWAVE/SWAN MODEL ($NH\overline{WAVE}$)

The wave-current interaction theory for waves propagating on a strongly sheared current has been presented in Chapter 2. The wave-averaged forces in the mean flow momentum equation are given in terms of the Craik-Leibovich vortex force formalism. The coupling of a wave-averaged version of the NHWAVE (Ma *et al.*, 2012) non-hydrostatic circulation model with the SWAN wave model has been recently developed by Dong (2016) (DK16), including both the vortex force formulation of McWilliams *et al.* (2004)(MRL04) and DK16 formulation based on strong currents with arbitrary shear. In this chapter we will study the application of the wave-current interaction theory by MRL04 in the circulation model $NHWAVE$ in studying the effect of non-breaking wave effects on current profiles. We will initially provide an introduction to the model $NH\overline{WAVE}$ and follow by presenting the numerical results of a test case of wave-current interaction in a laboratory flume studied by Kemp & Simons (1982).

5.1 Introduction to $NH\overline{WAVE}$

5.1.1 NHWAVE Model

A non-hydrostatic model (NHWAVE) for simulating dispersive free-surface hydrodynamics has been developed by Ma (2012). The model solves the incompressible Reynolds-averaged Navier-Stokes equations in surface and terrain-following form using a σ-coordinate transformation. A hybrid finite-volume and finite-difference scheme is adopted to discretize the equations. A different staggered grid framework is introduced, in which the velocity is at the cell center and the pressure is at the cell

vertical face. Thus the pressure boundary condition at the free surface can be precisely imposed. A shock-capturing Godunov-type scheme is used to solve the momentum equations. Bottom movement is considered in order to simulate the underwater landslide-generated tsunamis. The hydrostatic equations are solved by a well-balanced finite volume method. The fluxes at cell faces are estimated by HLL Riemann approximation. To obtain the second-order temporal accuracy, the nonlinear Strong Stability-Preserving (SSP) Runge-Kutta scheme is adopted for adaptive time stepping Gottlieb *et al.* (2001). The model is parallelized using the Message Passing Interface (MPI). The high performance pre-conditioner HYPRE software library is used to solve the Poisson equation (http://acts.nersc.gov/hypre/).

5.1.1.1 Governing equations

Here we will present the governing equations implemented in the phase averaged version of NHWAVE. In chapter 2 we separated the mean current and wave motions by defining the mean current variables with an overline and the wave part with tilde. The governing equations in this section correspond to the mean flow motions and we have omitted the overline for simplicity. All values hence correspond to the mean flow characteristics.

The σ coordinate (x, y, σ,t) is introduced in vertical direction. The relation between z coordinate and σ coordinates is linear.

$$\sigma = \frac{z^* + h}{d} \tag{5.1}$$

where d is defined as the total water depth as:

$$d = \overline{\eta} + h \tag{5.2}$$

with $\overline{\eta}$ being the mean water surface elevation including wave setup/setdown. σ ranges from 0 at the bottom ($z = -h$) to 1 at the surface ($z = \bar{\eta}$). Now any variable f^*

in the Cartesian coordinates can be transformed to the corresponding variable f in σ-coordinates.

$$f^*(x^*, y^*, z^*, t^*) = f(x, y, \sigma, t) \tag{5.3}$$

The vertical coordinate σ can be treated as a variable in Cartesian coordinates.

$$\sigma = \sigma(x^*, y^*, z^*, t^*) \tag{5.4}$$

Since there is no change in the horizontal and temporal coordinates in the transformation, let $x = x^*$,$y = y^*$,$t = t^*$. Considering the transition between derivatives of $\sigma(x^*, y^*, z^*, t^*)$ and $z^*(x, y, \sigma, t)$, the derivatives of variable f in Cartesian coordinates now become

$$\frac{\partial f^*}{\partial t^*} = \frac{\partial f}{\partial t} + \frac{\partial f}{\partial \sigma}(\frac{1}{d}\frac{\partial h}{\partial t} - \frac{\sigma}{d}\frac{\partial d}{\partial t}) \tag{5.5}$$

$$\frac{\partial f^*}{\partial x^*} = \frac{\partial f}{\partial x} + \frac{\partial f}{\partial \sigma}(\frac{1}{d}\frac{\partial h}{\partial x} - \frac{\sigma}{d}\frac{\partial d}{\partial x}) \tag{5.6}$$

$$\frac{\partial f^*}{\partial y^*} = \frac{\partial f}{\partial y} + \frac{\partial f}{\partial \sigma}(\frac{1}{d}\frac{\partial h}{\partial y} - \frac{\sigma}{d}\frac{\partial d}{\partial y}) \tag{5.7}$$

$$\frac{\partial f^*}{\partial z^*} = \frac{\partial f}{\partial \sigma}\frac{1}{d} \tag{5.8}$$

We define the vertical velocity ω in σ-coordinates.

$$\omega = d\frac{d\sigma}{dt^*} = d(\frac{\partial \sigma}{\partial t^*} + u\frac{\partial \sigma}{\partial x^*} + v\frac{\partial \sigma}{\partial y^*} + w\frac{\partial \sigma}{\partial z^*}) \tag{5.9}$$

ω is related to the vertical velocity w in Cartesian coordinates.

$$\omega = w - \frac{\partial z^*}{\partial t} - u\frac{\partial z^*}{\partial x} - v\frac{\partial z^*}{\partial y} \tag{5.10}$$

The continuity equation in σ-coordinates is expressed as

$$\frac{\partial d}{\partial t} + \frac{\partial du}{\partial x} + \frac{\partial dv}{\partial y} + \frac{\partial \omega}{\partial \sigma} = 0 \tag{5.11}$$

The depth-integral of the continuity equation yields

$$\frac{\partial d}{\partial t} + \frac{\partial}{\partial x}(d\int_0^1 u d\sigma) + \frac{\partial}{\partial y}(d\int_0^1 v d\sigma) = 0 \tag{5.12}$$

We separate the pressure terms into hydrostatic and non-hydrostatic pressure

$$p = q + \rho g(\overline{\eta} - z^*) + P \tag{5.13}$$

where P is the wave induced surface pressure as defined in equation 5.26. This term is added to the Bernoulli head which will result in a modified Bernoulli head ($\hat{\kappa}$) as defined in equation 5.25 and a modified boundary condition for the dynamic pressure at the surface

$$q(\overline{\eta}) = 0 \tag{5.14}$$

Finally, we obtain the momentum equations after adding the Reynolds stress terms and wave averaged forces in both x and y directions as

$$\begin{aligned}\frac{\partial du}{\partial t} + \frac{\partial}{\partial x}(duu + \frac{1}{2}gd^2) + \frac{\partial duv}{\partial y} + \frac{\partial u\omega}{\partial \sigma} &= gd\frac{\partial h}{\partial x} - \frac{d}{\rho}(\frac{\partial q}{\partial x} + \frac{\partial q}{\partial \sigma}\frac{\partial \sigma}{\partial x^*}) + dS_{\tau x} \\ &- d(\frac{\partial \kappa}{\partial x} + \frac{\partial \kappa}{\partial \sigma}\frac{\partial \sigma}{\partial x^*}) + dJ_x \end{aligned} \tag{5.15}$$

$$\begin{aligned}\frac{\partial dv}{\partial t} + \frac{\partial dvu}{\partial x} + \frac{\partial}{\partial y}(dvv + \frac{1}{2}gd^2) + \frac{\partial v\omega}{\partial \sigma} &= gd\frac{\partial h}{\partial y} - \frac{d}{\rho}(\frac{\partial q}{\partial y} + \frac{\partial q}{\partial \sigma}\frac{\partial \sigma}{\partial y^*}) + dS_{\tau y} \\ &- d(\frac{\partial \kappa}{\partial y} + \frac{\partial \kappa}{\partial \sigma}\frac{\partial \sigma}{\partial y^*}) + dJ_y \end{aligned} \tag{5.16}$$

The σ-direction momentum equation

$$\begin{aligned}\frac{\partial dw}{\partial t} + \frac{\partial dwu}{\partial x} + \frac{\partial dwv}{\partial y} + \frac{\partial w\omega}{\partial \sigma} &= -\frac{1}{\rho}\frac{\partial q}{\partial \sigma} + dS_{\tau z} \\ &- d\frac{\partial \kappa}{\partial \sigma} + dK \end{aligned} \tag{5.17}$$

The wave-averaged surface boundary condition is given by

$$w|_{\bar{\eta}} = \frac{\partial \bar{\eta}}{\partial t} + u|_{\bar{\eta}} \frac{\partial \bar{\eta}}{\partial x} + v|_{\bar{\eta}} \frac{\partial \bar{\eta}}{\partial y} + \nabla_h \cdot \mathbf{U}^{st} \tag{5.18}$$

The divergence of the depth-integrated Stokes drift $\nabla_H \cdot \mathbf{U}^{st}$ appears on the RHS of the kinematic surface boundary condition as a wave-induced mass source/sink term Hasselmann (1971). The Stokes drift expressions are defined as

$$\mathbf{u}^{st} = \frac{a^2 \sigma_w \mathbf{k}}{2 \sinh^2 kd} \cosh 2k(z+h) \tag{5.19}$$

$$\mathbf{U}^{st}(z) = \frac{a^2 \sigma_w \mathbf{k}}{4k \sinh^2 kh} \sinh 2kd = \frac{E}{\rho c} \frac{\mathbf{k}}{k} = \frac{N}{\rho} \mathbf{k} \tag{5.20}$$

$$w^{st}(z) = -\nabla_H \cdot \int_{-h}^{z} \mathbf{u}^{st} dz' \tag{5.21}$$

where a is the wave amplitude; $\mathbf{k}$ is its wave number vector and k is its magnitude and σ_w is the intrinsic frequency (not to be confused with the σ coordinate in NHWAVE). These wave characteristics are provided either through the passage of data for the peak frequency from the wave model SWAN or as an input to NHWAVE without the need to run the wave model for monochromatic waves.

The wave vortex force $(\mathbf{J}, K)$and Bernoulli head κ from MRL04 presented in Chpater 4 are re-written in σ-coordinates as:

$$J_x = v^{st}\chi - \frac{w^{st}}{d} \frac{\partial u}{\partial \sigma} \tag{5.22}$$

$$J_y = -u^{st}\chi - \frac{w^{st}}{d} \frac{\partial v}{\partial \sigma} \tag{5.23}$$

$$K = \frac{u^{st}}{d} \frac{\partial u}{\partial \sigma} + \frac{v^{st}}{d} \frac{\partial v}{\partial \sigma} \tag{5.24}$$

$$\hat{\kappa} = \frac{{\sigma_w}^2 a^2}{4} \frac{\cosh 2kd\sigma}{\sinh^2 kd} + \frac{\sigma_w a^2}{4k \sinh^2 kd} [-(\frac{k_x}{d} \frac{\partial u}{\partial \sigma}|_{-h} + \frac{k_y}{d} \frac{\partial v}{\partial \sigma}|_{-h}) \sinh 2kd\sigma + 2k \int_0^{\sigma} \frac{\partial (\mathbf{k} \cdot \mathbf{u})}{\partial \sigma'} \cosh 2kd(\sigma - \sigma') d\sigma'] + \frac{1}{\rho} P \tag{5.25}$$

P is the wave induces surface pressure defined as:

$$\begin{aligned} P &= -\rho\frac{{\sigma_w}^2 a^2}{2} - \rho\frac{gka^2\tanh kd}{\sigma_w}\Big(\frac{2k}{\sinh 2kd}\int_0^1 (\mathbf{k}\cdot\mathbf{u})\cosh 2k(d(\sigma-1))dz \\ &\quad -[(\mathbf{k}\cdot\mathbf{u})|_{\overline{\eta}} + (\mathbf{k}\cdot\mathbf{u})|_{-h}]\Big) \end{aligned} \tag{5.26}$$

The 3D momentum equations in $NH\overline{\text{WAVE}}$ are

$$\frac{\partial \mathbf{U}}{\partial t} + \frac{\partial \mathbf{F}}{\partial x} + \frac{\partial \mathbf{G}}{\partial y} + \frac{\partial \mathbf{H}}{\partial \sigma} = \mathbf{S_h} + \mathbf{S_p} + \mathbf{S_w^{(1)}} + \mathbf{S_w^{(2)}} + \mathbf{S}_\tau \tag{5.27}$$

$$\mathbf{U} = (du, dv, dw)^T \tag{5.28}$$

$$\mathbf{F} = (duu + \frac{1}{2}gd^2, duv, duw)^T \tag{5.29}$$

$$\mathbf{G} = (dvu, dvv + \frac{1}{2}gd^2, dvw)^T \tag{5.30}$$

$$\mathbf{H} = (\omega u, \omega v, \omega w)^T \tag{5.31}$$

$$\mathbf{S_h} = (gd\frac{\partial h}{\partial x}, gd\frac{\partial h}{\partial y}, 0)^T \tag{5.32}$$

$$\mathbf{S_p} = (-\frac{d}{\rho}(\frac{\partial q}{\partial x} + \frac{\partial q}{\partial \sigma}\frac{\partial \sigma}{\partial x^*}), -\frac{d}{\rho}(\frac{\partial q}{\partial y} + \frac{\partial q}{\partial \sigma}\frac{\partial \sigma}{\partial y^*}), -\frac{1}{\rho}\frac{\partial q}{\partial \sigma})^T \tag{5.33}$$

$$\mathbf{S_w^{(1)}} = (-d(\frac{\partial \hat{\kappa}}{\partial x} + \frac{\partial \hat{\kappa}}{\partial \sigma}\frac{\partial \sigma}{\partial x^*}), -d(\frac{\partial \hat{\kappa}}{\partial y} + \frac{\partial \hat{\kappa}}{\partial \sigma}\frac{\partial \sigma}{\partial y^*}), -\frac{\partial \hat{\kappa}}{\partial \sigma})^T \tag{5.34}$$

$$\mathbf{S_w^{(2)}} = (dJ_x, dJ_y, dK)^T \tag{5.35}$$

$$\mathbf{S}_\tau = (dS_{\tau x}, dS_{\tau y}, dS_{\tau z})^T \tag{5.36}$$

$$S_{\tau x} = \frac{\partial \tau_{xx}}{\partial x} + \frac{\partial \tau_{xx}}{\partial \sigma}\frac{\partial \sigma}{\partial x^*} + \frac{\partial \tau_{xy}}{\partial y} + \frac{\partial \tau_{xy}}{\partial \sigma}\frac{\partial \sigma}{\partial y^*} + \frac{\partial \tau_{xz}}{\partial \sigma}\frac{\partial \sigma}{\partial z^*} \tag{5.37}$$

$$S_{\tau y} = \frac{\partial \tau_{yx}}{\partial x} + \frac{\partial \tau_{yx}}{\partial \sigma}\frac{\partial \sigma}{\partial x^*} + \frac{\partial \tau_{yy}}{\partial y} + \frac{\partial \tau_{yy}}{\partial \sigma}\frac{\partial \sigma}{\partial y^*} + \frac{\partial \tau_{yz}}{\partial \sigma}\frac{\partial \sigma}{\partial z^*} \tag{5.38}$$

$$S_{\tau z} = \frac{\partial \tau_{zx}}{\partial x} + \frac{\partial \tau_{zx}}{\partial \sigma}\frac{\partial \sigma}{\partial x^*} + \frac{\partial \tau_{zy}}{\partial y} + \frac{\partial \tau_{zy}}{\partial \sigma}\frac{\partial \sigma}{\partial y^*} + \frac{\partial \tau_{zz}}{\partial \sigma}\frac{\partial \sigma}{\partial z^*} \tag{5.39}$$

where τ_{ij} with $(i,j) = x, y, z$ is the turbulence stress defined as

$$\tau_{xx} = 2\nu_t(\frac{\partial u}{\partial x} + \frac{\partial u}{\partial \sigma}\frac{\partial \sigma}{\partial x^*}) \tag{5.40}$$

$$\tau_{yy} = 2\nu_t(\frac{\partial v}{\partial y} + \frac{\partial v}{\partial \sigma}\frac{\partial \sigma}{\partial y^*}) \tag{5.41}$$

$$\tau_{zz} = 2\nu_t(\frac{\partial w}{\partial \sigma}\frac{\partial \sigma}{\partial z^*}) \tag{5.42}$$

$$\tau_{xy} = \tau_{yx} = \nu_t(\frac{\partial u}{\partial y} + \frac{\partial u}{\partial \sigma}\frac{\partial \sigma}{\partial y^*} + \frac{\partial v}{\partial x} + \frac{\partial v}{\partial \sigma}\frac{\partial \sigma}{\partial x^*}) \tag{5.43}$$

$$\tau_{xz} = \tau_{zx} = \nu_t(\frac{\partial u}{\partial \sigma}\frac{\partial \sigma}{\partial z^*} + \frac{\partial w}{\partial x} + \frac{\partial w}{\partial \sigma}\frac{\partial \sigma}{\partial x^*}) \tag{5.44}$$

$$\tau_{yz} = \tau_{zy} = \nu_t(\frac{\partial v}{\partial \sigma}\frac{\partial \sigma}{\partial z^*} + \frac{\partial w}{\partial y} + \frac{\partial w}{\partial \sigma}\frac{\partial \sigma}{\partial y^*}) \tag{5.45}$$

ν_t is turbulent viscosity which has to be defined by the turbulence closure method of choice in NHWAVE. $\mathbf{S_w^{(1)}}$ is wave-induced Bernoulli head gradient. $\mathbf{S_w^{(2)}}$ is wave vortex force. $\mathbf{S_p}$ accounts for mean flow and long wave dynamic pressure. These forces are the conservative wave forcing terms. In case of breaking waves, non-conservative wave forces should be added to the equations. Since our study is focused on non-breaking waves we have not included these forces in the above equations. They can easily be added as discussed in Chapter 5 of DK16.

5.1.1.2 Boundary Conditions

In NHWAVE, boundary conditions are required to solve the governing equations. At the free surface, the continuity of normal and tangential stresses are enforced. Without wind stress, the tangential stress equals zero. If we assume that the mean water surface is never steep or wavy and neglect $\partial\sigma/\partial x^*$ and $\partial\sigma/\partial y^*$ terms in higher order derivatives Derakhti *et al.* (2016), the surface boundary condition can be written as

$$\frac{\partial u}{\partial \sigma}|_{z=\eta} = \frac{\partial v}{\partial \sigma}|_{z=\eta} = 0 \tag{5.46}$$

At the bottom, the tangential stress and normal velocity are prescribed. The normal velocity w includes the change rate of bottom with time to generate landslide.

$$w|_{z=-h} = -\frac{\partial h}{\partial t} - u\frac{\partial h}{\partial x} - v\frac{\partial h}{\partial y} \tag{5.47}$$

For the horizontal velocities, either free-slip boundary conditions

$$\frac{\partial u}{\partial \sigma}|_{z=-h} = \frac{\partial v}{\partial \sigma}|_{z=-h} = 0 \tag{5.48}$$

or bottom shear stresses are considered

$$\frac{\tau_{bot}}{\rho} = \nu_t \frac{1}{D}\frac{\partial \mathbf{u}}{\partial \sigma}|_{z=-h} = c_d|\mathbf{u}_b|\mathbf{u}_b \tag{5.49}$$

where c_d is the bottom drag coefficient and $\mathbf{u}_b$ is near bed current velocity. In the presence of waves, the wave motions enhance the bottom stress τ_{bot} (Soulsby, 1995). ν_t is determined by τ_{bot}.

$$\tau_{bot} = \tau_c[1.0 + 1.2(\frac{|\tau_w|}{|\tau_w| + |\tau_c|})^{3.2}] \tag{5.50}$$

$$\tau_c = \rho[\frac{\kappa}{\ln(z_m/z_0)}]^2|\mathbf{u}|\mathbf{u} \tag{5.51}$$

$$|\tau_w| = \frac{1}{2}\rho f_w|\tilde{\mathbf{u}}_{orb}|^2 \tag{5.52}$$

where $\tau_\mathbf{c}$ and τ_w are bottom stresses due to current and waves, respectively. κ is the von Karman constant; z_0 is the bed roughness; z_m is a reference depth above the bed, nominally equivalent to a half bottom-most grid cell height; $f_w = 1.39(\sigma_w z_0/|\tilde{\mathbf{u}}_{orb}|)^{0.52}$ is the wave friction factor given by Soulsby (1995). $|\tilde{\mathbf{u}}_{orb}| = \sigma_w a/(\sinh kd)$ is the bottom wave orbital velocity.

The Neumann boundary condition is used for getting the dynamic pressure,

which is directly obtained from the vertical momentum equation.

$$\frac{\partial q}{\partial \sigma}|_{z=-h} = -\rho d \frac{dw}{dt}|_{z=-h} \tag{5.53}$$

where w is given by the bottom boundary condition.

5.1.1.3 Turbulence Model

An appropriate turbulence model is needed. The Smagorinsky subgrid and $k-\epsilon$ models are commonly used turbulence models,depending on the grid resolution. Having relatively larger grid sizes, in this study, the nonlinear $k-\epsilon$ model is applied to simulate the turbulence generated by sheared current. The equations are given by

$$\begin{aligned}
\frac{\partial d k^{tur}}{\partial t} + \nabla\cdot(d\mathbf{u}_m k^{tur}) &= \nabla\cdot[d(\nu + \frac{\nu_t}{\sigma_k})\nabla k^{tur}] + d(P_s + P_b - \epsilon^{tur}) && (5.54)\\
\frac{\partial d \epsilon^{tur}}{\partial t} + \nabla\cdot(d\mathbf{u}_m \epsilon^{tur}) &= \nabla\cdot[d(\nu + \frac{\nu_t}{\sigma_\epsilon})\nabla \epsilon^{tur}] \\
&+ \frac{\epsilon^{tur}}{k^{tur}} d(C_{1\epsilon}P_s + C_{3\epsilon}P_b - C_{2\epsilon}\epsilon^{tur}) && (5.55)
\end{aligned}$$

where $\mathbf{u}_m$ is the mixture fluid phase velocity considering both liquid and bubble. k^{tur} is turbulent kinetic energy, ϵ^{tur} is turbulent dissipation rate, $\sigma_k = 1.0, \sigma_\epsilon = 1.3, C_{1\epsilon} = 1.44, C_{2\epsilon} = 1.92, C_{3\epsilon} = -1.4$ are empirical coefficients (Rodi, 1980). P_s is the shear production and P_b is the buoyancy production, which are described as

$$\begin{aligned}
P_s &= -\overline{u'_i u'_j}\frac{\partial u_i}{\partial x^*_j} && (5.56)\\
P_b &= -\frac{1}{\rho_0} g \nu_t \frac{\partial \rho_m}{\partial z} && (5.57)
\end{aligned}$$

where the Reynolds stress $u'_i u'_j$ is calculated by a nonlinear model proposed by Lin & Liu (1998). ρ_0 is the reference density of the incompressible liquid, and ρ_m is the mixture fluid phase density. In case of friction in the boundaries the kinetic energy is

imposed. The pertinent value is obtained by applying local equilibrium between production and dissipation of kinetic energy. This leads to Dirichlet boundary conditions

$$k^{tur}|_b = \frac{{u_*}^2}{\sqrt{c_\mu}} \quad , \epsilon^{tur}|_b = \frac{{u_*}^3}{\kappa z_b} \tag{5.58}$$

where κ is the Von Karman constant, z_b is the distance from the bed, and u_* is the friction velocity defined as the square root of bottom stress τ_{bot}/ρ (5.49).

5.1.2 Wave model SWAN

The calculation of the wave-averaged driving forces in the momentum equations requires wave properties such as wave height, wave direction, wave length and wave energy dissipation. Wave period and bottom orbital velocity are needed for wave-averaged bottom stress. In the coupled numerical model, these variables can be either obtained from the third-generation numerical wave model SWAN (Simulating Waves Nearshore) (Booij *et al.*, 1999) for spectral waves or as an input for monochromatic waves. The SWAN model governing equation is the wave action conservation equation for each discrete spectral component, which accounts for wave refraction by bathymetry and ambient currents. The model is driven by local winds and boundary data. Physical processes such as wind generation, white-capping, bottom dissipation and quadruplet wave-wave interactions are explicitly represented. Depth-induced wave breaking and triad wave-wave interactions are also included. The numerical propagation scheme is implicit. In SWAN, wave propagation is described using the two-dimensional wave action density spectrum $N(\sigma_w, \theta)$, where σ_w is wave intrinsic (relative) frequency and θ is wave direction. The reason to use the wave action as the computing property is because wave energy density is no longer conserved in the presence of the slowly varying ambient current Bretherton & Garrett (1968). Therefore the evolution of wave action spectrum is described in the Cartesian coordinates Hasselmann (1973).

$$\frac{\partial N}{\partial t} + \frac{\partial}{\partial x}(c_x N) + \frac{\partial}{\partial y}(c_y N) + \frac{\partial}{\partial \sigma_w}(c_\sigma N) + \frac{\partial}{\partial \theta}(c_\theta N) = \frac{S}{\sigma_w} \tag{5.59}$$

The first term on the LHS is the local changing rate of wave action density with time. The second and the third term account for the wave action density propagation in horizontal space. The fourth term stands for the shifting of the intrinsic frequency due to the variations in bathymetry and ambient currents. The fifth term represents wave refraction induced by varying bathymetry and currents. Both the wave action density and the propagation speeds in SWAN are based on linear wave theory. The term S on the RHS contains all the source terms such as wind-generation, dissipation and nonlinear wave-wave interactions. The introduction to each source term included in SWAN is given by Booij *et al.* (1999).

5.2 Interaction of currents with non-breaking waves

The correct modelling of interaction of waves and currents is of great importance for a good prediction of the vertical structure of the mean flow field. Horizontal and vertical velocities, as well as shear stresses, depend strongly on the interactions of waves and currents. The vertical profiles of these variables are modified, and the changes can effect bed friction, vertical mixing and horizontal dispersion/transport of dissolved or suspended mass in coastal seas.

Experiments designed to evaluate these modifications have shown that the near-surface velocity of an otherwise uniform current is reduced by following waves and increased by opposing waves. Kemp & Simons (1982, 1983) carried out laboratory experiments in a flume with rough and smooth beds, and with waves on following and opposing currents. They observed that when waves were following the current, the mean horizontal velocity reached a maximum value at a level between the bottom boundary layer and the wave trough. On the other hand, when waves were opposing the current, the mean horizontal velocity reached a maximum at the free surface which is higher than the value observed with the logarithmic profile for a current-only case. The reader is also referred to the references therein for a discussion of previous experiments. Similar results were obtained by Klopman (1994) in a series of experiments in a wave flume with a rough bed. His measurements included both the mean horizontal velocity

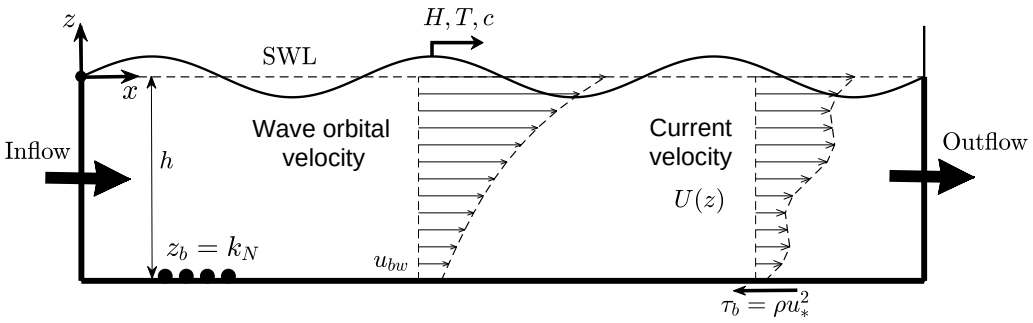

Figure 5.1: Definition sketch of wave propagation over underlying current of arbitrary profile

and the horizontal-velocity amplitude for regular and irregular waves with (i) waves opposing currents, (ii) waves following currents, (iii) only waves, and (iv) only currents. In the case of only currents, more detailed observations were made, including shear and normal stresses. The observed velocity shear is in agreement with the conclusions of Kemp & Simons (1982, 1983).

Experimentally, this decrease of the near surface velocity is opposite to the increase of velocity due to breaking waves, propagating with the current. Hence, in a three dimensional flow model the effect of breaking and non breaking waves can not be modelled with the same mathematical formulation. For the change of near surface velocity due to non-breaking waves in a laboratory flume, an explanation is needed.

Major studies have analyzed the interaction of waves and currents by analytical and numerical models. Analytical approaches consider a 1D wave-current interaction problem in which the vertical structure of the combined flow is solved relying on the concept of a simple vertical turbulence structure. The work of Grant & Madsen (1979) follows this approach, stating that the influence of waves on steady currents above the wave boundary layer can be parametrized by an apparent increase in the roughness experienced by the current. Additional examples of simplified wave boundary models include Christoffersen & Jonsson 1985; You 1996; Nielsen & You 1997; Huang & Mei 2003; Yang *et al.* 2006. Numerical simulations accommodate more sophisticated models

of the primitive equations. Dingemans *et al.* (1996) attributed the wave-induced change of the Eulerian mean velocity to Langmuir circulation induced by the lateral boundaries of the wave tank. The results of their three-dimensional computations based on a $k-\epsilon$ model agree reasonably well with the measurement of Klopman (1994) only for waves following, but not opposing currents. Allowing the current to be as strong as the phase velocity of waves, Groeneweg & Klopman (1998) treated the two-dimensional problem by combining the method of generalized Lagrangian mean (GLM) and a numerical turbulence model. By an empirical estimate of the eddy viscosity and numerical computations, they found good agreement between the computed and measured profiles of the longitudinal velocity for both flowing and opposing currents of Klopman (1994). Since the original experiment of Klopman (1994) only provided measurements in the center-line of the flume and not in the whole cross section, Klopman conducted additional tests in the same wave-current flume of the 1994 experiment in 1997 in order to determine the occurrence and strength of the secondary flow under waves following and opposing the current. Both results for waves following and opposing the current were in good agreement with the predictions form CL vortex force theory. According to the CL vortex force mechanism two counter-rotating secondary circulation cells are generated, anti symmetric with regard to the vertical center plane along the flume axis. For waves following the current the water flows upward near the side walls, to the center at the free surface and is down-welling at the center of the flume. The opposite occurs for waves opposing the current.

Groeneweg & Battjes (2003) further extended the method presented by Groeneweg & Klopman (1998) to study the sidewall effects in the three-dimensional motion in a long flume of finite width. Transverse circulation due to the presence of the vertical sidewalls was calculated. The 2DV model with vortex forces being implemented following Dingemans *et al.* (1996) are compared to their 2DV GLM based model. They conclude that the comparison proves that secondary circulation cannot be ruled out in laboratory experiments such as Kemp & Simons (1982) However the CL theory is

insufficient to predict the observed velocity profile changes. They provide an explanation for the wave induced changes in the mean velocity profile due to the interplay between the wave-induced shear stress and the Stokes correction of the shear stress, both acting in longitudinal direction. They state that these effects are dominant over the transport of longitudinal momentum by the secondary circulations.

Recently interactions between waves and currents was studied by Huang & Mei (2003), where the eddy viscosity was provided using an algebraic turbulence model from the flow variables. However their approach is not simple to apply. Olabarrieta *et al.* (2010) developed a 2DV non hydrostatic model in order to analyze the problem. The governing equations are solved in the classical Eulerian reference frame, but using a σ coordinate system, allowing the variation of free surface elevation. The model can simulate currents propagating at different angles with respect to the wave propagation direction. The numerical solution is able to take into account nonlinear terms without assuming small values of the wave steepness. However, some approximation has to be introduced in any case (e.g. nonlinear effects in the vertical component of momentum equations are neglected), and the numerical solution implies high computational costs which, in this case too, make it quite hard to consider arbitrary angles between the direction of the current and that of wave propagation. More recently Tambroni *et al.* (2015) propose an approach which provides the flow field generated by the interaction of waves and currents in the entire water column, avoiding the decomposition of the fluid domain into inviscid core region and viscous boundary layers. Their analysis can easily be modified to be added to other turbulence models.

In the next section considering a coastal region of constant water depth h, characterized by the presence of surface gravity waves of frequency ω, which propagates in positive x direction (Figure 5.1), we will validate our 3D wave-current coupled model with the inclusion of the wave averaged vortex force, with laboratory experiments. At this stage it is of importance to identify the dimensionless variables of the problem. The quantities wave length k and wave period T are used as spatial and temporal scales, respectively. Moreover the quantity $u_{bw} = a\omega/\sinh kh$ is used as velocity scale

Parameter	WCA5
Wave height H (m)	0.0444
Wave Length (m)	1.433
Mean centerline velocity for current alone (m/s)	0.183
Reynolds number Re_w	2026
Bottom Roughness (mm)	0.05

Table 5.1: Parameters of (Kemp & Simons, 1982) for wave-following current.

where a denotes the amplitude of waves. Current strength will be measured by the Froude number $Fr = U_s/c$ where U_s is the current velocity at the surface and c is the phase speed of the waves.We will compare the results of our 3D coupled model to a test case provided from data observed by Kemp & Simons (1982) for waves following currents. This test will represent the interaction of a regular wave with a weak current and weak shear $Fr \ll 1$ and therefore the vortex force formulation of MRL04 will be a reasonable model to use.

5.3 Model setup and validation

Kemp & Simons have reported the current profiles for wave-following currents over smooth (WCA1-WCA5) and rough (WCR1-WCR5) beds, in a small wave tank of $14.5\,m$ length, $0.457\,m$ width and $0.69\,m$ height. The still water depth was $0.2\,m$. Along the centerline, the depth-averaged mean current velocity was $0.185\,m/s$. Waves with period $T = 1\,s$ were added to the turbulent current. The wave amplitudes a ranged from 0.011 to $0.023\,m$ for the wave-following current of Kemp & Simons (1982). All full-depth profiles of currents were measured on top of a strip at a station $8.07\,m$ away from the wave maker. For a steady current, the bottom roughness z_B is usually determined by fitting the logarithmic profile with the measured profile of the pure current. Based on experiments Mathisen & Madsen (1996) have shown that the same value can be taken if waves are also present. For the purpose of our model validation we chose one wave-following current with a smooth bed and one case of on opposing current over the rough bed. The experimental parameters are summarized in table 5.1.

5.3.1 Current only

To setup the model we first need to apply the proper initial and boundary conditions to run the model with currents and after a steady logarithmic velocity profile is established we will add the wave forcing to the current. At inflow, the velocity is given as an input. At outflow we imposed the same outflow flux as the inflow flux.

In order to study if the wave effects on the current are a 2D or 3D effect, we have generated two runs for a 2D and 3D case by applying free slip and no slip boundaries in y direction. Using 550 grid cells in x. For the 2D case we have 5 grid points in y direction and for the 3D case we have 45 grid points in y. In both cases there are 20 vertical layers . The cell size is $dx = 0.04\,m$ and $dy = 0.01\,m$. Based on the constant depth of $0.20\,m$ throughout the test the vertical resolution would be $0.01\,m$.

Another important step in the model setup is the built-in turbulence closure model. We here choose a $k-\epsilon$ model bearing in mind that the use of this model needs adequate simulation time and space to make sure the turbulence model fully develops.

For the situation of current alone (no waves) the computed vertically averaged horizontal velocity, evaluated at the center line was taken as reference for the vertically averaged velocity as resulting from the measurements, likewise taken in the center of the flume. This approach will give the required input flux for modeling and has been applied to all measurements.

Figure 5.2 (a) and (b) illustrate the mid-section velocities and surface velocity in the flume at time $300\,s$ for 3D run where the current profile is fully developed before waves are added. Figure 5.2 (c) shows the vertical profile of the horizontal velocity for 2D and 3D model along with the calculated logarthmic profile given $u*$ and bottom roughness z_B. It can be seen that the two cases are in good agreement with the measurements from the experiment.The quantities wave length k and wave orbital amplitude $u_{bw} = a\omega/\sinh kh$ are used as length and velocity scale where a denotes the amplitude of waves. Figure 5.2 (d) shows the vertical profile of eddy viscosities from the $k-\epsilon$ model non-dimensionalized by the molecluar viscosity $\nu = 1e^{-6}$, in the 2D and 3D simulations and the eddy viscisty based on the Prandlt mixing length theory

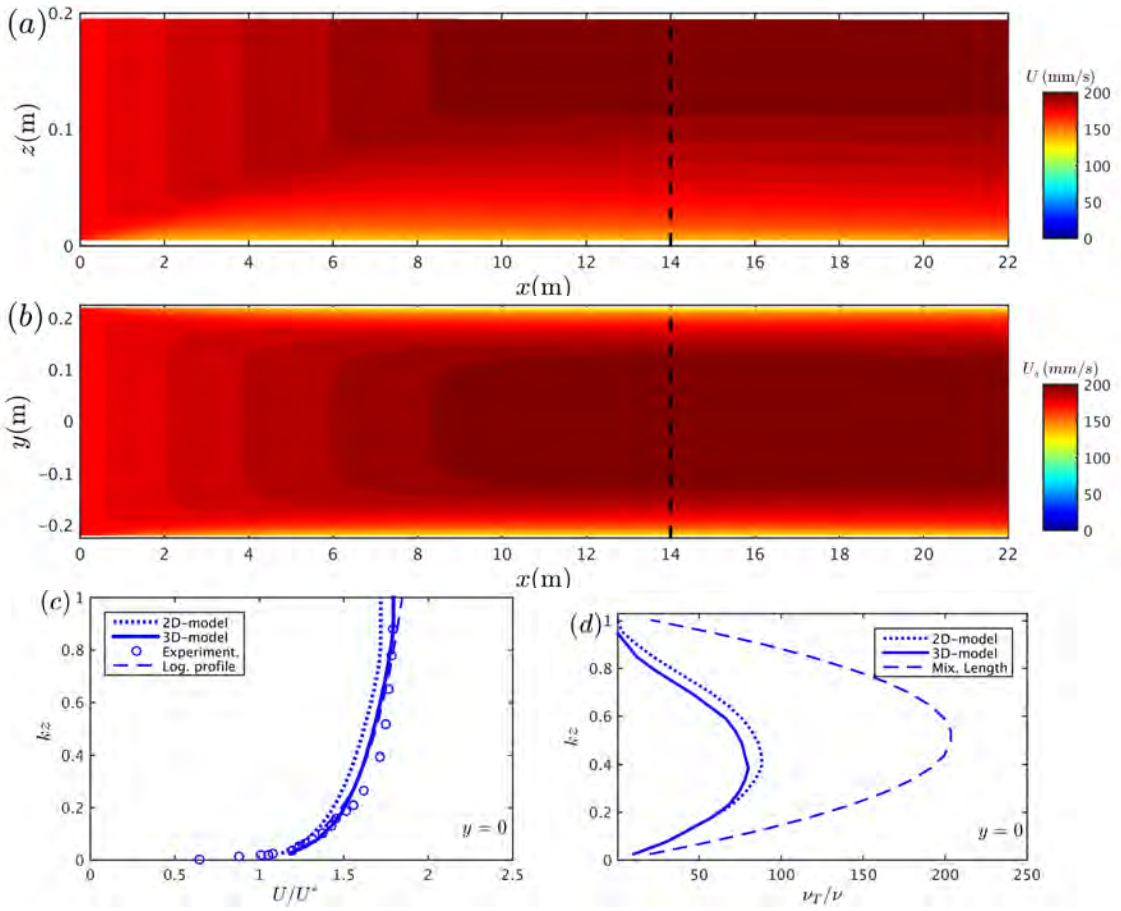

Figure 5.2: Kemp & Simons (1982) (WCA5)- Current only simulation: (a) 3D model; horizontal velocity in mid-section of the flume (b) 3D model; surface velocity in the flume (c) Vertical structure of the horizontal velocity in the comparison section illustrated in upper panels with dashed line. (d) Vertical structure of eddy viscosity in comparison section

(ν_{ml}), given by the following expression:

$$\nu_{ml} = {l_m}^2 (\frac{\partial u}{\partial z}) \tag{5.60}$$

where l_m represents the mixing length. Following Bakker & Van Doorn (1978) and Kim *et al.* (2001), the length scale is assumed to increase with the distance from the bed. Nezu & Rodi (1986), based on experimental measurements made with stationary currents, concluded that the length scale tends to zero near the water surface. Thus, a reduction factor for the length scale is included to take into account this tendency. The equation that includes this linear increase of the mixing length and its reduction near the free surface is given by the following expression:

$$l_m = \kappa z \sqrt{1 - \frac{z}{h + \bar{\eta}}} \tag{5.61}$$

where κ is the von Karman constant ($= 0.4$), $\bar{\eta}$ the sea surface elevation and h is the mean water depth.

5.3.2 Wave and currents

The wave parameters such as significant wave height and wave period are provided as input to NHWAVE without activating SWAN. Adding waves to the established current needs some caution considering the experiment conditions. In Kemp & Simons's experiment there is no wave current interaction in the inflow boundary, as they have designed their flume to have a wave paddle with a distance from the inflow valve. To simulate the same condition in our model we have added a tangent hyperbolic function for the wave height that has the value of zero at the inflow boundary and gradually increases to the actual wave height in the test case. After the turbulent logarithmic shear flow was developed sufficiently the wave forcings are taken into account and 120 seconds after a new steady state is obtained.Since the wave vortex force also acts on the vertical velocity it is important to also run simulations based on the same numerical and physical parameters but with a non-hydrostatic pressure.

Comparing the 2D and 3D hydrosttaic and non-hydrostatic model results with experimental data are shown in fig 5.3 for 3 different distances from the center line, where L_y is the total width of the flume and $y = 0$ corresponds to the center line. Figure 5.3 shows that the effects of waves on currents can not be simulated by a 2D model. It is also seen that the non-hydrostatic model is shown to give more realistic results.Further comparison and discussion on the wave forcing and momentum balances for the hydrostatic and non-hydrostatic case will be discussed in the following sections.

The development of eddies generated in the cross section in the 3D model is shown shown in Fig 5.4. It is noticeable that neglecting the non-hydrostatic pressure results in unrealistic eddies where the size of the vertical velocity w, can get as big as the horizontal velocity u. In the next section we will first discuss the details of the momentum balances and differences in the hydrostatic and non-hydrostatic case. We will also explain how these balances in the non-hydrostatic simulation cause the significant changes in the vertical profile of the horizontal velocity as reported by Kemp & Simons (1982).

5.3.3 Momentum balances

It was shown in the previous section how the hydrostatic and non-hydrostatic simulations lead to different results. The magnitude of the eddies shown in figure 5.4 (a) for the hydrostatic case were unreasonably large and an order of magnitude larger than the eddies shown in figure 5.4 (b) for the non-hydrostatic simulation. Here we will provide the momentum balances and a discussion on how the hydrostatic case leads to non satisfactory results. The wave-averaged momentum equations in the Cartesian coordinates can be written as:

$$\frac{\partial u}{\partial t} + u\frac{\partial u}{\partial x} + v\frac{\partial u}{\partial y} + w\frac{\partial u}{\partial z} + \frac{1}{\rho}\frac{\partial p}{\partial x} = -\frac{\partial \kappa}{\partial x} + J_x + S_{\tau x} \tag{5.62}$$

$$\frac{\partial v}{\partial t} + u\frac{\partial v}{\partial x} + v\frac{\partial v}{\partial y} + w\frac{\partial v}{\partial z} + \frac{1}{\rho}\frac{\partial p}{\partial y} = -\frac{\partial \kappa}{\partial y} + J_y + S_{\tau y} \tag{5.63}$$

$$\frac{\partial w}{\partial t} + u\frac{\partial w}{\partial x} + v\frac{\partial w}{\partial y} + w\frac{\partial w}{\partial z} + \frac{1}{\rho}\frac{\partial p}{\partial z} + g = -\frac{\partial \kappa}{\partial z} + K + S_{\tau z} \tag{5.64}$$

with p being the sum of hydrostatic and non-hydrostatic pressure as:

$$p = q + \rho g(\overline{\eta} - z^*) \tag{5.65}$$

From the definitions of vortex force in x direction in MRL04 we have:

$$J_x = -w^{st}u_{,z} + v^{st}\chi \tag{5.66}$$

$$J_y = -w^{st}v_{,z} - u^{st}\chi \tag{5.67}$$

with

$$w^{st} = -\nabla_H \cdot \int_{-h}^{z} \mathbf{u}^{st} dz' \tag{5.68}$$

and the current vorticity as

$$\chi = \nabla_H \times \mathbf{u} \tag{5.69}$$

Since the waves are in x direction, the v^{st} is zero. Also there are no changes in the wave properties in x direction therefore w^{st} can be neglected.

The results are taken at the time when the simulation reaches a steady state and is fully developed therefore all the derivatives with respect to time are zero. The nonlinear terms with x derivatives are also negligibly small.

The momentum equations will be simplified to:

$$v\frac{\partial u}{\partial y} + w\frac{\partial u}{\partial z} + \frac{1}{\rho}\frac{\partial p}{\partial x} = S_{\tau x} \tag{5.70}$$

$$v\frac{\partial v}{\partial y} + w\frac{\partial v}{\partial z} + \frac{1}{\rho}\frac{\partial p}{\partial y} = -\frac{\partial \kappa}{\partial y} + J_y + S_{\tau y} \tag{5.71}$$

$$v\frac{\partial w}{\partial y} + w\frac{\partial w}{\partial z} + \frac{1}{\rho}\frac{\partial p}{\partial z} + g = -\frac{\partial \kappa}{\partial z} + K + S_{\tau z} \tag{5.72}$$

Hence, the main forcing mechanism is in y and z direction. We will therefore look at the balances in equation 5.71 and 5.72 as shown in the figures 5.5 and 5.6.

It can be seen that in absence of the dynamic pressure the waves forcing and shear stress have to balance with the convection terms, which leads to large velocities

in y and z direction as also seen in figure 5.4. This will also cause unreasonable surface fluctuations which is evident in figure 5.5 (d), where the term $-\frac{1}{\rho}P_{,y}$ is equal to $-g\eta_{,y}$ in the absence of dynamic pressure. We can thus conclude that due to the dynamics of this problem and the 3D circulations the hydrostatic assumption does not apply here and hereinafter we will only discuss the balances in the non-hydrostatic simulation. In figure 5.7 the momentum balances in the x direction are shown. In the middle section it is seen that the main balance is between the $w\partial u/\partial z$ and the shear stress term. near the wall the balance is between all three terms shown in figure 5.7 and the pressure gradient term $-\frac{1}{\rho}P_{,x}$ which is solely due to $-g\eta_{,x}$. Figure 5.8 compares the shear stress and eddy viscosity in the 3D non-hydrostatic and 2D model. In absence of the side wall effect, the secondary circulations will not be generated and therefore there will not be a significant vertical velocity w in the mid section. Consequently in the 2D momentum balance the shear stress balancing the convection terms in the x momentum balance is smaller compared to the 3D non-hydrostatic model. The structure of the eddy viscosity is also seen to be significantly different. The eddy viscosity calculated by the 3D k-epsilon model stays constant in the upper part of the current.

5.3.4 Discussion

Recent studies have analyzed the change in the mean velocity profile interacting with non-breaking waves in laboratory flumes (e.g. studies by Kemp & Simons (1982, 1983); Klopman (1994)). Their main focus has been explaining the changes in the vertical profile of the velocity due to non-conservative shear stresses. Studies such as Huang & Mei (2003) and Tambroni *et al.* (2015) introduce eddy viscosity models to account for the wave effects on current. In both studies the 2D models have reasonable agreements with wave opposing currents such as experiments by Kemp & Simons (1983); Klopman (1994), but lack accuracy for wave following currents such as Kemp & Simons's 1982 experiment. In this Chapter without interfering with the eddy viscosities we examined the effect of the conservative wave forces on the current field. For this simulation it can be seen that using a non-hydrostatic model the conservative wave forces alone can

generate satisfactory results compared to experiment. The question on whether these forces could solely explain the changes in the current velocity in a variety of test cases still needs to be addressed. Son & Lynett (2014) study the effect of turbulence induced by interactions between waves and currents with arbitrary horizontal vorticity, by introducing new stress in their depth integrated equations. These stresses are functions of a parameter b that relates the relative importance of wave radiation stress and bottom friction stress to the wavecurrent interaction. Similar analysis could be further done using our 3D wave forcing to generate similar parameters where the importance of the conservative vs non-conservative wave effects could be investigated. The case of waves opposing currents also needs to be addressed. Dingemans *et al.* (1996) linked the wave-induced change of the Eulerian mean velocity to Langmuir circulation induced by the lateral boundaries of the wave tank. The results of their three-dimensional computations based on a $k\epsilon$ model agree reasonably well with the measurement of Klopman (1994) only for waves following, but not opposing, the current. The question on why no effect on the current profile was found for their waves opposing current case is yet not clear, and would be a starting point for future work.

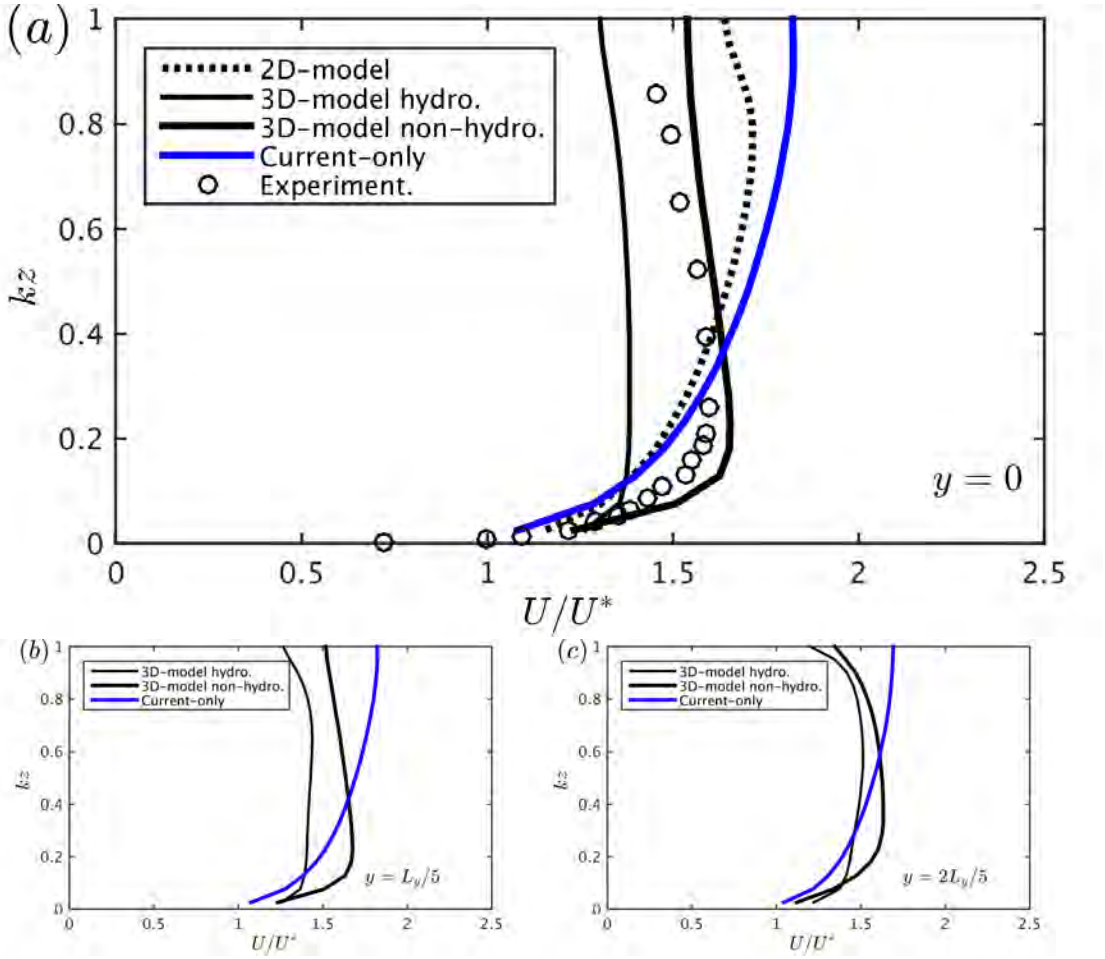

Figure 5.3: Kemp & Simons (1982) (WCA5)- Waves and Current simulation: Vertical structure of the normalized horizontal velocity; comparison of the 2D with 3D hydrostatic and non-hydrostatic simulations in sections (a)$y = 0$ (b) $y = L_y/5$ and (c) $y = 2L_y/5$

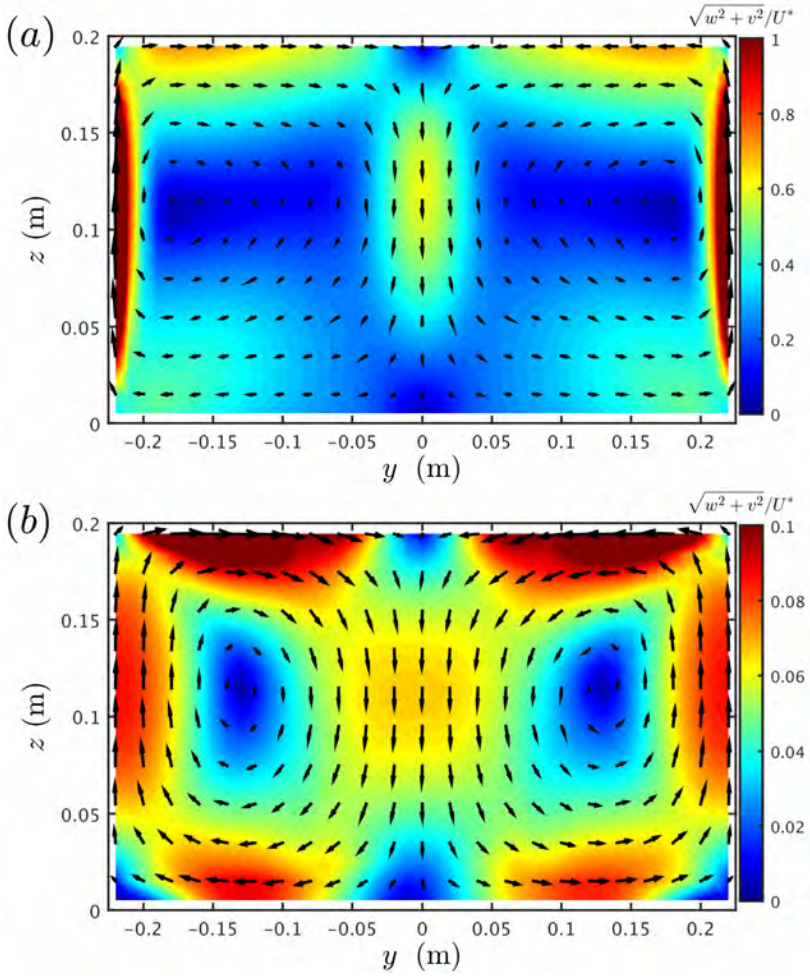

Figure 5.4: Kemp & Simons (1982) (WCA5)- Waves and Current simulation: Normalized velocity feild in the cross section (a) hydrostatic model; (b) non-hydrostatic model

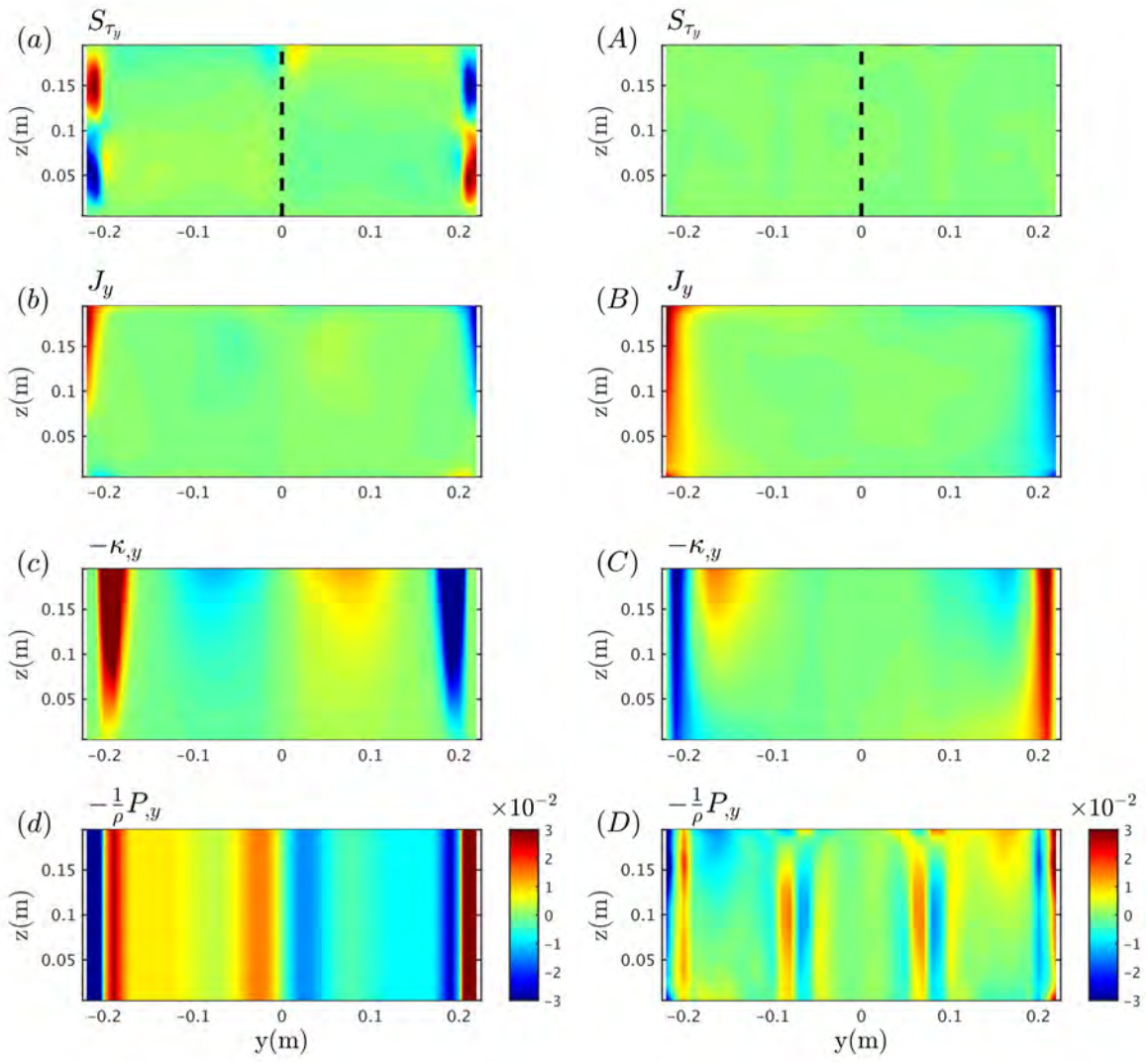

Figure 5.5: Kemp & Simons (1982) (WCA5)- Waves and Currents: Forcing terms in the Y momentum balance (a)-(d): Hydrostatic, (A)-(D): non-hydrostatic

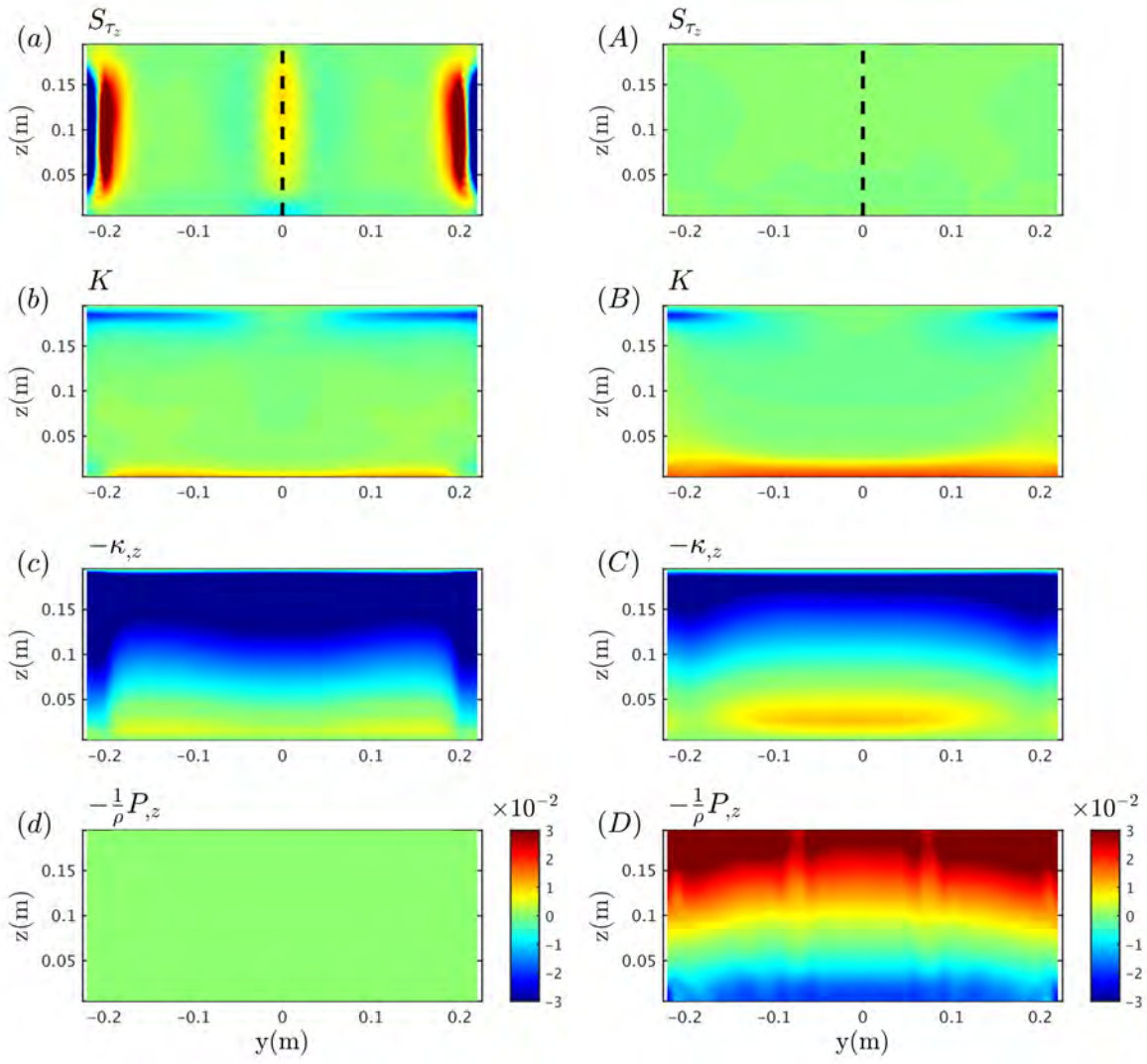

Figure 5.6: Kemp & Simons (1982) (WCA5)- Waves and Currents: Forcing terms in the Z momentum balance (a)-(d): Hydrostatic right, (A)-(D): non-hydrostatic

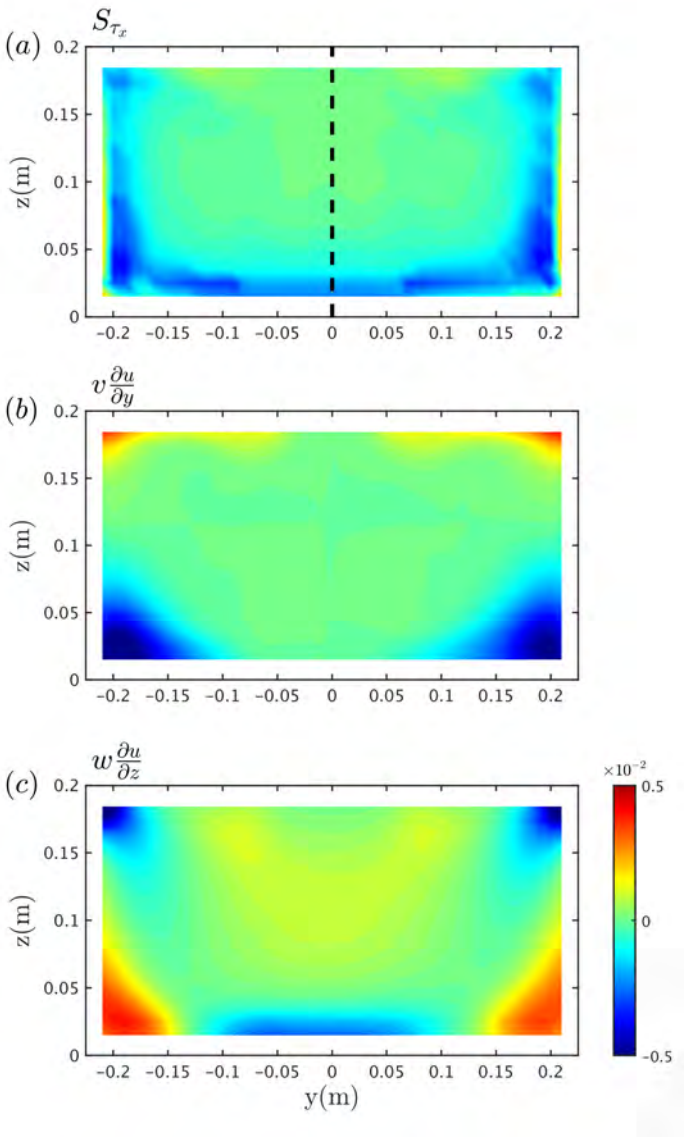

Figure 5.7: Kemp & Simons (1982) (WCA5)- Waves and Current- Non- hydrostatic simulation: momentum balances in X direction in cross section

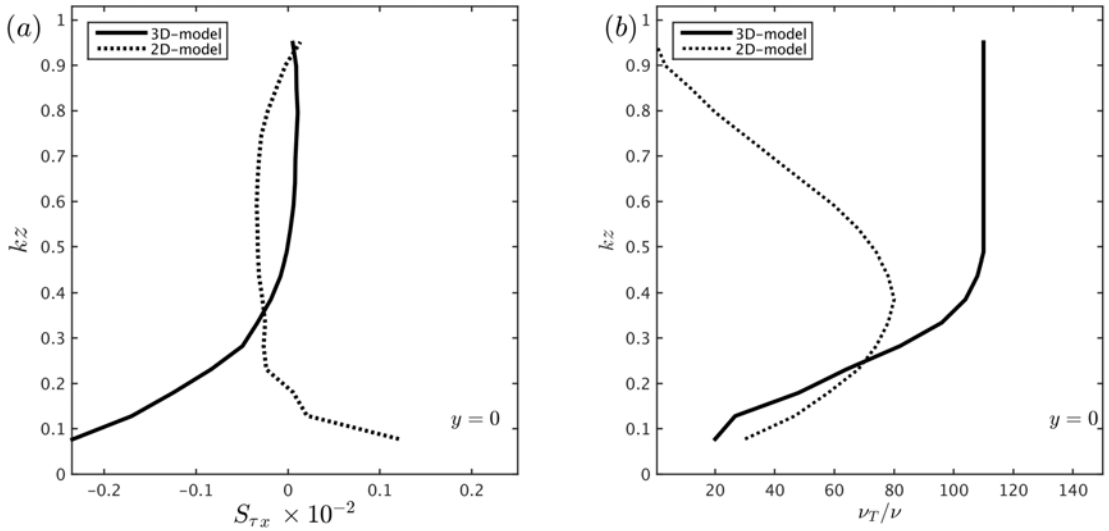

Figure 5.8: Kemp & Simons (1982) (WCA5)- Waves and Currents: 3D vs 2D comparison; (a) Shear stress $S_{\tau x}$ (b) Vertical structure of eddy viscosity

Chapter 6

SUMMARY AND FUTURE WORK

6.1 Summary of presented work

The interactions between surface gravity waves and vertically sheared currents have been discussed in the thesis. The study consists of three parts: (1) general wave-current interaction theory, (2) effect of sheared currents in wave action conservation and (3) Numerical study on wave effects on current profiles using the phase averaged non-hydrostatic model NHWAVE.

In the first part, the framework presented by DK16 to describe the wave-current interaction for arbitrarily sheared current is discussed. The flow motions are considered to be the superposition of waves and currents. The wave equations are then separated from the mean flow equations by applying multiple scale expansion and wave-averaging. The wave-averaged forces in terms of vortex force formulation are obtained from the mean flow equations. The reduction of the present vortex force formula for weak current assumption is compared with MRL04 results. The leading order wave equation results in the Rayleigh (or inviscid Orr-Sommerfeld) stability equation. The solvability condition of the second order wave Raleigh equation leads to the wave action equation for arbitrary current profile. In DK16 it is shown that the resulting wave action equation for strongly sheared current reproduces the work done by Voronovich (1976). After presenting the summary of the theoretical work on wave-current interaction for strongly sheared mean flows developed by DK16 and further verified in our study, we move to investigating the shortcomings in numerical modeling of waves and currents. Typical coastal circulation and wave models, still only employ theoretical formulations which take depth-uniform mean flows into account, with realistic, non-uniform flows treated

as being depth uniform through some chosen averaging procedure. Depending on the choice of average over depth, significant errors may arise in the estimation of properties such as group velocity and action density in realistic conditions. These errors, in turn, are fed back into the circulation model through incorrect representation of the vertical structure of wave forcing. In Chapter 3 we demonstrate that the widely used depth-weighted average current value KC89, is not the correct current speed to use directly in the action equation in SWAN or similar wave models, as this approach neglects the contribution from the derivative of the wavenumber-dependent weighted current during calculation if the group velocity. We correct this error and also suggest a strategy for determining the current contribution to group velocity as a function of frequency, employing a Taylor series expansion about the peak frequency, significantly extending the range of accuracy of current information with minimal additional programming or data passage. We then extend the results to two horizontal dimensions for use in the SWAN wave model. The expressions for energy density and intrinsic frequency used to construct the wave action density are similarly investigated, using perturbation approximations in the general action balance equation of Voronovich (1976). The results suggest that the action density $\mathcal{N} = E_0/\sigma$ may be consistently constructed using the usual expression for energy density, $E_0 = 1/2\rho g a^2$, together with a $\sigma = \omega - k\tilde{U}$ based on the KC89 current speed. The wave action flux approximation also suggests the use of the current $\hat{U}$ as the correct current speed to be used in the advection velocity which is the vector form of the advection velocity suggested by KC89 and discussed in chapter (3). We have further extended the suggested Taylor expansion around the peak wave number in a modeled spectrum, with extensions covering the specification of action, flux and intrinsic frequency as well as an extension to a general 2D horizontal setting. These results provide an avenue for calculating wave action and action flux in spectral wave models, using a compact set of information about the current field evaluated at the spectral peak wave number. The final part of this study is focused on the effect of wave vortex forces presented by MRL04 in wave current interaction in laboratory flumes. In doing so we have used the coupled NHWAVE-SWAN model ($NH\overline{WAVE}$)

without activating the SWAN model and instead using the second option implemented in the code to give wave characteristics as an input data to the phase averaged model NHWAVE. To validate our model we have chosen the experiments done by Kemp & Simons (1982) on the interaction of non-breaking waves with currents in a laboratory flume. The results from our 3D non-hydrostatic model agree reasonably well with data from the experiment. The changes in the vertical profile of the current are successfully modeled with the wave averaged vortex forces. Further simulations to investigate the effect of flume width, bottom roughness and wave direction will be considered as future work.

6.2 Future work

Future work can be listed as bellow:

- Implementation of work done in Chapters (3) and (4) in phase averaged models such as SWAN:

  This has been an ongoing project in collaboration with USGS Woods Hole and University of Washington to implement the proposed method in Banihashemi *et al.* (2017) and Banihashemi & Kirby (2019) in the coupled wave, current, and sediment-transport model (COAWST).

- Extend the wave-current interaction theory to incorporate spectral wave conditions:

  Quantities calculated based on spectral information in SWAN are simply based on monochromatic theory expressions using the peak frequency and direction. Guidance on this issue can be obtained from Bennis *et al.* (2011) where they assume that in the case of random waves the corresponding forcing is simply the sum of the monochromatic wave forcing. For example they replace the wave energy E with is the spectral density of the surface wave elevation variance $E(f,\theta)$ (where f and θ are, respectively, the wave frequency and direction). So if the Stokes drift velocity is defined as

$$\mathbf{u}^{st}(z) = \frac{E\sigma\mathbf{k}}{2\sinh^2 kd}\cosh 2k(z+h) \tag{6.1}$$

  then for random waves the stokes drift velocity could be defined as

$$\mathbf{u}^{st}(z) = \int \frac{E(f,\theta)\sigma\mathbf{k}}{2\sinh^2 kd}\cosh 2k(z+h)\,df\,d\theta \tag{6.2}$$

- Further investigation on wave conservative vs non-conservative wave effects on the mean current.

  In chapter 5 we studied the interaction of non-breaking waves with currents. Our non-hydrostatic model results were in good agreement with wave following currents from the laboratory study of Kemp & Simons (1982). However the effect of bottom roughness, flume width and the direction of the waves still needs to be addressed. Further simulations would be required to investigate the effect of each parameter in generating the secondary circulations and modifying the vertical profile of the mean current.

Bibliography

Akan, C., Moghimi, S., Özkan-Haller, H. T., Osborne, J. & Kurapov, A. 2017 On the dynamics of the mouth of the columbia river: Results from a three-dimensional fully coupled wave-current interaction model. *J. Geophys. Res* **122** (7), 5218–5236.

Ardhuin, F. Jenkins, A.D. & Belibassakis, K.A. 2008 Comments on "The depth-dependent current and wave interaction equations: A revision". *J. Phys. Oceanogr.* **38**, 1340–1350.

Ardhuin, F., Rascle, N. & Belibassakis, K. A. 2008 Explicit wave-averaged primitive equations using a generalized Lagrangian mean. *Ocean Modelling* **20**, 35–60.

Bakker, W. T. & Van Doorn, T. 1978 Near-bottom velocities in waves with a current. *Coastal Engineering Proceedings* **1** (16), 82.

Banihashemi, Saeideh & Kirby, James T 2019 Approximation of wave action conservation in vertically sheared mean flows. *Ocean Modelling* **143**, 101460.

Banihashemi, S., Kirby, J. T. & Dong, Z. 2017 Approximation of wave action flux velocity in strongly sheared mean flows. *Ocean Modelling* **116**, 33–47.

Benetazzo, A, Carniel, S, Sclavo, M & Bergamasco, A 2013 Wave–current interaction: Effect on the wave field in a semi-enclosed basin. *Ocean Modelling* **70**, 152–165.

Bennis, A.C., Ardhuin, F. & Dumas, F. 2011 On the coupling of wave and three-dimensional circulation models: Choice of theoretical framework, practical implementation and adiabatic tests. *Ocean Modelling* **40** (3), 260–272.

Bennis, A.-C. & Ardhuin, F. 2011 Comments on" the depth-dependent current and wave interaction equations: A revision". *J. Phys. Oceanogr.* **41**, 2008–2012.

Booij, N., Ris, R. C. & Holthuijsen, L. H 1999 A third-generation wave model for coastal regions: 1. model description and validation. *J. Geophys. Res* **104** (C4), 7649–7666.

Bretherton, F. P. & Garrett, C. J. R. 1968 Wavetrains in inhomogeneous moving media. *Proc. of R. Soc. London* **302**, 529–554.

Caires, S., Doorn, N., Groeneweg, J. & van Dongeren, A. R. 2006 Storm hindcasts norderneyer seegat and amelander zeegat. *H4803* .

Chawla, A. & Kirby, J. T. 2002 Monochromatic and random wave breaking at blocking points. *J. Geophys. Res* **107** (C7), 1–19.

Christoffersen, J. B. & Jonsson, I. G. 1985 Bed friction and dissipation in a combined current and wave motion. *Ocean Engineering* **12** (5), 387–423.

Constantin, A. Escher, J. 2011 Analyticity of periodic traveling free surface water waves with vorticity. *Ann. of Math.* **173**, 559–568.

Craik, A. D. D. 1968 Resonant gravity-wave interactions in a shear flow. *Journal of Fluid Mechanics* **34** (3), 531–549.

Craik, A. D. D. & Leibovich, S. 1976 A rational model for Langmuir circulations. *J. of Fluid Mechanics* **73** (03), 401–426.

Derakhti, M., Kirby, J. T., Shi, F. & Ma, G. 2016 Nhwave: Consistent boundary conditions and turbulence modeling. *Ocean Modelling* **106**, 121 – 130.

Dingemans, M. W. 1997 *Water Wave Propagation over Uneven Bottoms. Part I: Linear Wave Propagation*. World Scientific.

Dingemans, M. W., Radder, A. C. & De Vriend, H. J. 1987 Computation of the driving forces of wave-induced currents. *Coastal Engineering* **11** (5), 539–563.

Dingemans, M. W., van Kester, J. T. M., Radder, A. C. & Uittenbogaard, R. E. 1996 The effect of the CL-vortex force in 3D wave-current interaction. In *Coastal Engineering 1996*, pp. 4821–4832.

Dong, Z. 2016 Wave-current interaction in strongly sheared mean flows. PhD thesis, University of Delaware.

Dong, Z. & Kirby, J. T. 2012 Theoretical and numerical study of wave-current interaction in strongly-sheared flows. In *Proc. 33d Int. Conf. Coastal Eng.* (ed. P. Lynett & J. M. Smith). Santander, Spain.

Elias, E. P. L., Gelfenbaum, G. & van der Westhuysen, A. J. 2012 Validation of a coupled wave-flow model in a high-energy setting: The mouth of the Columbia River. *J. Geophys. Res* **117**, C09011, doi:10.1029/2012JC008105.

Ellingsen, S. A. 2016 Oblique waves on a vertically sheared current are rotational. *European J. of Mechanics B/Fluids* **56**, 156–160.

Ellingsen, S. A. & Li, Y. 2017 Approximate dispersion relations for waves on arbitrary shear flows. *Journal of Geophysical Research: Oceans* **122**, 9889–9905.

Fenton, J. D. 1973 Some results for surface gravity waves on shear flows. *J. Inst. Math. Appl.* **12** (1), 1–20.

Garrett, C. 1976 Generation of Langmuir circulations by surface waves feedback mechanism. *J. Mar. Res.* **34**, 117–130.

Gong, W., Chen Y. Zhang H. Chen Z. 2018 Effects of wave–current interaction on salt intrusion during a typhoon event in a highly stratified estuary. *Estuaries and Coasts* pp. 1–20.

Gottlieb, S., Shu, C. & Tadmor, E. 2001 Strong stability-preserving high-order time discretization methods. *SIAM Review* **43** (1), 89–112.

Grant, W. D. & Madsen, O. S. 1979 Combined wave and current interaction with a rough bottom. *J. of Geophys. Res* **84** (C4), 1797–1808.

Groeneweg, J & Battjes, JA 2003 Three-dimensional wave effects on a steady current. *J. Fluid Mech.* **478**, 325–343.

Groeneweg, J & Klopman, G 1998 Changes of the mean velocity profiles in the combined wave–current motion described in a glm formulation. *J. Fluid Mech.* **370**, 271–296.

Groeneweg, J., van Vledder, Gh., Doorn, N., Caires, S. & van der Westhuysen, AJ 2007 Storm hindcasts for wadden sea .

Haskoning, R. 2007 Hindcast tidal inlet of ameland storms january and march 2007. *Royal Haskoning Report 9S8833. A* .

Hasselmann, K., et al. 1973 Measurements of wind-wave growth and swell decay during the joint north sea wave project (jonswap). *Ergänzungsheft 8-12* .

Hasselmann, K. 1971 On the mass and momentum transfer between short gravity waves and larger-scale motions. *J. Fluid Mech.* **50** (01), 189–205.

Hickey, B. M., Pietrafesa, L. J., Jay, D. A. & Boicourt, W. C. 1998 The Columbia River plume study: Subtidal variability in the velocity and salinity fields. *J. Geophys. Res.* **103** (C5), 10,339–10,368.

Huang, Z. & Mei, C. C. 2003 Effects of surface waves on a turbulent current over a smooth or rough seabed. *J. Fluid Mech.* **497**, 253–287.

Janssen, T. T. & Herbers, T. H. 2014 Wave-current interaction in coastal inlets and river mouths. *Tech. Rep.*.

Jonsson, I. G. 1990 Wave-current interactions. *The Sea. Ocean Engineering Science* **9**, 65–120.

Jonsson, I. G., Brink-Kjaer, O. & Thomas, G. P. 1978 Wave action and set-down for waves on a shear current. *J. Fluid Mech.* **87**, 401–416.

Karageorgis, P. 2012 Dispersion relation for water waves with non-constant vorticity. *European J. of Mechanics B/Fluids* **34**, 7–12.

Kemp, P. H. & Simons, R. R. 1982 The interaction between waves and a turbulent current: waves propagating with the current. *J. Fluid Mech.* **116**, 227250.

Kemp, P. H. & Simons, R. R. 1983 The interaction of waves and a turbulent current: waves propagating against the current. *J. Fluid Mech.* **130**, 7389.

Kilcher, L. F. & Nash, J. D. 2010 Structure and dynamics of the Columbia River tidal plume front. *J. Geophys. Res.* **115**, C05S90, doi:10.1029/2009JC006066.

Kim, H., O'Connor, B. A. & Park, I.and Lee, Y. 2001 Modeling effect of intersection angle on near-bed flows for waves and currents. *Journal of waterway, port, coastal, and ocean engineering* **127** (6), 308–318.

Kirby, J. T & Chen, T. 1989 Surface waves on vertically sheared flows: approximate dispersion relations. *J. Geophys. Res.* **94**, 1013–1027.

Klopman, G 1994 Vertical structure of the flow due to waves and currents-laser-doppler flow measurements for waves following or opposing a current. *WL report H840-30, part II, for Rijkswaterstaat,* .

Kumar, N., Voulgaris, G. & Warner, J. C. 2011 Implementation and modification of a three-dimensional radiation stress formulation for surf zone and rip-current applications. *Coastal Eng.* **58** (12), 1097–1117.

Kumar, N., Voulgaris, G., Warner, J. C. & Olabarrieta, M. 2012 Implementation of the vortex force formalism in the coupled ocean-atmosphere-wave-sediment transport (COAWST) modeling system for inner shelf and surf zone applications. *Ocean Modelling* **47**, 65–95.

Leibovich, S. 1980 On wave-current interaction theories of Langmuir circulations. *J. Fluid Mech.* **99** (04), 715–724.

Lesser, G.R., Roelvink, J.A., van Kester, J.A.T.M. & Stelling, G.S. 2004 Development and validation of a three-dimensional morphological model. *Coastal Eng.* **51** (8), 883–915.

Lesser, G. R. 2009 An Approach to Medium-term Coastal Morphological Modelling. PhD thesis, Delft University of Technology.

Li, Y. & Ellingsen, S. Å. 2019 A framework for modeling linear surface waves on shear currents in slowly varying waters. *Journal of Geophysical Research: Oceans* **124** (4), 2527–2545.

Lin, P. & Liu, P. L. F. 1998 Turbulence transport, vorticity dynamics, and solute mixing under plunging breaking waves in surf zone. *Journal of Geophysical Research: Oceans* **103** (C8), 15677–15694.

Longuet-Higgins, M. S. & Stewart, R.W. 1964 Radiation stresses in water waves; a physical discussion, with applications. *Deep Sea Research and Oceanographic Abstracts* **11**, 529–562.

Longuet-Higgins, M. S. & Stewart, R. W. 1960 Changes in the form of short gravity waves on long waves and tidal currents. *J. Fluid Mech.* **8**, 565–583.

Longuet-Higgins, M. S. & Stewart, R. W. 1961 The changes in amplitude of short gravity waves on steady non-uniform currents. *J. Fluid Mech.* **10** (04), 529–549.

Longuet-Higgins, M. S. & Stewart, R. W. 1962 Radiation stress and mass transport in gravity waves, with application to 'surf beats'. *J. Fluid Mech.* **13** (04), 481–504.

Ma, G. 2012 Multiscale numerical study of turbulent flow and bubble entrainment in the surf zone. PhD thesis, University of Delaware, Newark DE.

Ma, G., Shi, F. & Kirby, J. T. 2012 Shock-capturing non-hydrostatic model for fully dispersive surface wave processes. *Ocean Modelling* **43**, 22–35.

Maïssa, P., Rousseaux, G. & Stepanyants, Y. 2016 Wave blocking phenomenon of surface waves on a shear flow with constant vorticity. *Physics of Fluids* **28** (032102).

Mathisen, P. P. & Madsen, O. S. 1996 Waves and currents over a fixed rippled bed: 1. bottom roughness experienced by waves in the presence and absence of currents. *J. Geophys. Res.* **101** (C7), 16533–16542.

McWilliams, J. C., Restrepo, J. M. & Lane, E. M. 2004 An asymptotic theory for the interaction of waves and currents in coastal waters. *J. Fluid Mech.* **511**, 135–178.

Mellor, G. 2003 The three-dimensional current and surface wave equations. *J. Phys. Oceanogr.* **33** (9), 1978–1989.

Mellor, G. L. 2008 The depth-dependent current and wave interaction equations: a revision. *J. Phys. Oceanogr.* **38** (11), 2587–2596.

Mellor, G. L. 2011a Corrigendum. *J. Phys. Oceanogr.* **41**, 1417–1418.

Moritz, H. R., Gelfenbaum, G. R., Kaminsky, G. M., Ruggiero, P., Oltman-Shay, J. & Mckillip, D. J. 2007 Implementing regional sediment management to sustain navigation at an energetic tidal inlet. In *Coastal Sediments 2007*, pp. 1768–1786.

Newberger, P. A. & Allen, J. S. 2007 Forcing a three-dimensional, hydrostatic, primitive-equation model for application in the surf zone: 1. formulation. *J. Geophys. Res* **112** (C08019).

Nezu, I. & Rodi, W. 1986 Open-channel flow measurements with a laser doppler anemometer. *Journal of Hydraulic Engineering* **112** (5), 335–355.

Nielsen, P. & You, Z. J. 1997 Eulerian mean velocities under non-breaking waves on horizontal bottoms. In *Coastal Engineering 1996*, pp. 4066–4078.

Olabarrieta, M., Geyer, W. R. & Kumar, N. 2014 The role of morphology and wave-current interaction at tidal inlets: An idealized modeling analysis. *J. Geophys. Res.* **119** (12), 8818–8837.

Olabarrieta, M., Medina, R. & Castanedo, S. 2010 Effects of wave–current interaction on the current profile. *Coastal Engineering* **57** (7), 643–655.

Olabarrieta, M., Warner, J. C. & Kumar, N. 2011 Wave-current interaction in willapa bay. *J. Geophys. Res.* **116** (C12).

Peregrine, D. H. 1976 Interaction of water waves and currents. *Adv. Appl. Mech.* **16**, 9–117.

Phillips, O. M. 1977 *The Dynamics of the Upper Ocean*. Cambridge University Press, London.

Quinn, B. E., Toledo, Y. & Shrira, V. I. 2017 Explicit wave action conservation for water waves on vertically sheared flows. *Ocean Modelling* **112**, 33–47.

Rong, Z., Hetland, R. D., Zhang, W. & Zhang, X. 2014 Current–wave interaction in the mississippi–atchafalaya river plume on the texas–louisiana shelf. *Ocean Modelling* **84**, 67–83.

Shi, F., Kirby, J. T. & Haas, K. 2006 Quasi-3D nearshore circulation equations: a CL-vortex force formulation. In *Proc. 30th Int. Conf. Coastal Eng*, pp. 1028–1039. San Diego.

Shrira, V. I. 1993 Surface waves on shear currents: solution of the boundary-value problem. *J. Fluid Mechanics* **252**, 565–584.

Skop, R. A 1987 Approximate dispersion relation for wave-current interactions. *J. Waterway, Port, Coastal, and Ocean Eng.* **113**, 187–195.

Smith, J. A. 1980 Waves, currents, and Langmuir circulation. *Ph.D. thesis, Dalhousie University* .

Smith, J. A. 2006 Wave-current interactions in finite depth. *J. of Phys. Oceanogr.* **36** (7), 1403–1419.

Son, S. & Lynett, P. J. 2014 Interaction of dispersive water waves with weakly sheared currents of arbitrary profile. *Coastal Engineering* **90**, 64–84.

Soulsby, R. L. 1995 Bed shear-stresses due to combined waves and currents. *Advances in coastal morphodynamics* .

Stewart, R. H. & Joy, J. W. 1974 Hf radio measurements of surface currents. *Deep Sea Research and Oceanographic Abstracts* **21**, 1039–1049.

Tambroni, N., Blondeaux, P. & Vittori, G. 2015 A simple model of wave–current interaction. *Journal of Fluid Mechanics* **775**, 328–348.

Thomas, G.P. & Klopman, G. 1997 Wave-current interactions in the near shore region. *Int. Series on Advances in Fluid Mechanics* **10**, 255–319.

Thompson, P. D. 1949 The propagation of small surface disturbances through rotational flow. *Annals of the New York Academy of Sciences* **51**, 463–474.

Thomson, J., Horner-Devine, A. R., Zippel, S., Rusch, C. & Geyer, W. 2014 Wave breaking turbulence at the offshore front of the Columbia River Plume. *Geophys. Res. Lett.* **41** (24), 8987–8993.

Uchiyama, Y., McWilliams, J. C. & Shchepetkin, A. F 2010 Wave-current interaction in an oceanic circulation model with a vortex-force formalism: Application to the surf zone. *Ocean Modelling* **34** (1), 16–35.

van der Westhuysen, A. & Lesser, G. 2007 Evaluation and development of wave-current interaction in SWAN: activity 6.4 of SBW project Waddenzee. *Tech. Rep.*. Deltares (WL).

Voronovich, A. G. 1976 Propagation of internal and surface gravity waves in the approximation of geometrical optics. *Izvestia Atmospheric and Oceanic Physics* **12**, 850–857.

Warner, J. C., Armstrong, B., He, R. & Zambon, J. B. 2010 Development of a coupled ocean–atmosphere–wave–sediment transport (COAWST) modeling system. *Ocean modelling* **35** (3), 230–244.

Warner, J. C., Sherwood, C. R., Signell, R. P., Harris, C. K. & Arango, H. G. 2008 Development of a three-dimensional, regional, coupled wave, current, and sediment-transport model. *Computers and Geosciences* **34** (10), 1284–1306.

Whitham, G. B. 1974 *Linear and Nonlinear Waves*. John Wiley , New York.

Wu, J. & Tsanis, I. K. 1995 Numerical study of wind-induced water currents. *Journal of Hydraulic Engineering* **121** (5), 388–395.

Yang, S., Tan, S., Lim, S. & Zhang, S. 2006 Velocity distribution in combined wave–current flows. *Advances in water resources* **29** (8), 1196–1208.

You, Z. J. 1996 The effect of wave-induced stress on current profiles. *Ocean Engineering* **23** (7), 619–628.

Appendix A

DEPTH-WEIGHTED CURRENT VELOCITIES BASED ON POLYNOMIAL FORM OF $U(Z)$

We define the ambient current profile $U(z)$ in polynomial form as

$$U(z) = U_s \sum_{n=0}^{N} a_n (\frac{z}{h})^n \tag{A.1}$$

where the a_n are defined by fitting to measurements or to grid-based numerical values. Evaluating $\tilde{U}$ from (3.1) then gives

$$\begin{aligned} \tilde{U} &= \frac{U_s G}{h} \sum_{n=0}^{N} a_n \int_{-h}^{0} (\frac{z}{h})^n \cosh[2k(h+z)]\, dz \\ &= \frac{U_s}{h} \sum_{n=0}^{N} \frac{a_n}{h^n} J_n \end{aligned} \tag{A.2}$$

with J_n given by

$$J_n = G \int_{-h}^{0} z^n \cosh[2k(h+z)]\, dz \tag{A.3}$$

The first two terms J_0 and J_1 may be simply evaluated, after which the remaining J_n's are defined by a recurrence relation:

$$\begin{aligned} J_0 &= h \\ J_1 &= -\frac{h^2 \mu}{2} \\ J_n &= \frac{n}{4k^2} \left[G(-h)^{(n-1)} + (n-1) J_{n-2} \right] \end{aligned} \tag{A.4}$$

For the polynomial of order $N = 6$ used in Section 5, $\tilde{U}$ is given by

$$\begin{aligned}\tilde{U} = \quad & U_s \left[a_0 - \frac{\mu}{2} a_1 + \frac{(1-G)}{2(kh)^2} a_2 + \frac{3(G-\mu)}{4(kh)^2} a_3 \right. \\ & + \left(\frac{3(1-G)}{2(kh)^4} - \frac{G}{(kh)^2} \right) a_4 + \left(\frac{15(G-\mu)}{4(kh)^4} + \frac{5G}{4(kh)^2} \right) a_5 \\ & \left. + \left(\frac{45(1-G)}{4(kh)^6} - \frac{15G}{2(kh)^4} - \frac{3G}{2(kh)^2} \right) a_6 \right]\end{aligned} \tag{A.5}$$

The derivative of $\tilde{U}$ w/r k is given by

$$\tilde{U}_k = \frac{U_s}{h} \sum_{n=0}^{N} \frac{a_n}{h^n} (J_n)_k \tag{A.6}$$

where subscript k denotes the derivative, and where $(J_n)_k$ can be expressed as

$$\begin{aligned}(J_0)_k &= 0 \\ (J_1)_k &= -\frac{h^2}{2} \mu_k \\ (J_n)_k &= \frac{-2J_n}{k} + \frac{n}{4k^2} \left[(-h)^{n-1} G_k + (n-1)(J_{n-2})_k \right]\end{aligned} \tag{A.7}$$

with

$$\begin{aligned}\mu_k &= \frac{\mu}{k}(G-1) \\ G_k &= \frac{G}{k}(1 - G\cosh 2kh)\end{aligned} \tag{A.8}$$

For $N = 6$, using (A.6) results in

$$\begin{aligned} k\tilde{U}_k &= U_s\Big[-\frac{k}{2}\mu_k a_1 - \frac{(kG_k - 2G + 2)}{2(kh)^2}a_2 + \frac{3(k(G_k - \mu_k) - 2(G - \mu))}{4(kh)^2}a_3 \\ &+ \frac{-k(2h^2k^2 + 3)G_k + 4G(h^2k^2 + 3) - 12)}{2(kh)^4}a_4 \\ &+ \frac{5(h^2k^3G_k + 3kG_k - 2G(h^2k^2 + 6) - 3k\mu_k + 12\mu)}{4(kh)^4}a_5 \\ &+ \frac{-k(2h^4k^4 + 10h^2k^2 + 15)G_k + G(4h^4k^4 + 40h^2k^2 + 90) - 90)}{4(kh)^6}a_6\Big] \end{aligned} \tag{A.9}$$

The resulting $O(F)$ correction to the group velocity is finally given by

$$\hat{U} = \frac{U_s}{h}\sum_{n=1}^{N}\frac{a_n}{h^n}\left(kJ_n\right)_k \tag{A.10}$$

At $O(F^2)$, the expression for C_2 is given by (3.10), and can be written as

$$C_2 = \frac{\tilde{U}}{2C_0}A + \frac{k^2C_0}{2gf_0^2(0)}B + \frac{2k^3C_0}{gf_0^2(0)}C \tag{A.11}$$

where

$$\begin{aligned} A &= [4kI_1(0) - (1 + 2\cosh 2kh)\tilde{U}] \\ B &= \int_{-h}^{0} U^2(z)[1 + 2\cosh^2 k(h + z)]\,dz \\ C &= \int_{-h}^{0} [I_2(z)I_1^{'}(z) - I_1(z)I_2^{'}(z)]\,dz \end{aligned} \tag{A.12}$$

with

$$\begin{aligned} I_1(z) &= \int_{-h}^{z} U(\xi)\sinh 2k(h + \xi)\,d\xi \\ I_2(z) &= \int_{-h}^{z} U(\xi)\cosh 2k(h + \xi)\,d\xi \end{aligned} \tag{A.13}$$

We first evaluate the expressions for $I_1(z)$ and $I_2(z)$. Using the current profile (A.1), we obtain

$$\begin{aligned} I_1(z) &= U_s \sum_{n=0}^{N} \frac{a_n}{h^n} \int_{-h}^{z} \xi^n \sinh 2k(h+\xi)\, dz \\ &= U_s \sum_{n=0}^{N} \frac{a_n}{h^n} I_{1,n}(z) \end{aligned} \tag{A.14}$$

with

$$\begin{aligned} I_{1,0}(z) &= \frac{\cosh 2k(h+z) - 1}{2k} \\ I_{1,1}(z) &= \left[\frac{z \cosh 2k(h+z) + h}{2k} - \frac{\sinh[2k(h+z)]}{4k^2} \right] \\ I_{1,n}(z) &= \frac{1}{4k^2} \left[2k \left(z^n \cosh 2k(h+z) - (-h)^n \right) - n z^{n-1} \sinh 2k(h+z) \right. \\ &\quad \left. + n(n-1) I_{1,n-2} \right] \end{aligned} \tag{A.15}$$

Similarly, $I_2(z)$ can be expressed as

$$\begin{aligned} I_2(z) &= U_s \sum_{n=0}^{N} \frac{a_n}{h^n} \int_{-h}^{z} \xi^n \cosh 2k(h+\xi)\, dz \\ &= U_s \sum_{n=0}^{N} \frac{a_n}{h^n} I_{2,n}(z) \end{aligned} \tag{A.16}$$

with

$$\begin{aligned} I_{2,0}(z) &= \frac{\sinh 2k(h+z)}{2k} \\ I_{2,1}(z) &= \left[\frac{z \sinh 2k(h+z)}{2k} - \frac{\cosh 2k(h+z) - 1}{4k^2} \right] \\ I_{2,n}(z) &= \frac{1}{4k^2} \left[2k \left(z^n \sinh 2k(h+z) \right) - n z^{n-1} \cosh 2k(h+z) \right. \\ &\quad \left. + n(-h)^{n-1} + n(n-1) I_{2,n-2} \right] \end{aligned} \tag{A.17}$$

The expression A in (A.12) is evaluated using (A.14) and (A.16). Moving to the second term in (A.12), we have

$$\begin{aligned} B &= \int_{-h}^{0} U^2(z)[1+2\cosh^2 k(h+z)]\,dz \\ &= \int_{-h}^{0} U^2(z)[2+\cosh 2k(h+z)]\,dz \\ &= {U_s}^2 \sum_{n=0}^{N}\sum_{m=0}^{N} \frac{a_n a_m}{h^{n+m}} \int_{-h}^{0} z^{n+m}(2+\cosh 2k(h+z))\,dz \\ &= {U_s}^2 \sum_{n=0}^{N}\sum_{m=0}^{N} a_n a_m \left[\frac{2h}{m+n+1}(-1)^{n+m+2} + \frac{1}{h^{n+m}} I_{2,n+m}(0)\right] \end{aligned} \tag{A.18}$$

The last term in (A.12) is given by

$$\begin{aligned} C &= \int_{-h}^{0} [I_2(z)I_1^{'}(z) - I_1(z)I_2^{'}(z)]\,dz \\ I_1^{'}(z) &= U(z)\sinh 2k(h+z) \\ I_2^{'}(z) &= U(z)\cosh 2k(h+z) \end{aligned} \tag{A.19}$$

and can be written as

$$C = {U_s}^2 \sum_{n=0}^{N}\sum_{m=0}^{N} \frac{a_n a_m}{h^{n+m}} H_{n,m} \tag{A.20}$$

with

$$H_{n,m} = \int_{-h}^{0} z^m \left[I_{2,n}(z)\sinh 2k(h+z) - I_{1,n}(z)\cosh 2k(h+z)\right]\,dz \tag{A.21}$$

For the polynomial form, $H_{n,m}$ is given by

$$\begin{aligned} H_{0,m} &= \frac{1}{2k}\left[\frac{(-h)^{m+1}}{m+1} + I_{2,m}(0)\right] \\ H_{1,m} &= \frac{1}{2k}\left[\frac{(-h)^{m+2}}{m+2} + (-h)I_{2,m}(0) + \frac{I_{1,m}(0)}{2k}\right] \\ H_{n,m} &= \frac{1}{2k}\left[\frac{(-h)^{n+m+1}}{n+m+1} + (-h)^n I_{2,m}(0) + \frac{n(-h)^{n-1}}{2k} I_{1,m}(0) + \frac{n(n-1)}{2k} H_{n-2,m}\right] \end{aligned} \tag{A.22}$$

The resulting second order correction to group velocity will be

$$\begin{aligned} C_{g2} =& \frac{\partial k C_2}{\partial k} = C_2 + k\frac{\partial C_2}{\partial k} \\ =& C_2 + k\Big[\frac{\partial}{\partial k}(\frac{\tilde{U}}{2C_0})A + \frac{\tilde{U}}{2C_0}A_k + \frac{\partial}{\partial k}(\frac{k^2 C_0}{2gf_0^2(0)})B + \frac{k^2 C_0}{2gf_0^2(0)}B_k \\ &+ \frac{\partial}{\partial k}(\frac{2k^3 C_0}{gf_0^2(0)})C + \frac{2k^3 C_0}{gf_0^2(0)}C_k\Big] \end{aligned} \tag{A.23}$$

We also need an expression for $\tilde{U}_{kk}$ to be used in the Taylor series in section 6. This is given by

$$\tilde{U}_{kk} = \frac{U_s}{h}\sum_{n=0}^{N}\frac{a_n}{h^n}(J_n)_{kk} \tag{A.24}$$

where $(J_n)_{kk}$ can be expressed as

$$\begin{aligned} (J_0)_{kk} &= 0 \\ (J_1)_{kk} &= -\frac{h^2}{2}\mu_{kk} \\ (J_n)_{kk} &= \frac{2J_n}{k^2} + \frac{-1}{2k^3}\Big[n(-h)^{n-1}G_k + n(n-1)(J_{n-2})_k\Big] \\ &\quad -\frac{2(J_n)_k}{k} + \frac{1}{4k^2}\Big[n(-h)^{n-1}G_{kk} + n(n-1)(J_{n-2})_{kk}\Big] \end{aligned} \tag{A.25}$$

with

$$\begin{aligned} \mu_{kk} &= \frac{\mu}{k^2}\Big[(G-1)^2 - (G-1) + G(1 - G\cosh 2kh)\Big] \\ G_{kk} &= \frac{G^2}{k^2}(G + G\cosh^2 2kh - 2\cosh 2kh) \end{aligned} \tag{A.26}$$

For $N = 6$ (A.24) leads to

$$\begin{aligned}\tilde{U}_{kk} = U_s\Big[&\frac{\mu_{kk}}{2}a_1 - \frac{(k^2G_{kk} - 4kG_k + 6G - 6)}{2k^4h^2}a_2 \\ &+\frac{3(k^2G_{kk} - 4kG_k + 6G - k^2\mu_{kk} + 4k\mu_k - 6\mu)}{4k^4h^2}a_3 \\ &-\frac{(k^2(2h^2k^2+3)G_{kk} - 4(2k(h^2k^2+3)G_k + 15) + 12G(h^2k^2+5))}{2k^6h^4}a_4 \\ &+\frac{5(k^2(h^2k^2+3)G_{kk} - 4h^2k^3G_k - 24kG_k + 6G(k)(h^2k^2+10) - 3k^2\mu_{kk} + 24k\mu_k - 60\mu)}{4k^6h^4}a_5 \\ &-\frac{3}{4k^8h^6}\Big(3(k^2(2h^4k^4+10h^2k^2+15) - 2((4h^4k^5+40h^2k^3+90k)G_k + 315) \\ &+2Gk(6h^4k^4+100h^2k^2+315))\Big)a_6\Big]\end{aligned} \tag{A.27}$$

Appendix B

SCALING AND PERTURBATION SOLUTION FOR THE STRONG CURRENT, WEAK SHEAR CASE

The theoretical development in KC89 and BKD17 is based on a framework that assumes that the steady current is small compared to wave phase speed, with current shear and profile curvature comparably small. Here, we provide a scaling analysis and perturbation solution that generalizes the problem to the case of a strong depth-uniform current component and arbitrary current orientation in horizontal coordinates, but with deviations from depth-uniformity assumed to be weak. Conceptually, the approach is to write the mean current vector $\mathbf{U}(z)$ as $\mathbf{U}_0 + \mathbf{U}_1(z)$, where the second component carries the information about weak shear and rotation over depth. We do not make an *a priori* choice of how to make this split into two components, and, as will be seen below, the solution itself suggests that $\mathbf{U}_1$ be chosen so as to have a weighted depth-average value of 0 when weighted according to the KC89 procedure.

To develop the non-dimensional form of (4.4a) - (4.4c), we introduce the scales ω_0 for frequency or inverse time, k_0 for wavenumber or inverse horizontal distance, and scale vertical coordinate z by uniform depth h. Vertical velocity is scaled by its value at the free surface (determined by the kinematic boundary condition) as

$$w(z) = -i\sigma_s a f(z) \tag{B.1}$$

where σ_s is intrinsic frequency at $z = 0$, a is surface wave amplitude, and $f(z)$ is a

dimensionless shape function. Intrinsic frequency σ is given by

$$\begin{aligned} \sigma(z) &= \omega - \mathbf{k}\cdot\mathbf{U}(z) = \omega - \mathbf{k}\cdot\mathbf{U}_0 - \mathbf{k}\cdot\mathbf{U}_1(z) \\ &= \sigma_0 + \sigma_1(z) \end{aligned} \tag{B.2}$$

We define a reference phase speed $c_0 = \omega_0/k_0$ and use $c_0 = \sqrt{gh}$, which fixes the relationship between ω_0 and k_0. For the monochromatic case studied here, we identify ω_0 with ω. Finally, we scale strong depth uniform current $\mathbf{U}_0$ by U and weak current $\mathbf{U}_1$ by $h\Omega$, where Ω represents the strength of current shear or rotation over depth. Referring to (4.4a) - (4.4c), we introduce dimensionless parameters $\sigma' = \sigma/\omega_0$ and $k' = k/k_0$. The resulting dimensionless problem (with primes dropped) is then given by

$$\begin{aligned} \sigma(z)(f_{,zz} - k^2\mu^2 f) &= \epsilon\sigma_{1,zz} f; \quad -1 \le z \le 0 \\ \sigma_s^2 f_{,z}(0) &= k^2 + \epsilon\sigma_s\sigma_{1,z}(0) \\ f(0) &= 1; \quad f(-1) = 0 \end{aligned} \tag{B.3}$$

with

$$\sigma(z) = \sigma_0 + \epsilon\sigma_1(z) = (1 - F\mathbf{k}\cdot\mathbf{U}_0) + \epsilon(-\mathbf{k}\cdot\mathbf{U}_1(z)) \tag{B.4}$$

Dimensionless parameters are $\mu = k_0 h = O(1), F = U/c_0 = O(1)$, and $\epsilon = \mu\Omega/\omega_0 \ll 1$, where μ is the usual dispersion parameter resulting from scaling depth by h and horizontal distance by k_0^{-1}, F is a Froude number, and $\epsilon \ll 1$ is a small parameter characterizing current shear. (The alternate approach employed by Ellingsen & Li (2017), where shear is allowed to be strong but curvature weak, would employ the regime $F, \epsilon = O(1)$, with a new small parameter required to characterize the weak curvature.)

Following KC89, we next solve the system (B.3) using a regular perturbation

expansion

$$f(z) = \sum_{n=0}^{N} \epsilon^n f_n(z). \tag{B.5}$$

with $f_n(-1) = 0$. In contrast to KC89, we take $f_0(0) = 1$ to satisfy the entire surface boundary condition for f, giving homogeneous conditions $f_n(0) = 0$ for $n > 0$. Introducing (B.4) and (B.5) in (B.3) and sorting by powers of ϵ gives the governing equations and surface boundary conditions

$$\sigma_0 \left(f_{n,zz} - k^2 \mu^2 f_n \right) = H_n(z) \tag{B.6}$$

$$\sigma_0^2 f_{n,z}(0) = S_n \tag{B.7}$$

At $n = 0$, we have $H_0 = 0$, $S_0 = 1$, and we get the solution

$$f_0(z) = \frac{\sinh \mu k(1+z)}{\sinh \mu k} \tag{B.8}$$

with

$$\sigma_0^2 = \frac{k \tanh \mu k}{\mu} \tag{B.9}$$

which is the usual solution for waves on a depth uniform current. For higher orders $n \geq 1$, use of Green's law for f_0 and f_n leads to a solvability condition

$$\int_{-1}^{0} f_0 H_n dz = S_n \tag{B.10}$$

At $n = 1$, the leading order at which current shear has an effect, we have

$$H_1(z) = \frac{\sigma_{1,zz}}{\sigma_0} f_0(z); \qquad S_1 = \frac{\sigma_{1,z}(0)}{\sigma_0} - \frac{2k^2 \sigma_1(0)}{\sigma_0^3} \tag{B.11}$$

Using (B.11) in (B.10) leads, after cancellations, to the identity

$$\int_{-1}^{0} \sigma_1(z) \cosh 2\mu k(1+z) dz = -\mathbf{k} \cdot \int_{-1}^{0} \mathbf{U}_1(z) \cosh 2\mu k(1+z) dz = 0 \tag{B.12}$$

But $\mathbf{U}_1 = (\mathbf{U} - \mathbf{U}_0)/\epsilon$, which, when substituted in (B.12), gives the result

$$\mathbf{U}_0 = \tilde{\mathbf{U}} = \frac{2\mu k}{\sinh 2\mu k} \int_{-1}^{0} \mathbf{U}(z) \cosh 2\mu k(1+z) dz \tag{B.13}$$

where $\tilde{\mathbf{U}}$ is the depth-weighted current from KC89, extended to allow for $F = O(1)$ and arbitrary direction relative to the wave direction. We thus have the leading order expression for intrinsic frequency $\sigma_0 = \tilde{\sigma} = 1 - F\mathbf{k} \cdot \tilde{\mathbf{U}}$, with leading order dispersion relation

$$\tilde{\sigma}^2 = \frac{k \tanh \mu k}{\mu} \tag{B.14}$$

The expression for phase speed $\mathbf{c}_a$ in a fixed frame is given by

$$\mathbf{c}_a = \frac{\omega}{\mathbf{k}} = \frac{\tilde{\sigma}}{\mathbf{k}} + \tilde{\mathbf{U}} + O(\epsilon^2) \tag{B.15}$$

with no further correction to phase speed at $O(\epsilon)$. Equations (B.6) - (B.7) may then be solved for $f_1(z)$ following the procedure in KC89, giving the result

$$\begin{aligned} f_1(z) \;=\; & \left[A_1 + \frac{1}{\mu k} \int_{-1}^{z} H_1(\xi) f_{0,\xi}(\xi)\, d\xi \right] f_0(z) \\ & + \left[B_1 - \frac{1}{\mu k} \int_{-1}^{z} H_1(\xi) f_0(\xi)\, d\xi \right] f_{0,z}(z) \end{aligned} \tag{B.16}$$

with the coefficients A_1 and B_1 of the homogeneous solution resolved by applying the boundary conditions $f_1(0) = f_1(-1) = 0$. Dimensional forms of the results are given in Section 4.3.1.

Appendix C

APPROXIMATIONS FOR WEAK CURRENT SHEAR

Starting with the expressions (4.9a) and (4.9b) for action density and flux, we develop expansions in powers of ϵ consistent with the approach in B. In (4.9a) and (4.9b), explicit appearances of σ_s and $\mathbf{U}_s$ occur due to the satisfaction of the surface boundary condition and the transformation (4.7). We assume these should be common to all versions of the expansion that follows. Subsequently, we express $f(z)$ as in (B.5) and use (4.14) and (4.16). We then introduce an arbitrary version of the depth uniform current and resulting intrinsic frequency, $\mathbf{U}_0$ and σ_0, as representations of the leading order solution,

$$\begin{aligned} \mathbf{U}(z) &= \mathbf{U}_0 + \epsilon \mathbf{U}_1(z) \\ \sigma(z) &= \sigma_0 + \epsilon \sigma_1(z) \end{aligned} \tag{C.1}$$

where $\sigma_0 = \omega - \mathbf{k}\cdot\mathbf{U}_0$ and $\sigma_1 = -\mathbf{k}\cdot\mathbf{U}_1 = -\mathbf{k}\cdot(\mathbf{U}-\mathbf{U}_0)$, and with associated dispersion relation

$$\sigma_0^2 = gk \tanh kh \tag{C.2}$$

After some simplification of the resulting forms of $\mathcal{N}$ and $\boldsymbol{\mathcal{F}}$, we obtain approximate forms consistent with the present derivation through the choice $\mathbf{U}_0 = \tilde{\mathbf{U}}$ and $\sigma_0 = \tilde{\sigma}$. We also develop an alternate version based on the choice $\mathbf{U}_0 = \mathbf{U}_s$ and $\sigma_0 = \sigma_s$, which leads to expressions for action and flux defined in terms of surface variables, as in Quinn *et al.* (2017). It was our initial expectation that this procedure should reproduce the results in Quinn *et al.* (2017), which are described as being based on the approximate wave-current formulation here and in KC89, but we have not been able to reproduce the results given by Quinn *et al.* (2017), as discussed in Section 4.7.1.

Substituting the expressions (C.1) and the expansion for $f(z)$ into the formulae (4.9a) and (4.9b) and retaining terms to $O(\epsilon)$ leads to the generic version of the expansion, where any remaining occurrences of frequency or current are expressed in terms of σ_0 and $\mathbf{U}_0$. During this process, expressions occurring in terms of $O(\epsilon)$ may be manipulated by choosing $\sigma_0 = \sigma_s$ or $\tilde{\sigma}$ freely, since transformations between these quantities would occur at $O(\epsilon^2)$. In contrast, occurrences of σ_0 in $O(1)$ terms must retain the implied ambiguity, as it's resolution would occur within the accuracy of the approximation.

Proceeding with (4.9a) for the action density, we note that the integral term is of $O(\epsilon)$, since $\sigma'' = \epsilon\sigma_1''$ for any choice of reference frame. Recognizing that $\sigma_s/\sigma_0 = 1 + O(\epsilon)$ for any choice of reference frame making σ_1 small, we obtain the approximate expression

$$\mathcal{N} = \frac{E_0}{\sigma_s}\left[1 + \epsilon\frac{\sigma_s}{2gk^2}\left(\sigma_{1,z}(0) - \int_{-h}^{0}\sigma_{1,zz}f_0^2 dz\right)\right] + O(\epsilon^2) \tag{C.3}$$

The expression in the interior parentheses may be integrated immediately, and we obtain the approximation

$$\mathcal{N}_0 = \frac{E_0}{\sigma_s}\left[1 + \epsilon\frac{\sigma_s}{\sigma_0^2}(\sigma_s - \tilde{\sigma})\right] + O(\epsilon^2) \tag{C.4}$$

where the single appearance of σ_0 results from a resolution of the combination $gk\tanh kh$.

Turning to the expression for action flux (4.9b), we note that the first integral term involving f^2 occurs at leading order, and thus the ambiguity of the value of σ_0 must be retained there. We proceed as before by substituting the expansions (C.1). The expression $A(z)$ may be expanded as $\mathbf{A} = \mathbf{A}_0 + \epsilon\mathbf{A}_1 + O(\epsilon^2)$, and we find that $\mathbf{A}_0 = 0$ and

$$\mathbf{A}_1(z) = \sigma_0\mathbf{U}_{1,z} - \mathbf{U}_0\sigma_{1,z} \tag{C.5}$$

so that the integral involving $\mathbf{A}_{,z}$ is reduced to

$$\sigma_s^2 \int_{-h}^{0} \sigma^{-2} \mathbf{A}_{,z} f^2 dz = \epsilon \frac{\sigma_s^2}{\sigma_s^2 + O(\epsilon)} \int_{-h}^{0} \mathbf{A}_{1,z} f_0^2 dz + O(\epsilon^2) \tag{C.6}$$

The entire bracketed expression involving $\mathbf{A}$ in (4.9b) is then evaluated as

$$\epsilon \left[-\mathbf{A}_1(0) + \int_{-h}^{0} \mathbf{A}_{1,z} f_0^2 dz \right] = -\epsilon \frac{k}{\sinh^2 kh} \mathbf{I}_3 \tag{C.7}$$

where

$$\mathbf{I}_3 = \int_{-h}^{0} \mathbf{A}_1(z) \sinh 2k(h+z) dz \tag{C.8}$$

The integral of f^2 is expanded to give

$$\int_{-h}^{0} f^2 dz = I_4 + 2\epsilon I_5 + O(\epsilon^2) \tag{C.9}$$

with

$$I_4 = \int_{-h}^{0} f_0^2 dz; \qquad I_5 = \int_{-h}^{0} f_0 f_1 dz \tag{C.10}$$

and with f_1 given by (4.16). The resulting expression for the approximation $\boldsymbol{\mathcal{F}}_0$ is then

$$\boldsymbol{\mathcal{F}}_0 = \frac{E_0}{\sigma_s} \left[\mathbf{U}_s + \mathbf{c}_{rs} \left(1 - \frac{\sigma_s^2}{g} I_4 \right) \right] - \epsilon \frac{E_0}{\sigma_s} \left[\mathbf{c}_{rs} \frac{2\sigma_s^2}{g} I_5 + \frac{\sigma_s}{\sigma_0^2 \sinh 2kh} \mathbf{I}_3 \right] \tag{C.11}$$

Integrals $\mathbf{I}_3$ and I_4 are given to the required order by

$$\begin{aligned} \mathbf{I_3} &= \sinh 2kh \left[\sigma_0 (\mathbf{U}_s - \tilde{\mathbf{U}}) + \mathbf{U}_0 (\tilde{\sigma} - \sigma_s) \right] \\ I_4 &= \frac{g}{2\sigma_0^2} (1 - G); \qquad G = \frac{2kh}{\sinh 2kh} \end{aligned} \tag{C.12}$$

The expression for I_5 is complex, and is given after some initial effort by

$$I_5 = \frac{1}{4\tilde{\sigma} \sinh^2 kh} \left[\frac{G \cosh^2 kh}{k} I_2(0) - I_6 \right] \tag{C.13}$$

where (from (4.17))

$$I_2(0) = 2\sinh^2 kh(\hat{\mathbf{k}} \cdot \mathbf{U}_{,z}(0)) + 2\sinh 2kh(\sigma_s - \tilde{\sigma}) \tag{C.14}$$

and

$$I_6 = \int_{-h}^{0} \hat{\mathbf{k}} \cdot \mathbf{U}_{,zz}(z)(h+z)\sinh 2k(h+z)dz \tag{C.15}$$

An expression for I_6 is obtained by first expressing $\tilde{\mathbf{U}}$ in terms of $\mathbf{U}_{,zz}$ using two integrations by parts, differentiating the resulting expression with respect to wavenumber k, and taking the dot product with the unit wavenumber $\hat{\mathbf{k}}$ to obtain (after rearrangement)

$$I_6 = \sinh 2kh\left[\mathbf{k} \cdot \tilde{\mathbf{U}}_{,k} + h\hat{\mathbf{k}} \cdot \mathbf{U}_{1,z}(0) + \frac{1}{k}\left((1-G) + 2G\cosh^2 kh\right)(\sigma_s - \tilde{\sigma})\right] \tag{C.16}$$

Using (C.14) and (C.16) in (C.13) leads to a relatively compact expression for I_5 given by

$$I_5 = -\frac{1}{2\tilde{\sigma}\tanh kh}\left[\mathbf{k} \cdot \tilde{\mathbf{U}}_{,k} + \frac{1}{k}(1-G)(\sigma_s - \tilde{\sigma})\right] \tag{C.17}$$

Using the results for $\mathbf{I}_3, I_4$ and I_5 in (C.11) leads finally to

$$\begin{aligned}
\boldsymbol{\mathcal{F}}_0 \;=\; & \frac{E_0}{\sigma_s}\left[\mathbf{U}_s + \mathbf{c}_{rs}\left(1 - \frac{1}{2}\left(\frac{\sigma_s}{\sigma_0}\right)^2(1-G)\right)\right] \\
& + \epsilon\frac{E_0}{\sigma_s}\left[\frac{\sigma_s^3\hat{\mathbf{k}}}{\tilde{\sigma}\sigma_0^2}\left(\mathbf{k} \cdot \tilde{\mathbf{U}}_{,k} + \frac{1}{k}(1-G)(\sigma_s - \tilde{\sigma})\right)\right. \\
& \left. - \frac{\sigma_s}{\sigma_0^2}\left(\sigma_0(\mathbf{U}_s - \tilde{\mathbf{U}}) + (\tilde{\sigma} - \sigma_s)\mathbf{U}_0\right)\right]
\end{aligned} \tag{C.18}$$

From this point, the resolution of the expressions for $\mathcal{N}_0$ and $\boldsymbol{\mathcal{F}}_0$ involves the choice of σ_0. Following the procedure of referencing all quantities to surface conditions leads to an expression for $\mathcal{N}_0$ given by

$$\mathcal{N}^* = \mathcal{N}_0(\sigma_s) = \frac{E_0}{\sigma_s}\left[1 + \epsilon\frac{(\sigma_s - \tilde{\sigma})}{\sigma_s}\right] + O(\epsilon^2) \tag{C.19}$$

This result is similar in form to that in Quinn *et al.* (2017), equation (4.2), but there is no clear relation between the residual $O(\epsilon)$ terms in the two results, as discussed further in Section 4.7.1.

Taking the alternate approach of referencing quantities to the frame moving with speed $\tilde{\mathbf{U}}$ leads to the expression

$$\tilde{\mathcal{N}} = \mathcal{N}_0(\tilde{\sigma}) = \frac{E_0}{\tilde{\sigma}} + O(\epsilon^2) \tag{C.20}$$

where all information about the approximation within the order of accuracy is contained in the simple ratio of E_0 and $\tilde{\sigma}$.

The same process applied to $\boldsymbol{\mathcal{F}}_0$ in (C.18) leads to the expressions

$$\boldsymbol{\mathcal{F}}^* = \frac{E_0}{\sigma_s}\left[\hat{\mathbf{U}} + \mathbf{c}_{grs} + \epsilon\left(\mathbf{U}_s\left(\frac{\sigma_s - \tilde{\sigma}}{\sigma_s}\right) + \frac{\hat{\mathbf{k}}}{k}(1-G)(\sigma_s - \tilde{\sigma})\right)\right] + O(\epsilon^2) \tag{C.21}$$

and

$$\tilde{\boldsymbol{\mathcal{F}}} = \frac{E_0}{\tilde{\sigma}}\left[\hat{\mathbf{U}} + \tilde{\mathbf{c}}_{gr}\right] + O(\epsilon^2) \tag{C.22}$$

where $\mathbf{c}_{grs}$ and $\tilde{\mathbf{c}}_{gr}$ are relative group velocities (defined in the usual sense for a depth uniform current) relative to the surface and depth weighted velocities respectively.

Appendix D

RESULTS FOR ERRORS IN WAVE ACTION DENSITY FLUX FOR ADDITIONAL CASES

We first report % errors in estimates of action density $\mathcal{N}$ relative to exact results for a linear shear current, using the depth-weighted current $\tilde{\mathbf{U}}$ (Figures D.1 - D.2), surface current U_s (Figures D.3 - D.5) or depth-average velocity $\overline{U}$ (Figures D.6 - D.8) for oblique angles $\beta = 0, \pi/4$ and $\pi/2$ between the surface current and shear current, for ranges of kh and wave angle θ relative to the surface current. Figures D.9 - D.16 report the % errors in the estimate of action flux $\boldsymbol{\mathcal{F}}$ for the same distributions of parameters.

Figures D.17 - D.20 show results for action density and flux estimates for the Mouth of the Columbia River example for expressions based on depth uniform current equal to the surface current or depth-average currents.

Figures D.21 - D.25 show error measures for cases constructed using the Taylor series expansion of Section 6, with values normalized by exact values for action density and flux.

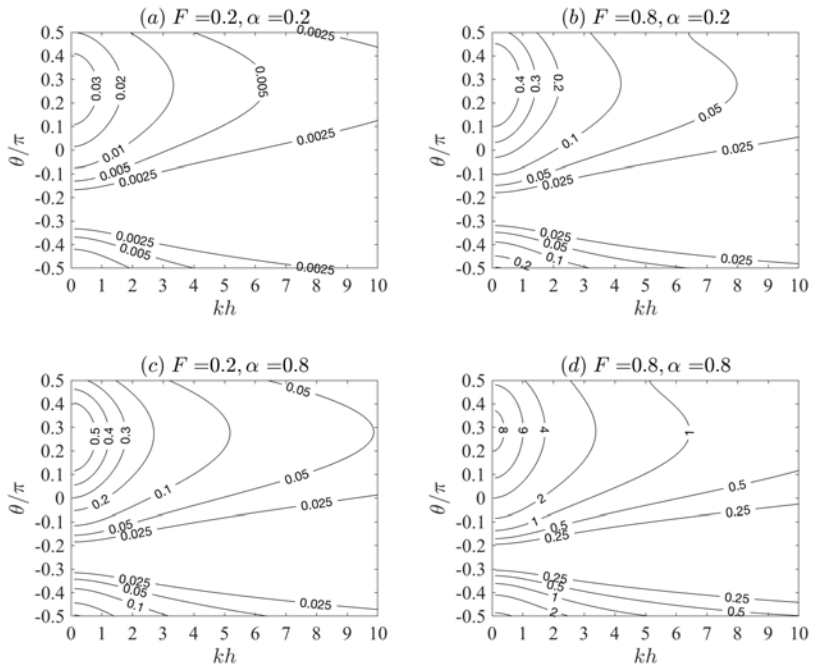

Figure D.1: % error in wave action density $100(1-\tilde{\mathcal{N}}/\mathcal{N})$: linear shear with variation of kh-θ, first order perturbation approximation, $\beta = \pi/4$.

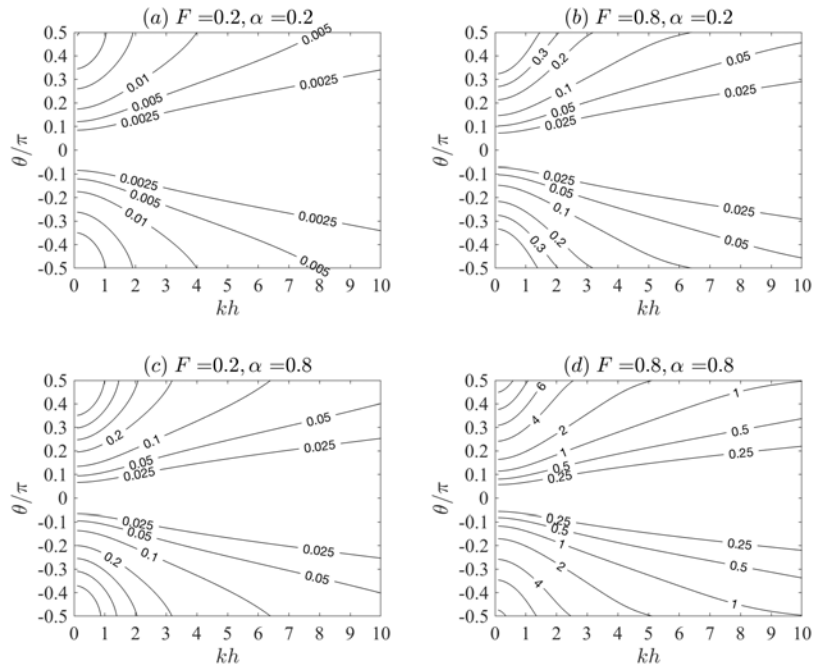

Figure D.2: % error in wave action density $100(1-\tilde{\mathcal{N}}/\mathcal{N})$: linear shear with variation of kh and θ, first order perturbation approximation, $\beta = \pi/2$.

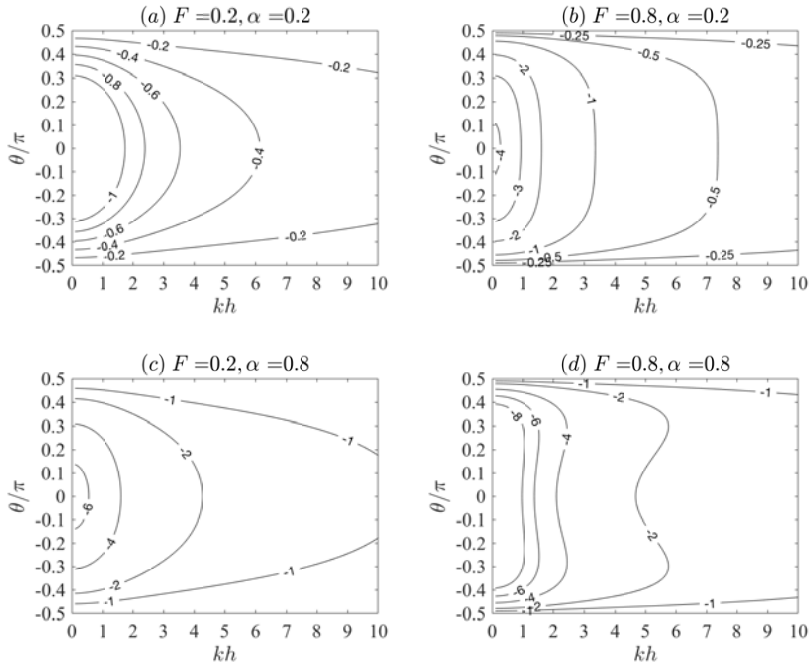

Figure D.3: % error in wave action density $\mathcal{N}_s$ based on surface current U_s relative to the exact value, $100(1-\mathcal{N}_s/\mathcal{N})$ with variation of kh and θ: Constant shear current, $\beta = 0$.

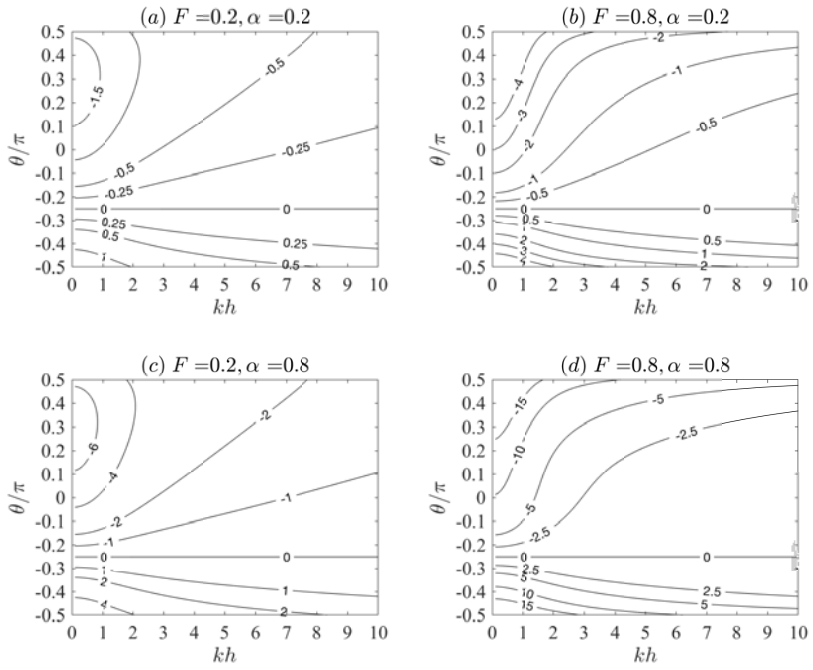

Figure D.4: As in Figure D.3: Constant shear current, $\beta = \pi/4$.

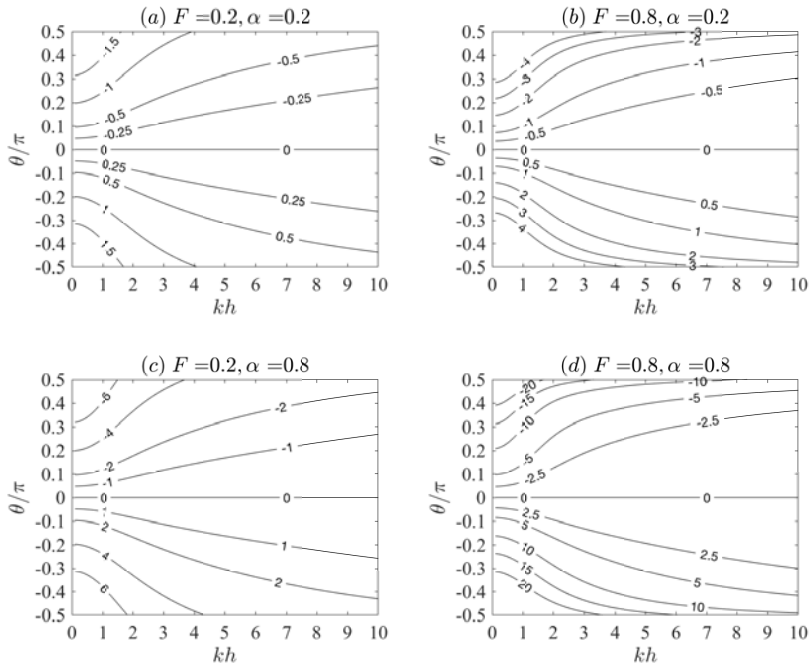

Figure D.5: As in Figure D.3: Constant shear current, $\beta = \pi/2$.

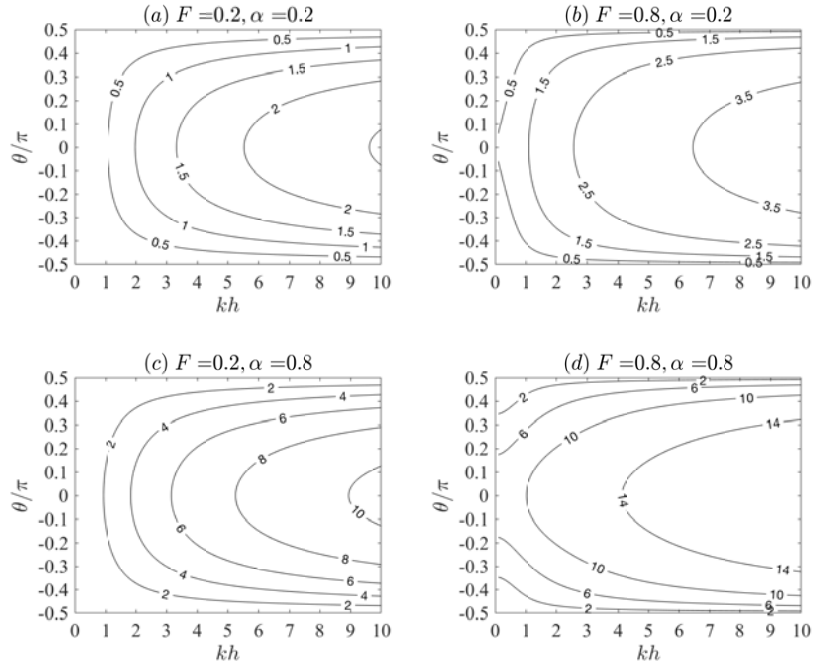

Figure D.6: % error in wave action density $\overline{\mathcal{N}}$ based on depth-average current $\overline{U}$ relative to the exact value, $100(1 - \overline{\mathcal{N}}/\mathcal{N})$ with variation of kh and θ: Constant shear current, $\beta = 0$.

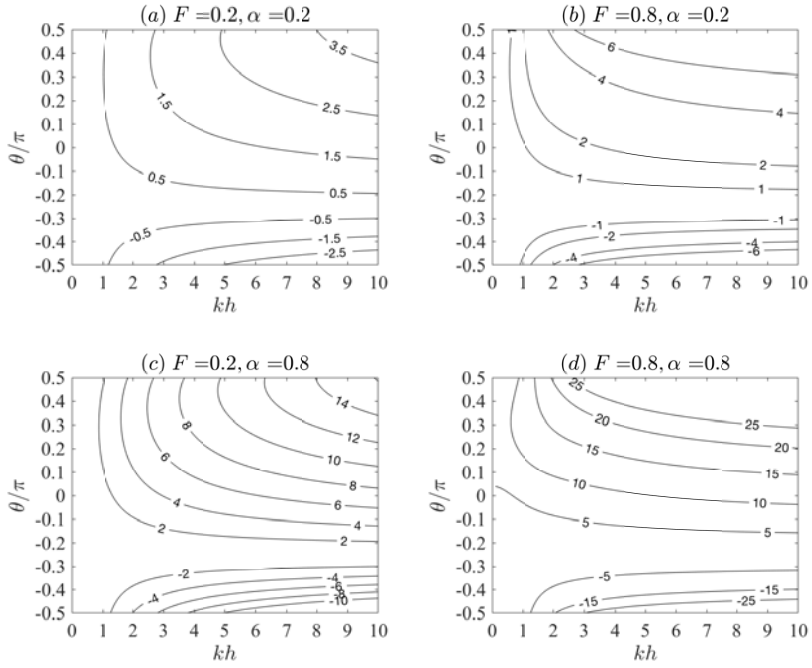

Figure D.7: As in Figure D.6: Constant shear current, $\beta = \pi/4$.

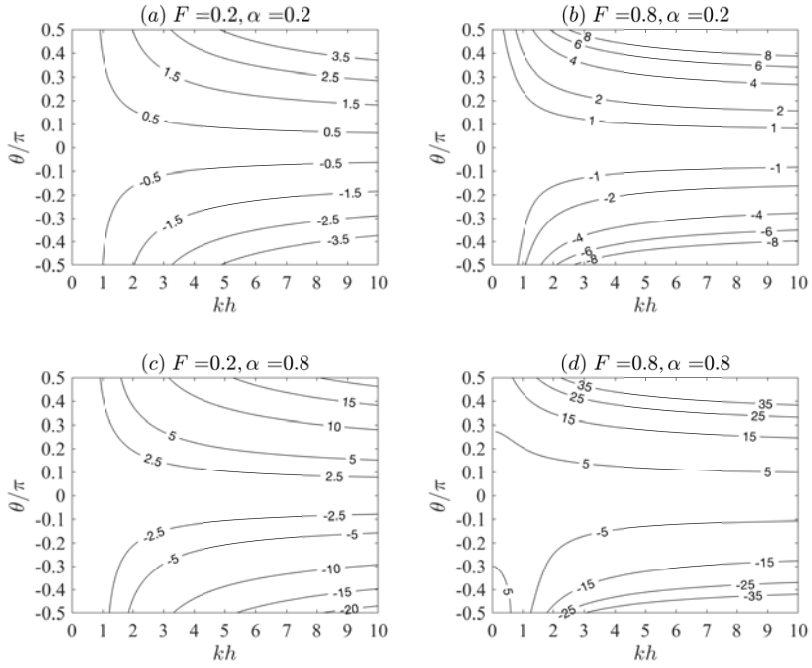

Figure D.8: As in Figure D.6: Constant shear current, $\beta = \pi/2$.

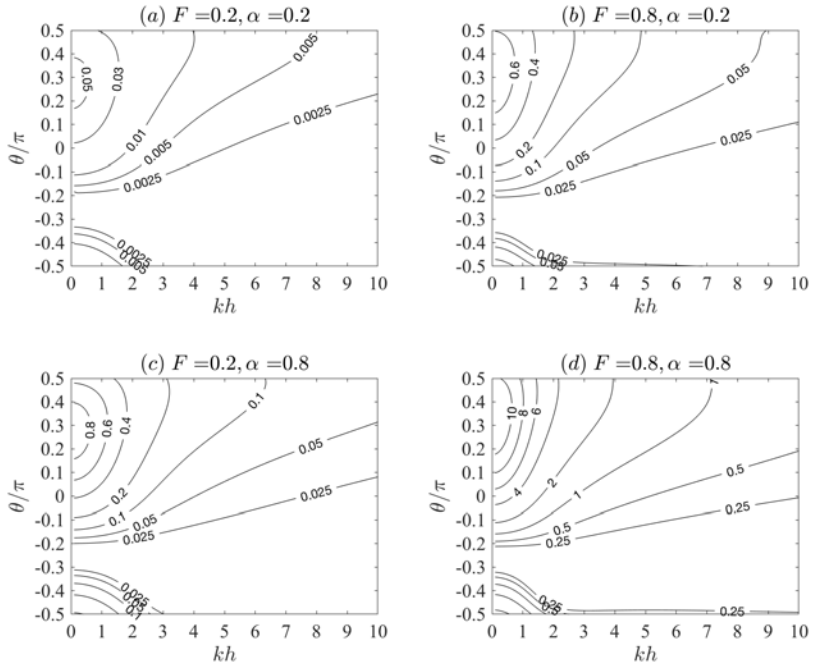

Figure D.9: % error in wave action flux $100(1-|\tilde{\boldsymbol{\mathcal{F}}}|/|\boldsymbol{\mathcal{F}}|)$: linear shear with variation of kh and θ, first order perturbation approximation, $\beta = \pi/4$.

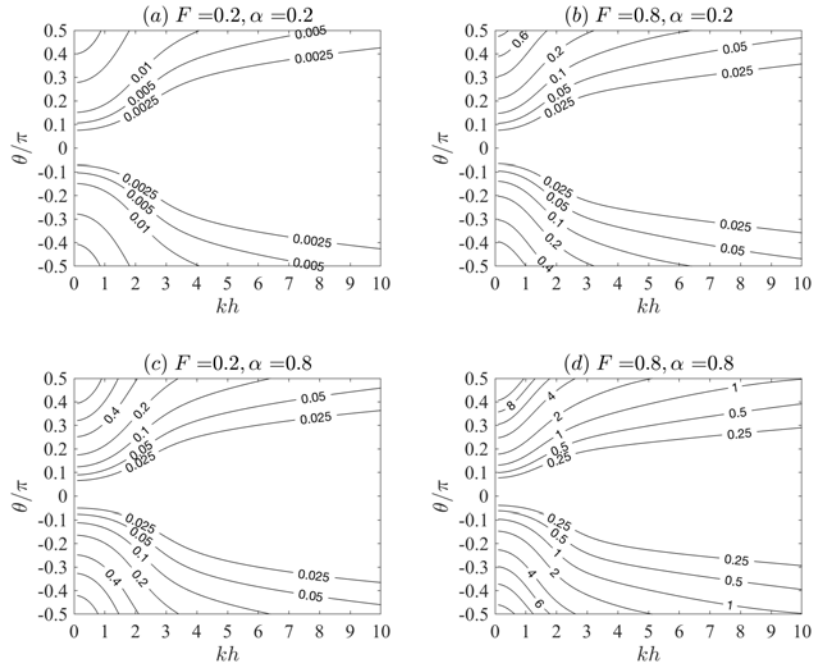

Figure D.10: % error in wave action flux $100(1-|\tilde{\boldsymbol{\mathcal{F}}}|/|\boldsymbol{\mathcal{F}}|)$: linear shear with variation of kh and θ, first order perturbation approximation, $\beta = \pi/2$.

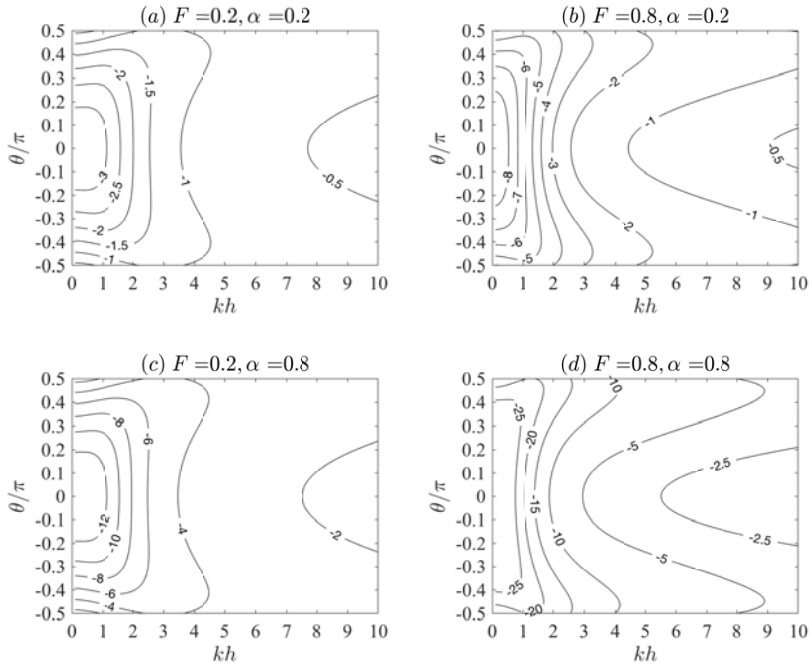

Figure D.11: % error in wave action flux $\boldsymbol{\mathcal{F}}_s$ based on surface current U_s relative to the exact value, $100(1 - \boldsymbol{\mathcal{F}}_s/\boldsymbol{\mathcal{F}})$ with variation of kh and θ: Constant shear current, $\beta = 0$.

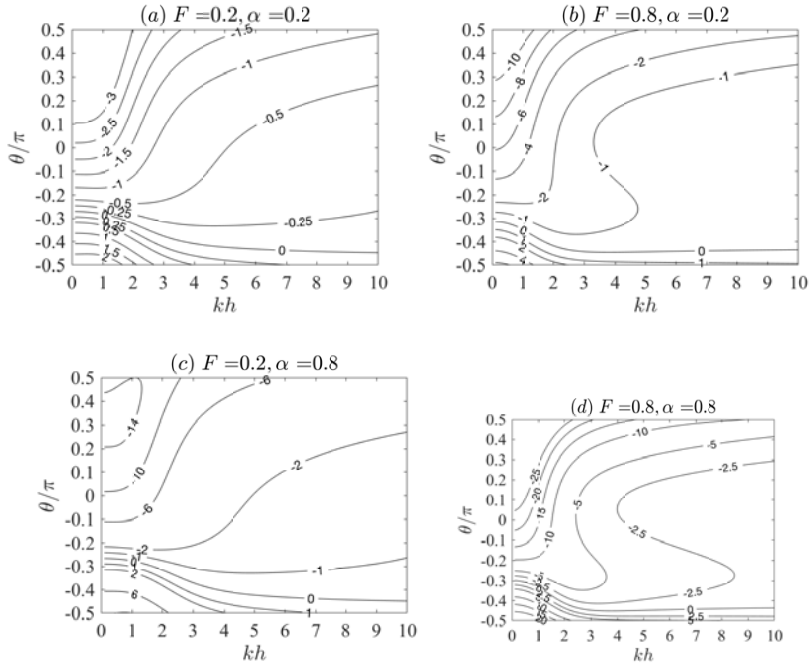

Figure D.12: As in Figure D.11: Constant shear current, $\beta = \pi/4$.

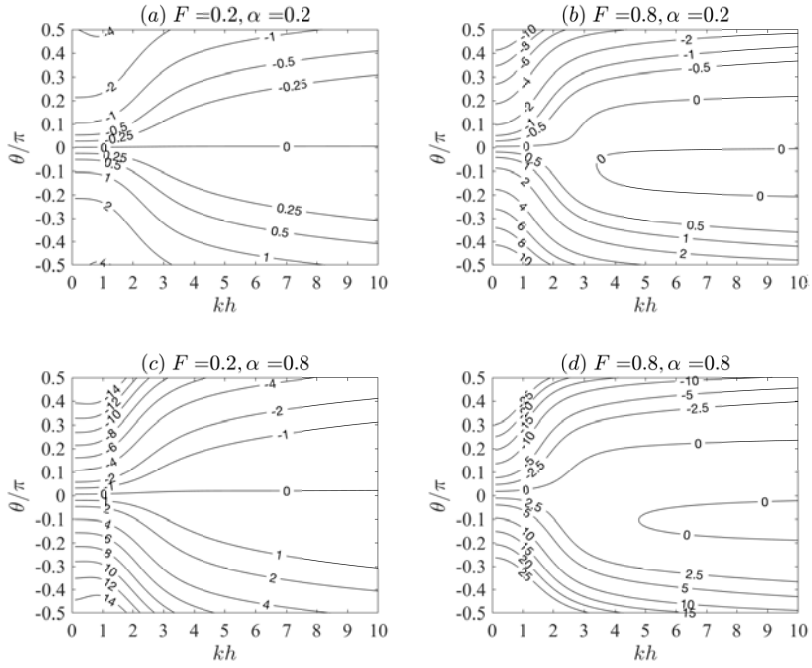

Figure D.13: As in Figure D.11: Constant shear current, $\beta = \pi/2$.

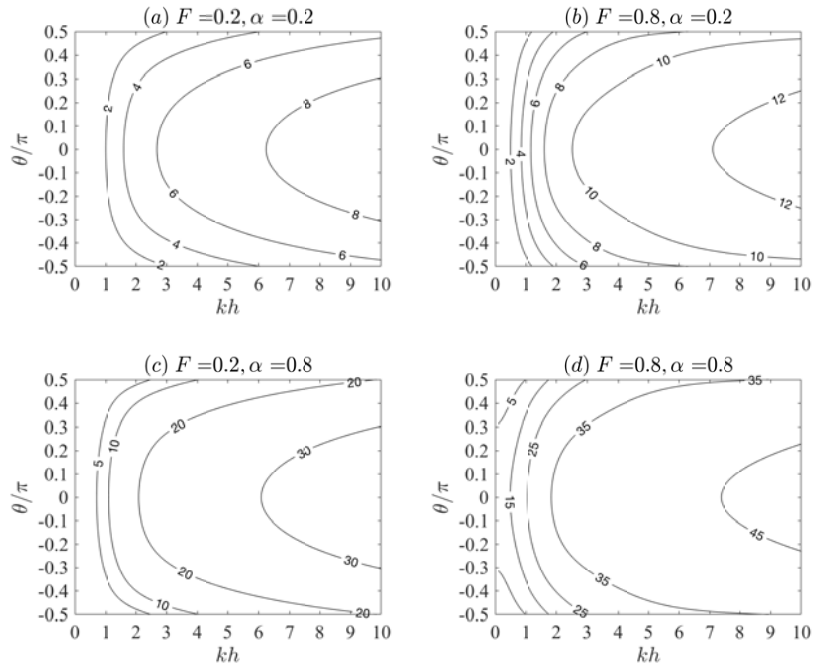

Figure D.14: % error in wave action flux $\overline{\boldsymbol{\mathcal{F}}}$ based on depth-averaged current $\overline{U}$ relative to the exact value, $100(1 - \overline{\boldsymbol{\mathcal{F}}}/\boldsymbol{\mathcal{F}})$ with variation of kh and θ: Constant shear current, $\beta = 0$.

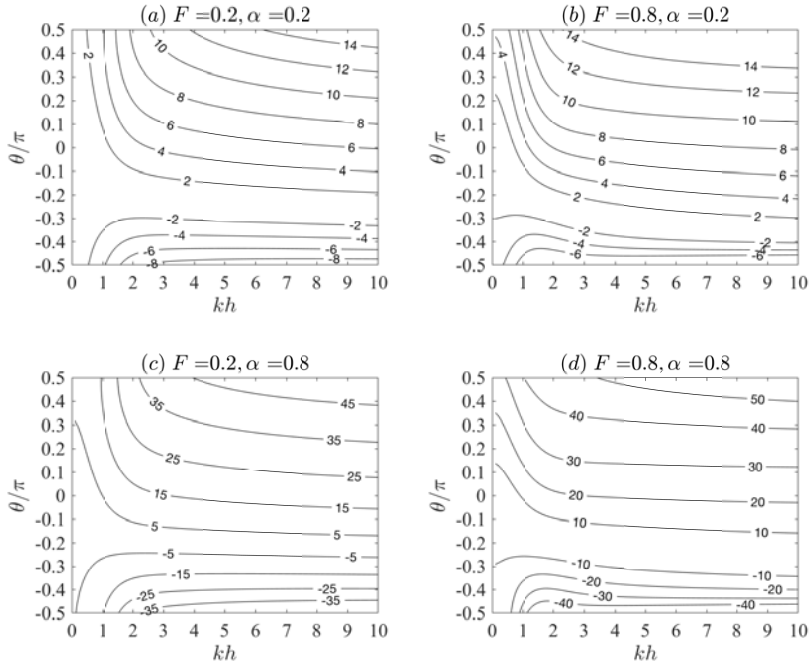

Figure D.15: As in Figure D.14: Constant shear current, $\beta = \pi/4$.

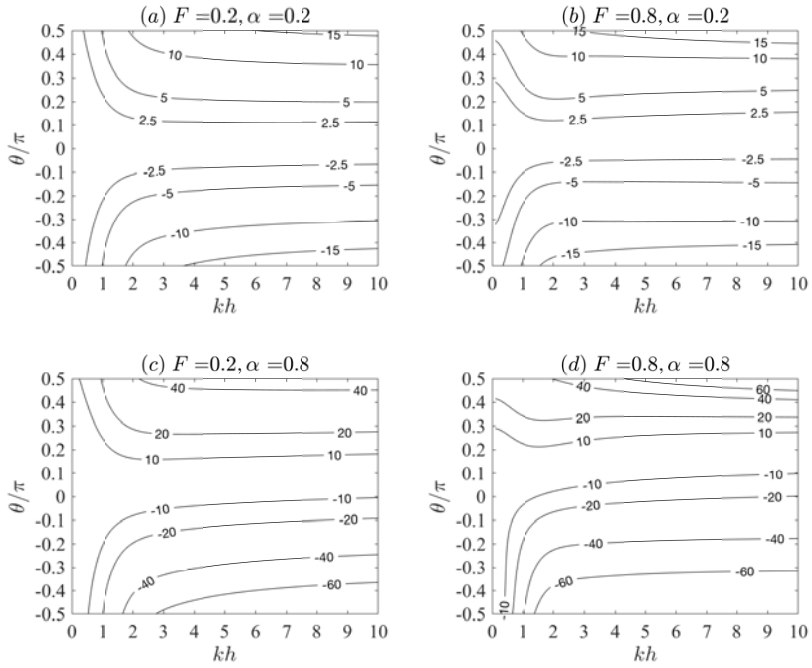

Figure D.16: As in Figure D.14: Constant shear current, $\beta = \pi/2$.

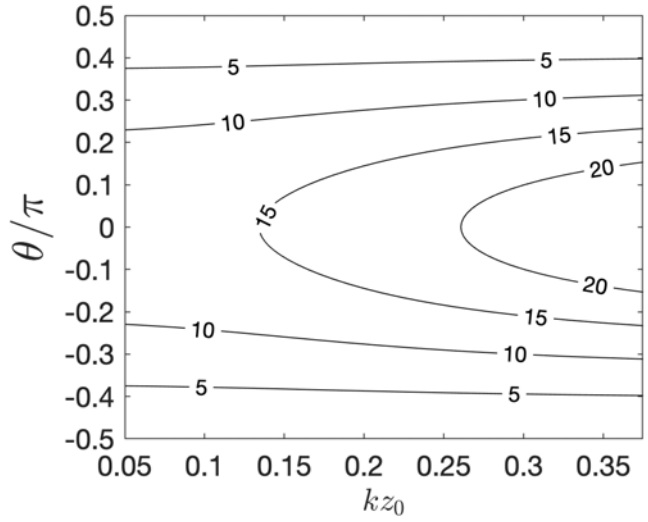

Figure D.17: % error in wave action density $100(1-\mathcal{N}_s/\mathcal{N})$ based on surface current: MCR current profile with variation of kz_0 and θ.

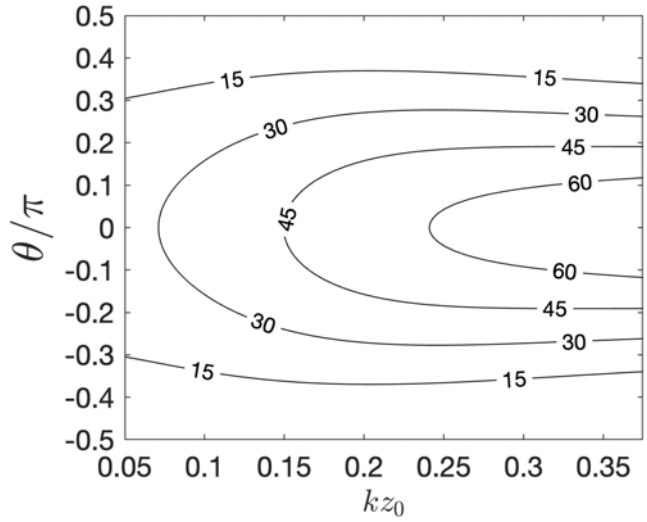

Figure D.18: % error in wave action flux $100(1-|\boldsymbol{\mathcal{F}}_s|/|\boldsymbol{\mathcal{F}}|)$ based on surface current: MCR current profile with variation of kz_0 and θ.

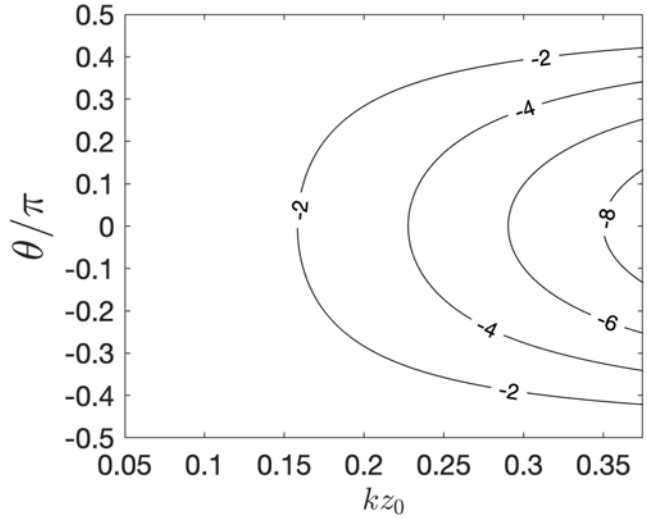

Figure D.19: % error in wave action density $100(1-\overline{\mathcal{N}}/\mathcal{N})$ based on depth-average current: MCR current profile with variation of kz_0 and θ.

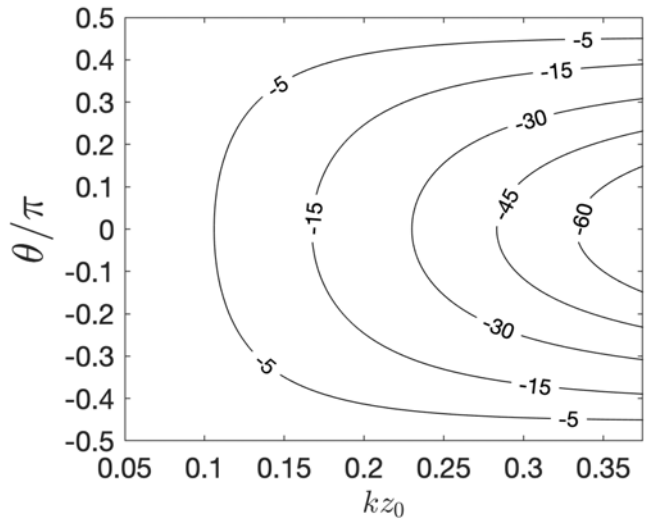

Figure D.20: % error in wave action flux $100(1 - |\overline{\boldsymbol{\mathcal{F}}}|/|\boldsymbol{\mathcal{F}}|)$based on depth-average current: MCR current profile with variation of kz_0 and θ with, average current value.

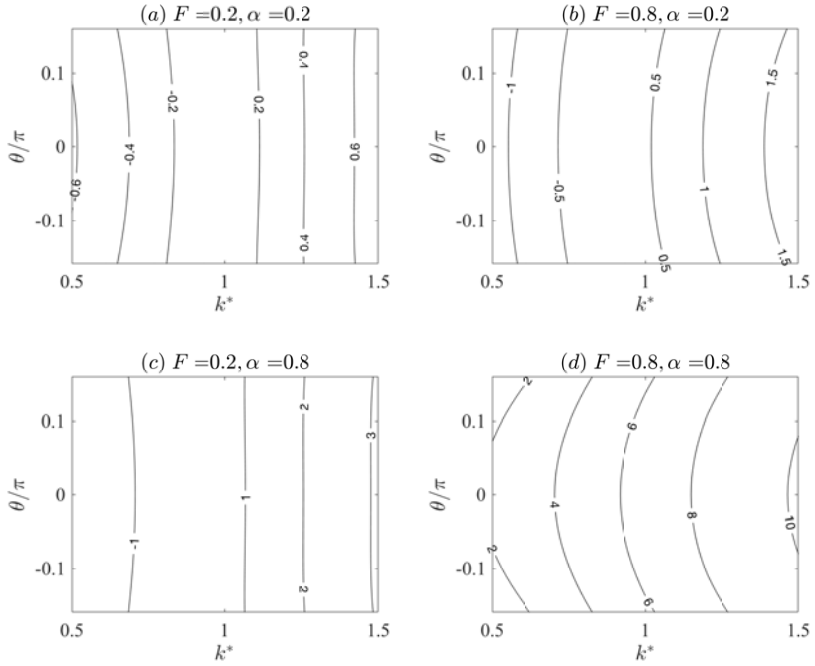

Figure D.21: % error in wave action flux $100(1-|\tilde{\boldsymbol{\mathcal{F}}}_T|/|\boldsymbol{\mathcal{F}}|)$ for current with constant shear, with variation of k^* and θ, with $k^* = k/k^p$, $k^p h = 1$: Taylor series expansion of $\tilde{\sigma}(k)$ and $\hat{\mathbf{U}}(k)$ around k^p, $\beta = 0$.

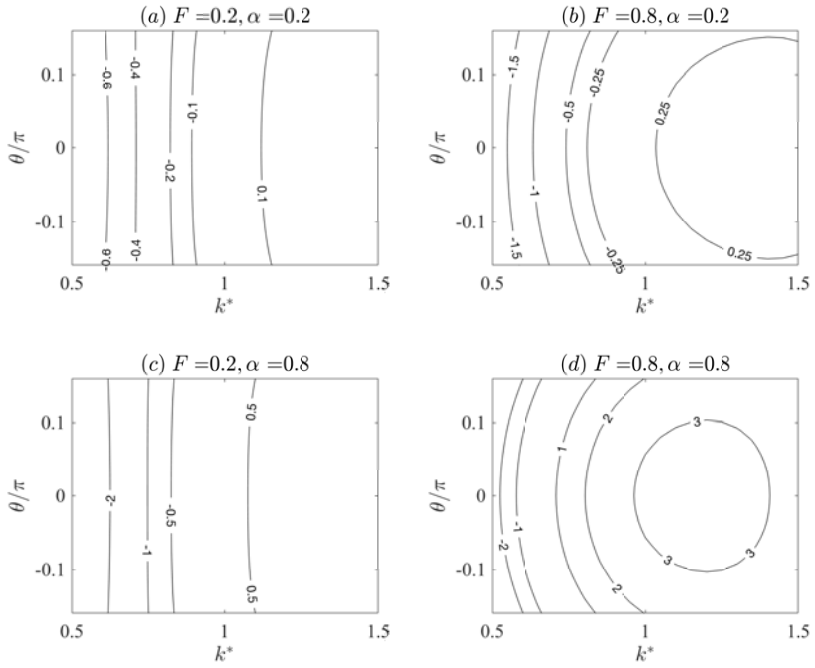

Figure D.22: % error in wave action flux $100(1-|\tilde{\boldsymbol{\mathcal{F}}}_T|/|\boldsymbol{\mathcal{F}}|)$ for current with constant shear, with variation of k^* and θ, with $k^* = k/k^p$, $k^p h = 2$: Taylor series expansion of $\tilde{\sigma}(k)$ and $\hat{\mathbf{U}}(k)$ around k^p, $\beta = 0$.

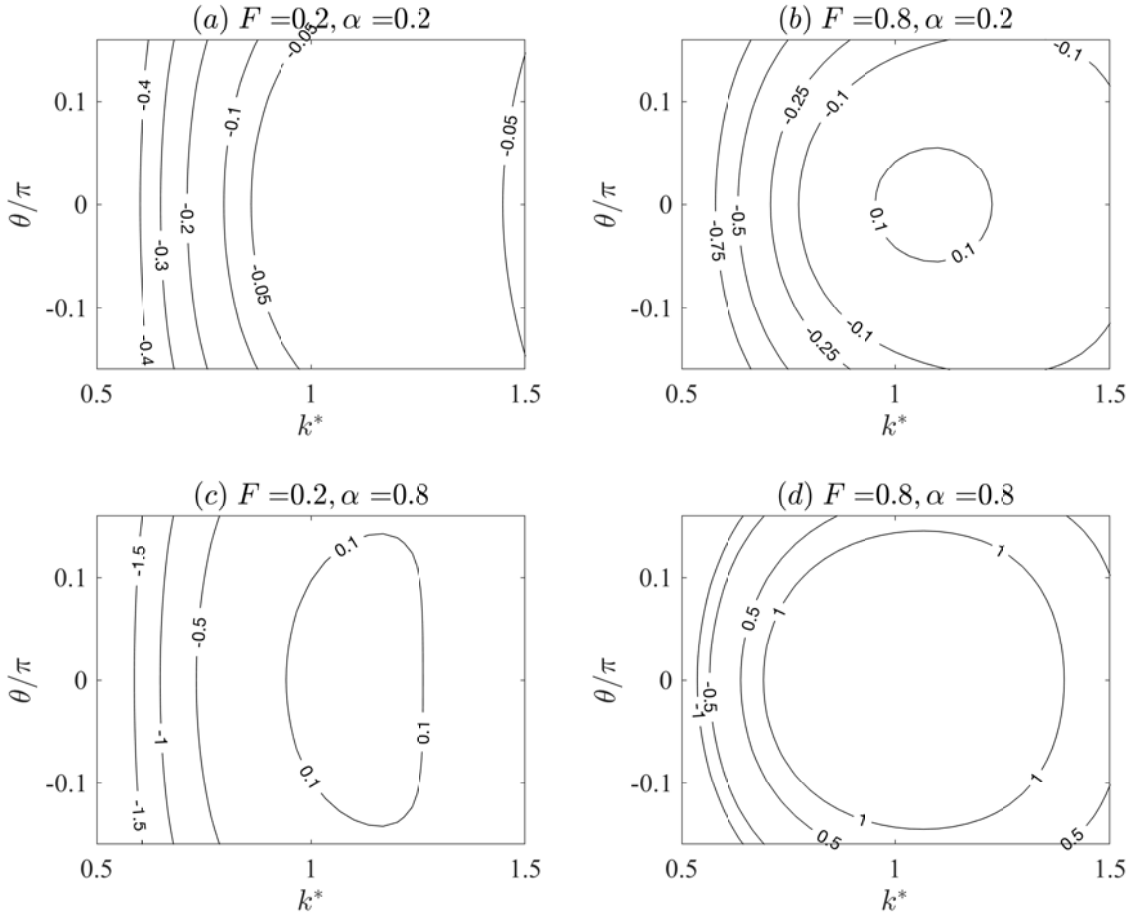

Figure D.23: % error in wave action flux $100(1-|\tilde{\boldsymbol{\mathcal{F}}}_T|/|\boldsymbol{\mathcal{F}}|)$ for current with constant shear, with variation of k^* and θ, with $k^* = k/k^p$, $k^p h = 3$: Taylor series expansion of $\tilde{\sigma}(k)$ and $\hat{\mathbf{U}}(k)$ around k^p, $\beta = 0$.

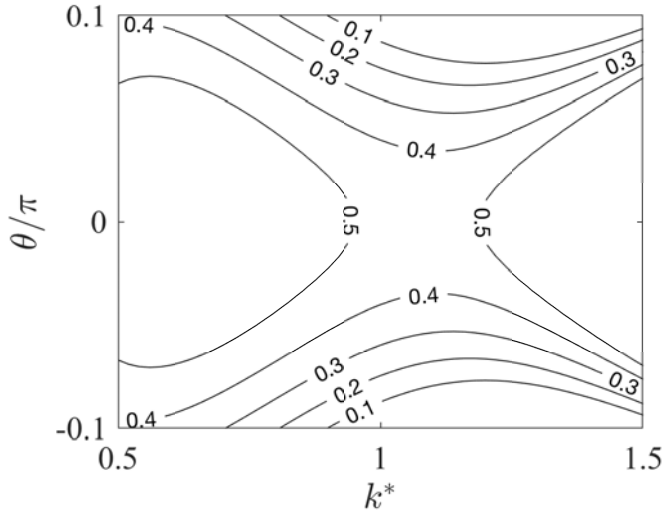

Figure D.24: % error in wave action flux $100(1 - |\tilde{\boldsymbol{\mathcal{F}}}_T|/|\boldsymbol{\mathcal{F}}|)$: MCR current profile with variation of k^* and θ with $k^* = k/k^p$ and $k^p h = 1$, first order perturbation approximation.

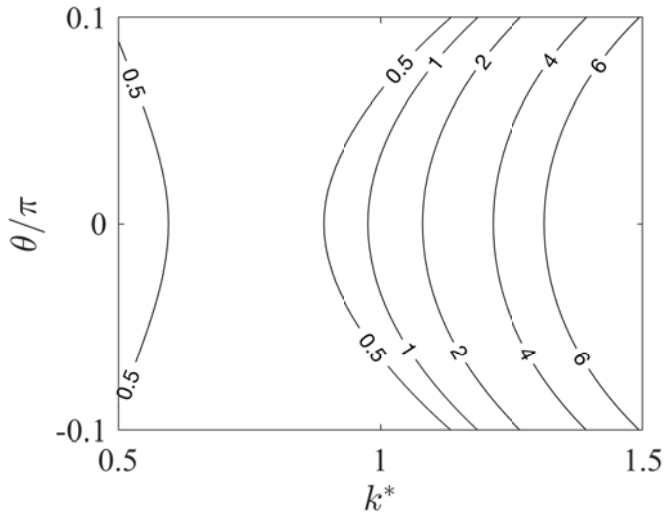

Figure D.25: % error in wave action flux $100(1 - |\tilde{\boldsymbol{\mathcal{F}}}_T|/|\boldsymbol{\mathcal{F}}|)$: MCR current profile with variation of k^* and θ with $k^* = k/k^p$ and $k^p h = 2$, first order perturbation approximation.

Appendix E

PERMISSIONS

Chapters 3 and 4 have been published in Ocean Modelling. Rights and content to include these publications in the thesis has been provided in this appendix.

Approximation of wave action flux velocity in strongly sheared mean flows

Author: Saeideh Banihashemi,James T. Kirby,Zhifei Dong

Publication: Ocean Modelling

Publisher: Elsevier

Date: August 2017

Approximation of wave action conservation in vertically sheared mean flows

Author: Saeideh Banihashemi,James T. Kirby

Publication: Ocean Modelling
Publisher: Elsevier
Date: November 2019